

SUPERVISED BATTERY CAPACITY ESTIMATION

by

Moinak Pyne



APPROVED BY SUPERVISORY COMMITTEE:

---

Stephen Yurkovich, Chair

---

Mark W. Spong

---

Babak Fahimi

---

Justin Ruths

Copyright © 2019

Moinak Pyne

All rights reserved

*To my parents and loved ones.*

SUPERVISED BATTERY CAPACITY ESTIMATION

by

MOINAK PYNE, BS, MS

DISSERTATION

Presented to the Faculty of  
The University of Texas at Dallas  
in Partial Fulfillment  
of the Requirements  
for the Degree of

DOCTOR OF PHILOSOPHY IN  
ELECTRICAL ENGINEERING

THE UNIVERSITY OF TEXAS AT DALLAS

August 2019

## ACKNOWLEDGMENTS

After an intensive period of six years, I am writing this note of thanks as the finishing touch on my dissertation. It has been a period of intense learning for me, not only in the scientific arena, but also on a personal level. Working on this dissertation has had a big impact on my life and I would like to reflect on the people who have supported and helped me throughout this endeavor.

I would first like to thank my advisor, Prof. Stephen Yurkovich, who has supported me immensely and always had an “open-door” policy for me. I would also like to thank him for all the opportunities I was given to conduct research at Ohio State and with individuals such as Benjamin J. Yurkovich, Dr. Ken Dudek and Prof. Giorgio Rizzoni.

In addition, I would like to thank my committee members Prof. Spong, Prof. Fahimi, and Prof. Ruths for their valuable guidance. They have definitely provided me with the tools that I needed to choose the right direction and successfully complete my dissertation.

I would especially like to thank Anandha Natarajan, with whom I extensively collaborated for the hardware implementation of the algorithms I had worked on.

I would also like to thank my parents, Amit Kumar Pyne and Lipika Pyne, and dear friend, Ipsita Konar, for their wise counsel, compassionate ear and patience.

Finally, there are my friends and colleagues. We were not only able to support each other by deliberating over our problems and findings, but also happily by talking about things other than just our work!

Thank you very much, everyone!

May 2019

# SUPERVISED BATTERY CAPACITY ESTIMATION

Moinak Pyne, PhD  
The University of Texas at Dallas, 2019

Supervising Professor: Stephen Yurkovich, Chair

Evaluation of capacity fade in Li-ion batteries in the ballparks of energy research has assumed significant importance in recent times extensively owing to growing demand and need for portable power supplies and electric vehicles. In terms of methodologies and analytics, with the accessibility of data becoming greatly simplified and computational capabilities being exceptionally improved, supervised intelligence has become the *approach-of-choice* for modern day analysts. Using supervised learning approaches, techniques generalized for clustering and regression can be used to systematically extract relevant information from operational data leading to effective prediction of capacity fade. Among the multiple learning tools, neural nets have garnered compelling importance in practical applications due to their flexibility and capabilities of learning in real-time. However, there is a lack of published research on the exercise of data mining and learning on capacity estimation. This investigation aims to study the abilities, drawbacks and applicability of supervised learning approaches in comparison to true capacity fade which is observed in Lithium ion batteries with extensive usage over time. For the effective identification and observation of changes in the battery pack's behavior, the focus will be on quantitatively analyzing the changes through various parameters, referred to as "*features*", and their related conditions. The capacity estimation problem will be primarily handled with the application of neural nets with the capabilities of real-time learning, with the primary focus being the data generated through the daily and regular

use of the packs. As and where imperative, there will be application of synthetically generated data by means of verified data generation techniques. The results of this endeavor will be applied to improved handling of Lithium ion cells and packs under the supervision of a battery management system, using experimental data for training, evaluation and synthetic fabrication of data.

## TABLE OF CONTENTS

ACKNOWLEDGMENTS . . . . .	v
ABSTRACT . . . . .	vi
LIST OF FIGURES . . . . .	xi
LIST OF TABLES . . . . .	xiii
CHAPTER 1 INTRODUCTION . . . . .	1
1.1 Problem Description . . . . .	4
1.2 Lithium ion Chemistry . . . . .	7
1.3 Mathematical Model of a Li-ion Cell . . . . .	9
1.4 Mechanism of Capacity Fade . . . . .	10
1.5 Literature Review . . . . .	14
1.5.1 Battery Capacity Fade Estimation . . . . .	14
1.5.2 Predictive Analytics in Energy Storage . . . . .	15
1.5.3 Synthetic Data . . . . .	16
1.5.4 Battery Management Systems . . . . .	17
CHAPTER 2 EXPERIMENTAL DATA . . . . .	19
2.0.1 Equipment Utilized . . . . .	19
2.0.2 Data Generation . . . . .	20
CHAPTER 3 FEATURE ENGINEERING . . . . .	38
3.1 K-Means Clustering . . . . .	40
3.2 Features Set . . . . .	42
3.3 Feature Characterization . . . . .	47
3.4 Summary . . . . .	49
CHAPTER 4 CAPACITY ESTIMATION USING STRUCTURED TESTS . . . . .	50
4.1 Introduction . . . . .	50
4.2 Data Sets Under Consideration . . . . .	52
4.2.1 Three Cell Pack . . . . .	52
4.2.2 Automotive Cell . . . . .	54
4.3 Neural Networks . . . . .	56

4.3.1	Definition of a Neural Network . . . . .	57
4.3.2	Data processing of a neuron . . . . .	57
4.3.3	Network Topologies . . . . .	59
4.3.4	Training of a Neural Network . . . . .	61
4.3.5	Optimization Algorithms . . . . .	65
4.3.6	Capacity Estimation in Three Cell Pack . . . . .	66
4.3.7	Capacity Estimation in Automotive Grade Battery . . . . .	70
4.4	On-Board Estimation . . . . .	75
4.4.1	Proposed Embedded System . . . . .	75
4.4.2	Algorithm Implementation . . . . .	76
4.4.3	Estimation Results . . . . .	77
4.4.4	Discussion . . . . .	79
4.4.5	Memory Considerations . . . . .	79
4.4.6	Future Scope . . . . .	80
4.5	Summary . . . . .	81
CHAPTER 5	CAPACITY ESTIMATION USING DRIVE CYCLES . . . . .	82
5.1	Introduction . . . . .	82
5.1.1	Feature Generation . . . . .	84
5.2	Validation . . . . .	88
5.3	Capacity Estimation Results . . . . .	88
5.4	Summary . . . . .	92
CHAPTER 6	SYNTHETIC DATA GENERATION . . . . .	93
6.1	Introduction . . . . .	93
6.2	Data Sets Under Consideration . . . . .	96
6.3	Synthetic Data Generation Methodology . . . . .	97
6.3.1	Current Profile Generation . . . . .	98
6.3.2	Voltage Profile Generation . . . . .	100
6.4	Results . . . . .	101
6.5	Summary . . . . .	106

CHAPTER 7 CONCLUSION . . . . .	108
7.1 Data Generation and Testing . . . . .	108
7.2 Characterization and mRPT Based Estimation . . . . .	109
7.3 Drive Cycle Based Estimation . . . . .	110
7.4 Synthetic Generation . . . . .	111
7.5 Final Comments . . . . .	111
REFERENCES . . . . .	113
BIOGRAPHICAL SKETCH . . . . .	119
CURRICULUM VITAE	

## LIST OF FIGURES

1.1	Li-ion battery pack. . . . .	1
1.2	Microgrid structure. . . . .	2
1.3	Battery management system layout. . . . .	3
1.4	Capacity fade determination procedure . . . . .	4
1.5	Overall work flowchart. . . . .	6
1.6	Schematic of the electrochemical process in a Li-ion cell. . . . .	7
1.7	Equivalent circuit representation of a cell. . . . .	9
1.8	Flowchart describing various capacity fade phenomena in Li-ion batteries. . . . .	10
2.1	Equipment used in testing. . . . .	20
2.2	$Q_i$ (characterization) test. . . . .	21
2.3	Battery pack aging timeline. . . . .	22
2.4	$Q_i$ (characterization) test. . . . .	23
2.5	Representative “drive” test I. . . . .	24
2.6	Representative “drive” test II. . . . .	25
2.7	Mini-reference performance test (mRPT). . . . .	26
2.8	Graphical representation of capacity variation at different temperatures. . . . .	28
2.9	Change in OCV voltage with prolonged testing at different temperatures. . . . .	29
2.10	Voltage plots from $Q_i$ characterization tests at 25°C. . . . .	31
2.11	Capacity test performed on the automotive batteries. . . . .	33
2.12	EV drive cycle (Example 1) . . . . .	34
2.13	EV drive cycle (Example 2) . . . . .	35
2.14	Voltage plots from capacity tests on the pack depicted as ‘Cell 1’ in Table 2.3. . . . .	36
2.15	Change in OCV voltage with prolonged testing at different temperatures. . . . .	37
3.1	Behavior of $\Delta$ Temperature. . . . .	43
3.2	Behavior of $\Delta$ Voltage. . . . .	44
3.3	Behavior of $\Delta$ Current. . . . .	44
3.4	Behavior of $\Delta$ rSoC1. . . . .	45
3.5	Behavior of Throughput. . . . .	46

3.6	Behavior of $R_0$ . . . . .	46
4.1	Estimation process flows. . . . .	51
4.2	$Q_i$ (characterization) test. . . . .	53
4.3	Behavior of variables. . . . .	53
4.4	Mini-reference performance test (mRPT). . . . .	54
4.5	Behavior of variables. . . . .	54
4.6	Voltage plots from capacity tests on the pack depicted as ‘Cell 1’ in Table 2.3. . . . .	55
4.7	Capacity test performed on the automotive batteries. . . . .	56
4.8	Behavior of variables. . . . .	56
4.9	Neuron components. . . . .	58
4.10	Feed forward neural network structure. . . . .	60
4.11	Recurrent neural network structure. . . . .	60
4.12	Comparison of experimental (“true”) and predicted SoC using full data from $Q_i$ tests 2, 4, 7, 10. . . . .	68
4.13	Comparison of experimental (“true”) and predicted SoC using mRPT tests 2, 4, 7, 10. . . . .	70
4.14	Behavior of Voltage centroids. . . . .	72
4.15	Behavior of Temperature centroids. . . . .	73
4.16	Behavior of Internal Resistance $R_0$ . . . . .	74
5.1	Comparison of predicted (dashed) and experimental $\Delta V_c$ . . . . .	88
5.2	Comparison of predicted (dashed) and experimental $\Delta T_c$ . . . . .	89
5.3	Comparison of predicted (dashed) and experimental $R_0$ . . . . .	90
5.4	Comparison of predicted (dashed) and experimental SoC. . . . .	91
6.1	Representative “drive” test II. . . . .	96
6.2	Sample Renault Twizy drive profile.. . . . .	97
6.3	Comparison of true and synthetic voltage centroids during mRPT tests 1,5,7,10. . . . .	103
6.4	Comparison of true and synthetic Voltage centroids during mRPT 1,5,7,10. . . . .	104
6.5	Synthetic drive cycle at different capacity values. . . . .	105

## LIST OF TABLES

2.1	Capacity variation at different ambient temperatures (drive cycle 1 used). . . . .	27
2.2	Capacity variation at different ambient temperatures (drive cycle 2 used). . . . .	30
2.3	Capacity variation of 5 LG Chem batteries. . . . .	32
2.4	Capacity variation of 5 LG Chem batteries. . . . .	32
3.1	Feature extraction. . . . .	42
3.2	Sensitivity analysis. . . . .	47
4.1	Capacity estimation results using full $Q_i$ test data. . . . .	69
4.2	Capacity estimation results using mRPT data. . . . .	71
4.3	Capacity estimation results in the SoC range 80% to 40%. . . . .	72
4.4	Capacity estimation results in the SoC range 60% to 20%. . . . .	73
4.5	Capacity estimation results in the SoC range 50% to 10%. . . . .	74
4.6	Capacity estimation results using $Q_i$ data. . . . .	77
4.7	Capacity estimation results using mRPT data. . . . .	78
4.8	Memory Consumption. . . . .	80
5.1	Features . . . . .	86
5.2	Training data . . . . .	86
5.3	Comparison of capacity estimation results using drive data. . . . .	91
6.1	mRPT mean square error comparison . . . . .	104
6.2	Capacity estimation results in the SoC range 50% to 10%. . . . .	106
6.3	Capacity estimation results in the SoC range 50% to 10%. . . . .	106

# CHAPTER 1

## INTRODUCTION

Over a span of four decades, Lithium ion (Li-ion) technology has undergone vast improvements in terms of reliability and safety, and also in terms of cost reduction of materials used (1). As a result, Li-ion (Figure 1.1) based batteries have become the battery of choice from portable electronics to electric vehicles and in stationary applications such as micro-grids (Figure 1.2). Generally speaking, compared to other chemistries, the typical Li-ion cell has high energy density, longer cycle and shelf life, useful open circuit voltage (OCV) characteristics and a low capacity fade rate. Due to their dependability, extensive research has also been conducted in order to understand and quantize the nonlinear behavior of these cells in terms of State-of-Charge (SoC), internal resistance, open circuit voltage, thermal characteristics and capacity fade.

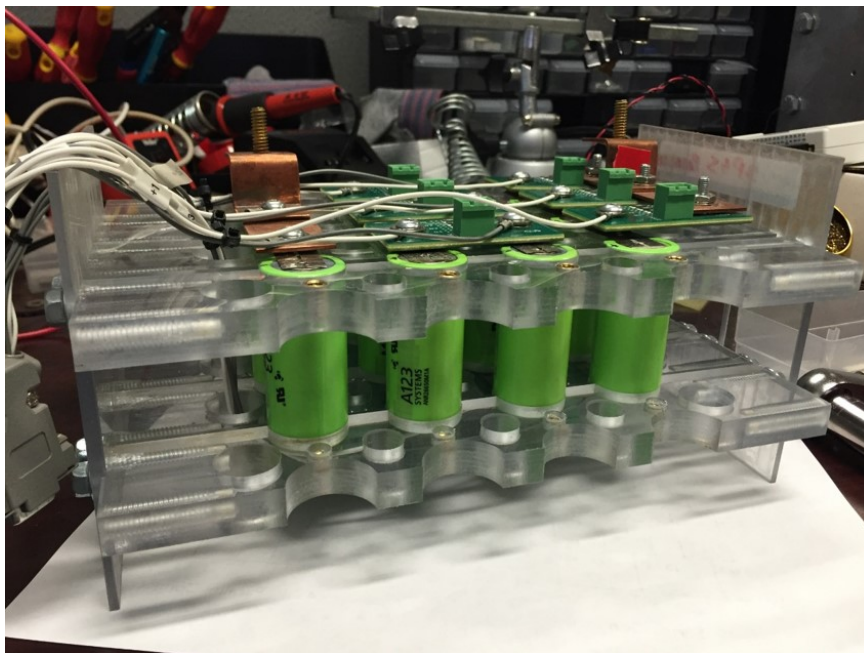


Figure 1.1: Li-ion battery pack.

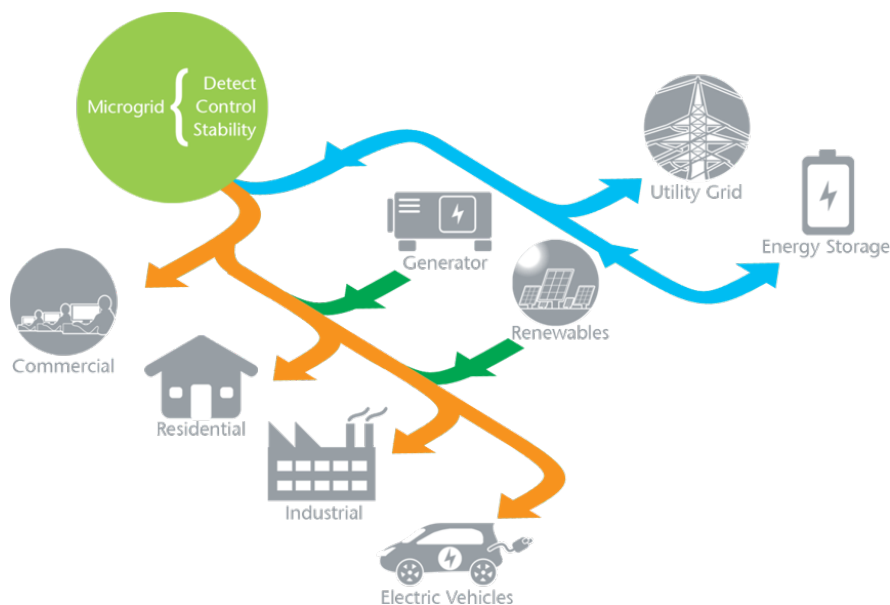


Figure 1.2: Microgrid structure.

Among these broad fields of research in batteries, prediction and estimation of capacity fade is a challenging problem due to the amount of data required over long time intervals, and also due to the complexity of the relationship between the intrinsic characteristics of the battery chemistry. Thus, being able to estimate, monitor, and predict capacity fade in battery packs is highly desirable for battery management systems (BMS) (Figure 1.3) (2) in the general State-of-Health (SoH) assessment. Along these lines, improving battery efficiency is also a significant topic of research for automotive and grid power related industries. Controlling cell performance and safety requires an in-depth understanding of the fundamental cell chemistry, performance characteristics and battery failure modes. The key objectives defining the working of a BMS are battery temperature, SoC, SoH and current and voltage thresholds. Hence, in order for the BMS to maintain the battery pack within permissible limits, capacity estimation during system operation assumes critical importance.

Present day BMSs provide safety and charge management for battery packs based on variations such as changes in internal chemical processes, temperature strain, state of charge

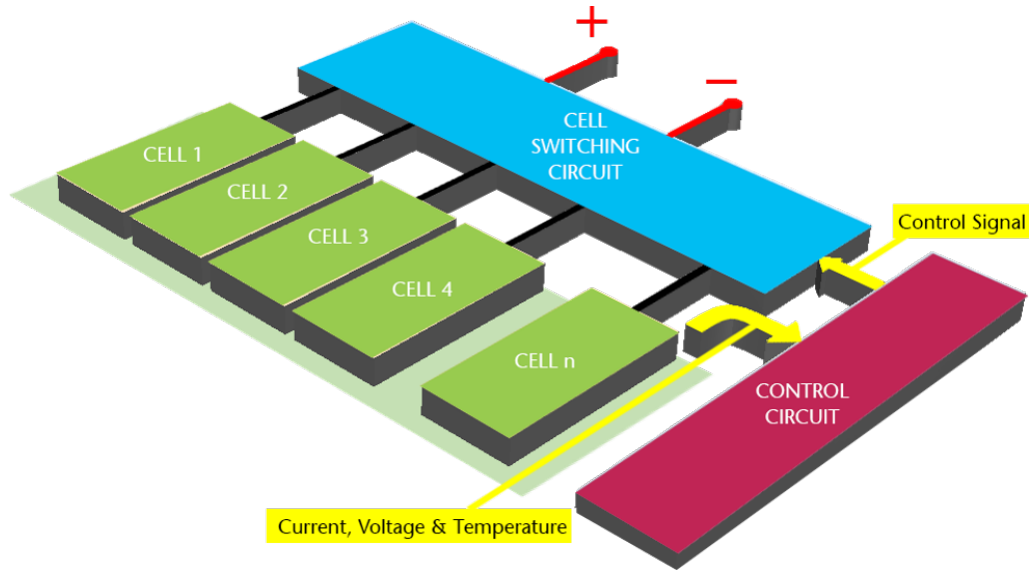


Figure 1.3: Battery management system layout.

variations, or high load variations, in a passive manner. Some go as far as estimating battery life, however typical algorithms are rudimentary at best and require specific capacity tests which can range between six to nine hours in length and also put undue strain on the battery.

Aimed at using a reduced amount of characterization data, while incorporating the impact of various factors affecting the performance of a battery, this research looks to estimate capacity in batteries with limited use of standard capacity tests, while the batteries or packs are employed in their intended applications.

The approach adopted to perform this task is portrayed in Figure 1.4, in which the first step is to extract “features” from the I-V-T data collected during the operation of the battery. The “features” are obtained by partitioning the entire data set into three periods: *charge*, *discharge*, and *rest*. Following this, each event data (I-V-T) are segmented into different events (e.g., a 10C discharge pulse is a separate event from a 20C discharge pulse). These events are fundamentally referred to as the “features”. This is followed by model based prediction of how these features should appear at a particular stage in life of the battery, and

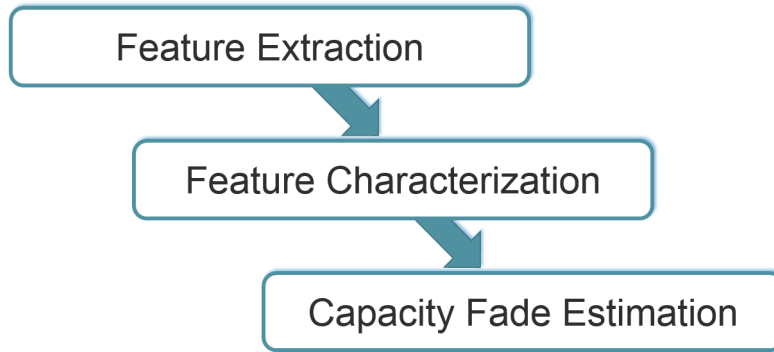


Figure 1.4: Capacity fade determination procedure

finally an optimized iterative approach to compare the extracted and characterized features in order to effectively determine the capacity of the battery.

The key enabling factor in this endeavor of capacity fade estimation is to incorporate a combination of supervised intelligence approaches, which conclusively facilitate the estimation algorithm to learn real-time as the battery is employed and be able to track the capacity variation with usage and time.

### 1.1 Problem Description

The problem investigated in this dissertation is:

*“To establish a standardized, adaptable and sensible estimation principle with the help of supervised learning techniques for the purpose of determining the variation in capacity in individual batteries and packs by fulfilling the objectives of minimizing the memory and data requirements along with the utilization of synthetically generated data and distributed computation”.*

To elaborate on the problem statement, in this research we have attempted to effectively utilize the trends in battery behavior over time and usage to determine the change in its capacity. First step in this process was the development of simplified neural net based

models, which were trained and tested on specific standardized capacity determination tests with the focus being on temperature and voltage as “features”. The second step was to utilize test data which comprised of higher dynamics than a capacity test but was simpler than an operational cycle that is essentially the utilization behavior of a battery when the electric vehicle is used and operated throughout the day. In order to accomplish this, along with the neural nets a clustering approach was adopted to extract and reduce the relevant data to “centroids” and use them as trends in the features in order to predict capacity. The third step involves the development of the overall algorithm which is fundamentally capable of learning from any operational data provided to it and be adept at providing an estimated capacity index which is within definitive tolerable bounds. This was accomplished with two additions, firstly, with a rule based structure which used multiple simplified neural nets that are windowed based on ranges in the features and thus affording us the flexibility of “used-only-when-needed”. Second, internal resistance was considered as an additional feature along with temperature and voltage. The data that was used throughout these first three steps has been generated from a non-automotive pack, which admittedly is not of the quality of an automotive grade battery, but for the purposes of accelerated aging and generation of data, such a battery pack has been preferred.

The penultimate step in this study is to test the robustness and applicability of the developed algorithm on automotive grade data. With the help of The Center for Automotive Research at The Ohio State University, we were granted access to an automotive data set, where the principles developed in estimating capacity as highlighted in the second step in this investigation, were applied and garnered favorable results. Such data sets, being laborious to generate experimentally and further challenging to acquire from commercial establishments, posed a significant hurdle to the completion of this investigation, and thus led to the final step in this endeavor, which is using limited amounts of experimental data along with probabilistic estimations in order to generate large amounts of synthetic data.

In turn, this synthetic data can be used by the algorithm refined in the previous steps to effectively train upon and generate sharpened capacity fade estimation statistics. An overview of the technologies that have been employed in this research endeavor is depicted in Figure 1.5.

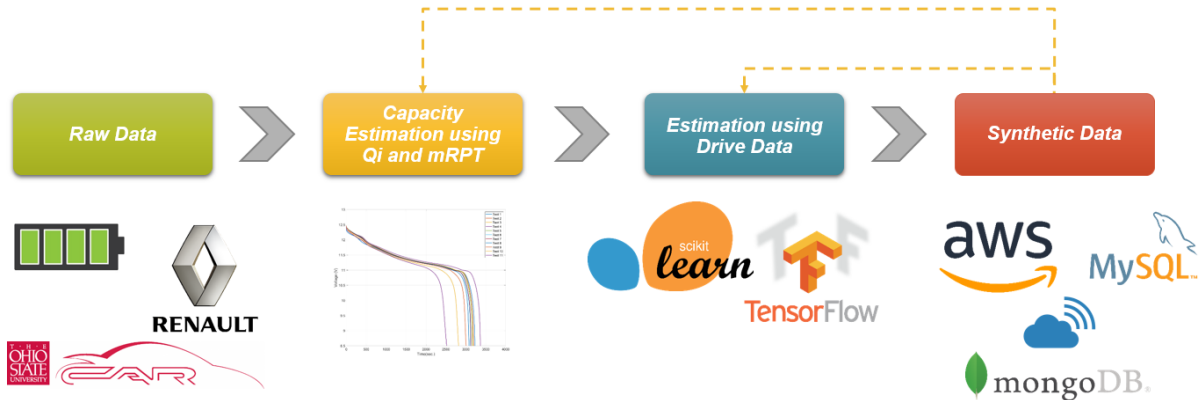


Figure 1.5: Overall work flowchart.

This dissertation is presented in the following order: In the remainder of Chapter 1, we talk about some of the basics of Li-ion batteries such as the chemistry behind its operating principle as well as the root causes of capacity fade in batteries. Chapter 2 talks about the capacity fade in batteries with in-depth description of the testing that has been done in-house to generate data. Chapter 3 depicts the analysis of features in the data that has been generated. The development and estimation of capacity fade using non-automotive grade data is presented in Chapter 4. In Chapter 5, we describe a similar approach to capacity fade but with the use of more dynamic drive-cycle data sets. Chapter 6 presents the finishing touch by characterizing the approach adopted for generating synthetic data and whereby the generated data aids in improved capacity fade estimation. At the end, Chapter 7 provides a culmination of all that has been achieved through this dissertation along with a few specific pointers, which could lead to future generations of this research.

## 1.2 Lithium ion Chemistry

The electro-chemically active material in electrodes inside Li-ion batteries are lithium metal oxide or a lithium metal phosphate for the positive electrode material and a lithiated graphite for the negative electrode material (3).

The active materials in conventional Li-ion cells operate by reversibly incorporating lithium in an intercalation process, a topotactic reaction where lithium ions (guests) are reversibly removed or inserted into a host without a significant structural change to the host. The positive material in a Li-ion cell is a metal oxide, with either a layered or a tunneled structure. The graphite carbon negative materials have a layered structure similar to graphite. Thus the metal oxide, graphite, and other materials act as hosts, reversibly incorporating the lithium ions to form sandwich-like structures Figure 1.6.

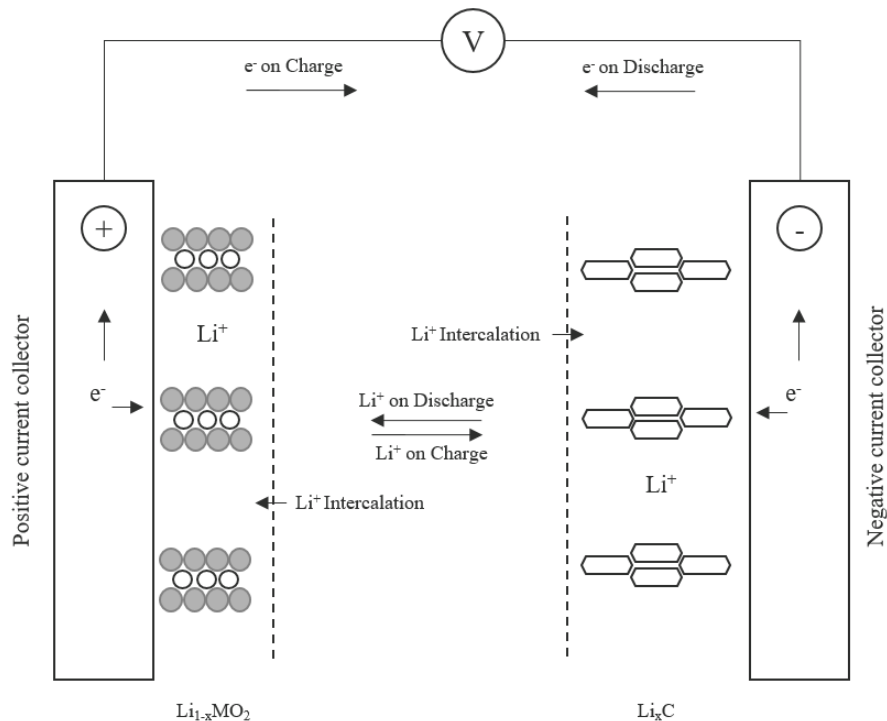
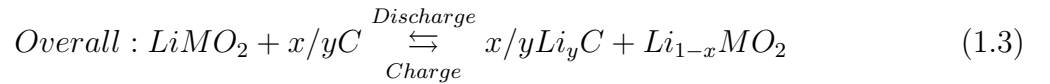
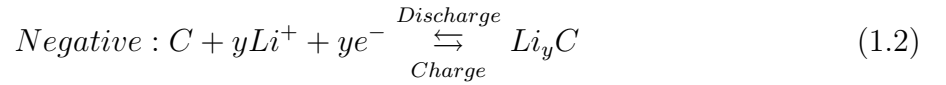
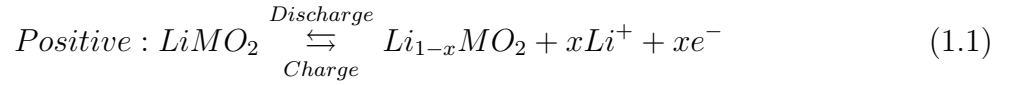


Figure 1.6: Schematic of the electrochemical process in a Li-ion cell.

In the field of Li-ion batteries, the work of alkali metal intercalation of graphite and related carbons, in particular  $Li_xC_6$  ( $0 \leq x \leq 1$ ), is of particular interest. When a Li-ion cell is charged active positive electrode material is oxidised and the active negative electrode material is reduced. In this process lithium ions ( $Li^+$ ) are deintercalated from the positive material and intercalated into the negative material, as illustrated in Equations 1.1, 1.2 and 1.3. In this scheme,  $LiMO_2$  represents the metal oxide positive material, such as  $LiCoO_2$ , and  $C$  represents the carbonaceous negative material, such as graphite (4) (5). That is,



where  $x$  and  $y$  are selected based on the molar capacities of the electrode materials for lithium.

Normally  $x$  is about 0.5 and  $y$  is about 0.16, therefore  $x/y$  about 3. The reverse occurs on discharge. The charge-discharge process is further depicted in Figure 1.6. It is to be noted that during discharge, due to the potential gradient between the positive and negative electrodes, the electrons rearrange themselves to get rid of this difference (high energy state), hence the electrons travel from the negative electrode to the positive electrode through the external load (low energy state). During charge, electrons flow from an external power source and the reaction happens in reverse with the positive and negative electrodes being restored to their original states. Hence, the main factors which cause electron flow are firstly, the requirement for the system to be at a low energy state, and second, the existence of a concentration gradient (6).

### 1.3 Mathematical Model of a Li-ion Cell

The convention of using AC impedance as a diagnostic tool for electrochemical systems was adopted in the 1970s and hence evolved the representation of a battery as a circuit consisting of standard electrical components, such as resistors and capacitors as depicted in Figure 1.7 (3).

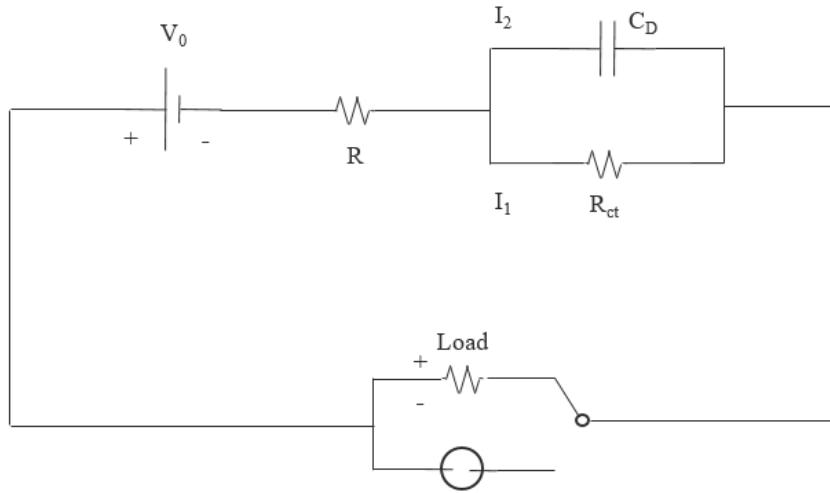


Figure 1.7: Equivalent circuit representation of a cell.

The behavior of the battery can be explained in terms of the values for the circuit elements in Figure 1.7. The voltage source  $V_0$  explains the open circuit voltage (OCV) of the battery, which essentially represents the thermodynamic limitations on the cell's performance. The resistance  $R$  refers to the ohmic drop inside the battery that arises from current passing through the electrolyte, contact resistances and the like.  $R_{ct}$  and  $C_D$  together represent the charge transport through the interface, where  $R_{ct}$  refers to the Faradaic part of the charge transfer resistance and  $C_D$  is a pseudocapacitance term often used to depict mass transfer limitations (7).

## 1.4 Mechanism of Capacity Fade

The capacity of a Li-ion battery reduces with repeated cycling over prolonged usage. This fade is caused by several mechanisms which are due to or caused by undesirable side reactions that occur in these batteries. A flowchart describing the various processes leading to capacity fade is highlighted in Figure 1.8 (8).

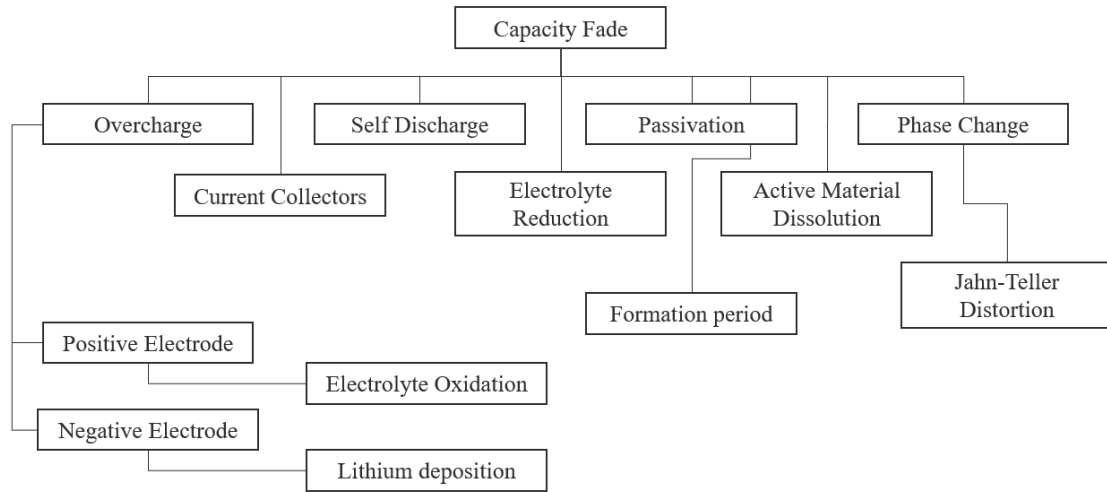


Figure 1.8: Flowchart describing various capacity fade phenomena in Li-ion batteries.

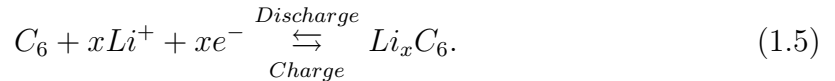
**Formation Cycles:** Li-ion batteries are characterized by a sharp decay initially during the first few cyclic operations. This is known as *formation period*, during which the cells get conditioned before being operational. It is generally required for this initial capacity drop after the formation period to be insignificant compared to total cell capacity, after which the the charge-discharge cycles are almost 100% efficient. The reason behind this sharp initial decay is the formation of Solid Electrolyte Interface (SEI) layer on the negative electrode, which is caused by the electrochemical decomposition of the electrolyte (9). The reason this layer is harmful is that it does not conduct electrons and is almost impenetrable to the electrolyte molecules.

**Overcharge Phenomena:** Li-ion batteries have poor overcharge resistance and as a result, capacity losses have been observed in all types of Li-ion cells during overcharge conditions. Overcharge losses can be classified into three categories:

- Overcharge of negative electrode: During overcharge, metallic lithium might get deposited on the coke or graphite based negative electrode surface due the primary side reaction. This reaction is common in cells with excess cyclable lithium either due to higher than required initial mass ratio or lower than expected lithium losses during the formation phase. The deposit of lithium covers the active surface area of the negative electrode causing loss of cyclable lithium and consumption of electrolyte due to the highly reactive nature of metallic lithium (10). The primary side reaction occurring during overcharge is,



and the intercalation-deintercalation reaction on the negative electrode is,



Also, formation of lithium metal is also a safety hazard owing to its extreme reactivity with liquid solvents. Li-ion deposition is more of a concern with graphite carbon electrodes than with coke electrodes because of the lower average open-circuit potential of graphite. For this reason, mass ratios of cells using graphite electrodes are preferably kept to a smaller number than the optimum to provide a buffer against lithium deposition (11).

- Overcharge of positive electrode: Overcharging of the positive electrodes leads to a wide array of reactions depending on the system chemistry. As was the case with the negative electrode, the extent to which overcharging is expected at the positive electrode depends on the system's capacity balance. For cells with a very low mass

ratio, the positive electrode is stressed further during charging and hence overcharging becomes a possibility. Overcharging the positive electrode leads to capacity loss due to inert material formation (e.g.,  $Co_3O_4$ ) or solvent oxidation due to the high positive electrode potential. Apart from these, formation of electrochemically inactive electrode decomposition products leads to a capacity imbalance between the electrodes. Furthermore, thermal overheating of the positive electrode can lead to oxygen loss from the metal oxide lattice and this oxygen can cause an increase in the pressure inside the cell, thus forming a potential safety concern (12).

- **Overcharge/high voltage electrolyte oxidation process:** In Li-ion cells, the electrolytes are a combination of solvents and one or more lithium salts. The more popular electrolytes use a mixture of linear and cyclic carbonates such as propylene carbonate, ethylene carbonate, dimethyl carbonate, diethyl carbonate, and ethyl methyl carbonate and salts such as  $LiPF_6$ ,  $LiBF_4$ ,  $LiAsF_6$ , and  $LiClO_4$ . High voltage positive electrodes used in Li-ion cells create a rigorous requirement for electrolyte stability and purity. Hence the choice of electrolyte is limited as the maximum voltage of the cell is governed by the decomposition potential of the electrolyte. Present day electrolytes decompose at a high voltages ( $>4.5$  V) and thus form insoluble products such as ( $Li_2CO_3$ , etc.), which block the pores of the electrodes and cause generation of gas. Such effects can cause both capacity loss upon further cycling and can be a cause of extreme safety hazard (8; 13).

**Electrolyte decomposition (reduction) processes:** Electrolyte reduction can be a hazard to the battery capacity as well as the cycle life of the cell by decomposing the salt and solvents, and thus compromising the safety of the system by generating gaseous products. Minimizing electrolyte reduction and the capacity losses incurred due to the reduction processes is a significant requirement for enhancing cycle life and high-temperature performance of Li-ion batteries (8; 14).

**Self-discharge processes:** Self-discharge is the phenomenon by which there is a drop in the cell voltage under open circuit conditions that occur spontaneously while the batteries are left standing. Li-ion cells undergo self-discharge, which although less significant than other battery chemistries, is still relatively rapid. The degree of self discharge is dependent on factors such as cathode and cell preparation, nature and purity of the electrolyte, temperature and time of storage. Self-discharge is more common in oxidized  $LiMn_2O_4$ ,  $LiCoO_2$  and  $LiNiO_2$  electrodes (15).

**Interfacial film formation:** A passive film gets formed at the negative electrode/electrolyte interface due to irreversible side reactions that occur between lithium ions and/or the solvent and electrode surface. These side reactions ideally form a stable and protective film of the surface of the negative electrode allowing the electrode to operate without further reaction. The initial loss in lithium ions in forming this film causes the capacity of the balance between the two electrodes to get altered. This sometimes results in diminished utilization and hence a decreased specific energy for the cell (16).

**Current collectors:** Aluminium and copper are the most commonly used current collectors for the positive and negative electrodes in a cell, respectively. Apart from these metals, nickel and stainless steel also have been employed as current collectors. The main concerns with current collectors are passive film formation, adhesion, localized corrosion such as pitting and general corrosion. These developments increase the internal impedance of the cell during cycling and can lead to capacity and rate capability losses (8; 17).

**Positive electrode dissolution:** The phenomena of positive electrode dissolution are both electrode and electrolyte specific. The factors affecting positive electrode dissolution are structural defects in the positive active material, high charging potentials and the carbon content in the composite positive electrode. Oxygen defects in the  $LiMn_2O_4$  and  $LiNiO_2$  structures tend to weaken the forces bonding transition metals and oxygen, resulting in  $Mn$  and  $Ni$  metal dissolution (3; 8).

**Phase changes in insertion electrodes:** The basic mechanism of phase changes is that large changes in lattice parameters lead to fractures of the particles and loss of contact from the electrode matrix. The three most popular metal oxide insertion compounds used in Li-ion batteries are fairly robust to phase changes or lattice expansions and show high reversibility and cycle life. However the constant development for higher capacity materials makes phase and structural changes difficult to avoid and require in-depth studies. The phase changes occurring in Li-ion batteries can be classified into two categories: first, in those that occur during normal insertion-deinsertion of lithium, and others that occur when the positive electrode is overcharged or overdischarged (for example the Jahn-Teller distortion in the overdischarge of  $Li_yMn_2O_4$  above  $y = 1$ ) (8).

## 1.5 Literature Review

This section presents a short informational review on the general field of capacity fade in batteries, use of supervised learning in battery based systems, possibilities of using synthetic battery operational data and the contemporary scenario of algorithms in Battery Management Systems.

### 1.5.1 Battery Capacity Fade Estimation

The challenge of characterizing capacity fade has to do with varying degrees of dependency on factors such as ambient temperature, C-rate, rest times, SoC levels, and duration of charge and discharge pulses along with shelf life or storage time of the batteries. More and more researchers are investigating the general SoH problem and, in particular, estimation of capacity fade, using approaches such as equivalent circuits (18), (19), empirical models (20), chemical models (21) and statistical evaluations (22). But one issue associated with such approaches is the effort required in identification of a large number of parameters, and hence cumbersome computations involving large volumes of data. Regrettably, the cost and

feasibility of performing purposeful aging experiments on high grade batteries limit such experiments; as a result, only limited volumes of data may be available and accessible. Along with internal and logistical considerations, time plays a central and pivotal agent in the experimentation with such batteries owing to the high number of cycles required for automotive grade batteries to show signs of deterioration in capacity. Unfortunately, there are no simple, “default” models for immediate capacity fade calculation.

### 1.5.2 Predictive Analytics in Energy Storage

Predictive analytics encompasses a variety of statistical techniques from predictive modeling, supervised and unsupervised intelligence, and data mining in the domain of battery technology.

Supervised learning as a data-driven approach to capacity fade estimation has been gaining interest in recent times and a number of techniques have been explored. Support Vector Machines which are characterized by flexible planes for dividing data sets have been explored in (23) and (24). Clustering has further been examined with principal component analysis in (25), and neural networks in (26) and (27). Other approaches in conjunction with learning techniques have also been explored, such as gray system theory in (28) and incremental capacity analysis with support vectors in (29). Rather disappointingly, two issues stick out. First, a major portion of the work that has appeared on capacity fade estimation is dependent on running characterization tests which discharge the battery from 100% to 0% SOC with C-rates ranging from 1C to 0.3C. Under controlled laboratory conditions, to determine the capacities of automotive grade battery packs, tests such as C/3 CC-CV, C/3 CC or 1C CC-CV tests are employed. Thus, challenges are the amount of testing time required and the amount of data to be generated, given that such tests can consume several hours each. Moreover, under normal operating conditions in vehicle operation, expecting an electric vehicle to remain stationary and inoperable for several hours at a time is not

only undesirable but also energy intensive. For such a test the entire charge available in the battery would need to be drained, followed by a full recharge. Another concern is the effect of temperature on capacity fade, the measurement of which is tedious; such studies have received very little attention in the literature. Keeping these drawbacks in mind, a data-driven approach which can extract relevant information from a limited data supply is the direction adopted in this research.

### 1.5.3 Synthetic Data

Among all the complexities of capacity fade in batteries, the most significant is undeniably the time and effort involved in acquiring data.

The variation in capacity of batteries that consists of multiple factors have been discussed comprehensively in (30), (31), (32). Among all the complexities of capacity fade in batteries, the most significant factor evidently turns out to be the time and effort required in effectively aging the batteries with the help of controlled experimentation such that the batteries not only lose their capacity retention capability, but also have a gradual decline in order to address the reliability concerns and to enable higher levels of efficiency in the energy storage systems. Also, by segregating and effectively incorporating all the features that display a change with the capacity fade, BMSs can be operated under flexible operation schedules to accommodate the variability introduced from the power requirements of modern EVs and stationary loads. However, these analyses are based on historical data collections from batteries tested at various facilities and hence only databases with a limited number of measurements are available. The novel idea of using a limited experimental data set to generate iterative synthetic drive cycles and study the technical performance of BMSs has been explored in (33). The concept of using synthetic data has been explored for used renewable energy systems (34) and health-care systems (35), quality data being vital to both fields.

In the domain of energy systems, synthetic data has found applications in modeling as well as large scale and domestic power consumption simulations. In (36) physics based modeling of batteries was presented, where computational challenges are tackled with particle Markov chain Monte Carlo methods, with an implementation specifically designed for the non-Markovian setting. In large scale power systems (37), synthetic PV and load demands are used to validate the control algorithms. In (38), a prototype demand-side load controller is validated using synthetically generated load data. It is evident in these examples that use of synthetic data as a validation tool is a well established practice in the research community.

Keeping the need for validation of our estimations systems on a diverse set of test data, and based of trends in the literature, generating synthetic battery data using Markov chains (31) based on actual experimental data is the method adopted for this work.

#### **1.5.4 Battery Management Systems**

The determination of control actions in a BMS is entirely based on how accurate the estimation capabilities are. Principally, a battery is an electrochemical unit, which is made up of two electrodes immersed in an ionically-conductive electrolyte. The electrolyte acts as a non conductor for electrons between the electrodes. With the introduction of an external circuit, the electrons are allowed to flow through the external circuit from the negative electrode to the positive electrode facilitating the oxidation-reduction reactions. Paradoxically, in this uncomplicated procedure, many complicated reactions and processes determine the battery's macroscopic behavior (specifically the current to voltage response). These processes include diffusion, charge transfer reaction, double layer capacitance and so on. Some of these processes are structurally distributed and thus require coupled partial differential equations to describe accurately (3). Despite partial differential equations accurately capturing the true nature of reactions going on inside the battery, they are not conducive to solving on-board or cloud-connected estimation problems owing to their computational complexities.

Traditionally, the estimation problems in a BMS encompassing SoC, terminal voltage and SoH has been looked at from an equivalent circuit point-of-view. Under small current assumption, the equivalent circuit approach can approximate the battery's input-output behavior. While equivalent circuits using only ideal resistors and capacitors can be used to approximate the battery behavior in a limited frequency range, these models are usually local to the operating conditions (temperature, SoC, and input current). For compensating for this drawback, attempts have been made to represent the circuit parameter as functions of operating conditions to arrive at better estimations (39). Given the identified parameter values in the differential equations represented by the equivalent circuits, a number of different methods have been shown to give good results, particularly Extended Kalman Filters (40) and Linear Parameter Varying methods (41). Two drawbacks with these methods are that they require substantial volumes of specific tests to be performed for identification and computational complexity. An approach gaining relevance in recent times has been the use of machine learning. While a number of publications have shown promise with the use of Fuzzy Logic (42) and Neural Networks (27), there is a lack of published results on using lesser volumes of data and extraction of parameters while the battery or battery pack is used in its intended application. This is an area where supervised learning may be able to provide an improvement.

## CHAPTER 2

### EXPERIMENTAL DATA<sup>1</sup>

When it comes to estimation of metrics related to batteries, the primary limiting factor has been the availability of accurate data with suitable variations in a wide range of parameters. This is a multi-faceted problem where, generation of effective data is a tedious process as the time and effort required in generating changes in parameters in batteries is substantial. On the other hand, accessing generated reliable test data from third parties can be a logistical ordeal. On this note, researchers in the domain of energy storage are left with a limited number of choices as to how to solve this dilemma. The path that was adopted by our research group was firstly, to perform in-house data generation by operating cyclic testing on batteries which were similar in chemistry to automotive grade batteries but where proven to show performance variations at a much accelerated pace. Second, keep the testing on-going in batches while the initially generated batches of data are used to develop preliminary models to serve as a base-line and use the results of these models as a convincing factor in order to obtain automotive grade data from specialized testing facilities. Finally, a crucial step is to validate the previous models on the newly obtained data.

In order to accomplish the in-house generation of data, customized and sophisticated laboratory equipment were utilized and the number of representative cyclic profiles were used to run the tests on the batteries at multiple temperature points. The details of these two broad points are elaborated upon in the following sections.

#### **2.0.1 Equipment Utilized**

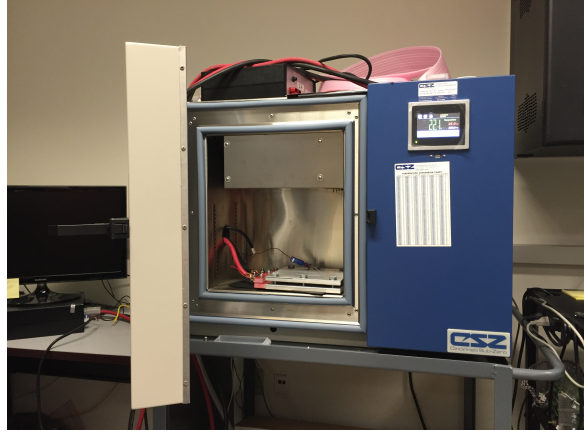
The primary equipment employed in the data generation endeavors were a thermal chamber and a custom designed cycling station, as shown in Figure 2.1.

---

<sup>1</sup>©2017 IEEE. Portions Adopted, with permission, from M. Pyne, B. J. Yurkovich, S. Yurkovich, “Capacity Fade Estimation Using Supervised Learning,” IEEE Conference on Control Technology and Applications (CCTA), August 2017.



(a) Cycling station.



(b) Thermal chamber.

Figure 2.1: Equipment used in testing.

The cycling station is managed by an HP server running a Red Hat Linux operating system that is used to run special purpose software for control and data acquisition. The station consists of two TDK Lambda GEN8-400 power supplies capable of a maximum voltage of 16 volts and 400 amps for charging; a Kepco EL 3k-25-400DG programmable load with rated power of 3000 watts, rated voltage of 25 volts and rated maximum current of 400 amps, for discharging; a T-type thermocouple for temperature sensing; and a NI USB-6008 data acquisition device that is used in sampling voltage, current and temperature. The cycler software evaluates the data and plots the real time sampling result. The thermal chamber is a Cincinnati Sub-Zero (CSZ), MicroClimate Benchtop Test Chamber, which is used to maintain isothermal ambient temperature conditions for modules and packs under testing (39).

## 2.0.2 Data Generation

The design of commercially available battery packs are such that they are able to withstand prolonged stress levels in terms of high C-rates. Moreover, Li-ion batteries are characterized

by high cycle-life which enables them to maintain capacity for prolonged periods of time. In order to observe degradation of capacity of such batteries, a very large number of test cycles is needed. For this study, experimental work was carried out in the Energy Storage Systems Laboratory, UT Dallas (30), utilizing the special purpose software and high accuracy instrumentation for battery data generation along with a thermal chamber for control over ambient temperatures. Custom profiles enable automated and rapid charge-discharge cycles on a pack, and also provide characterization tests after regular intervals of time. Manufactured by Turnigy Power Systems, the battery pack considered in this preliminary study consists of three Li-ion cells in series and is rated at 11.4 V/2200 mAh (Figure 2.2).



Figure 2.2:  $Q_i$  (characterization) test.

For battery pack cycling and data gathering, three test profiles have been developed: (i) a characterization test, (ii) a representative charge-discharge profile “drive” test, and (iii) a mini-reference performance test (henceforth, mRPT). Collection of data consists of recording relevant current, voltage and temperature signals for these test profiles at different temperatures.

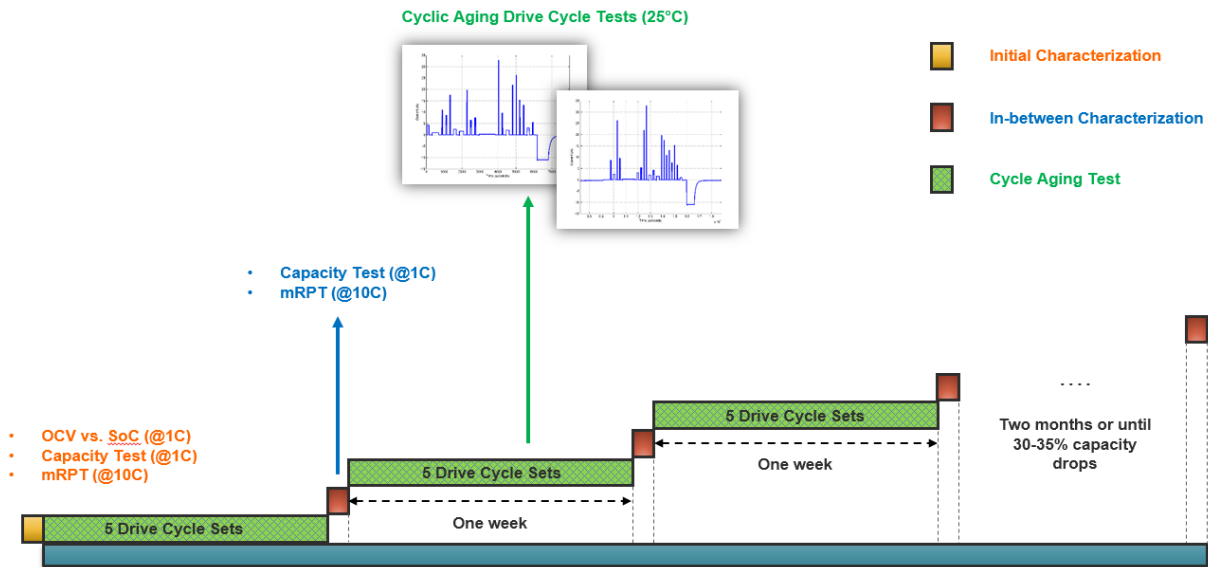


Figure 2.3: Battery pack aging timeline.

The time-line followed for the cycling and subsequent aging of the aforementioned battery is shown in Figure 2.3. The first step in the testing sequence is to characterize the battery pack as well as determine its Beginning-of-life (B-o-L) capacity ( $Q_i$  test) along with an mRPT. This is followed by five drive cycle sets. After these drive cycle sets, a  $Q_i$  and an mRPT are held at this point in order to record the change in capacity as the battery is used. This cycle of five drive cycle sets followed by a  $Q_i$  and mRPT are repeated until the battery loses about 30 to 35% of its B-o-L capacity.

## Test Profiles

For a typical cycle in this work, the “characterization” test is executed first, followed by ten cycles of the drive test, and finally followed by the mRPT. This sequence is repeated until the capacity of the battery is close to 60% of the rated capacity. The typical characterization test for capacity is referred to herein as the  $Q_i$  test for an initial  $Q_0$  (fresh pack) and subsequent capacity characterizations ( $i = 1, 2, \dots$ ) as the pack ages. The  $Q_i$  test has two parts: first,

a discharge from 100% to 0% SOC at 1C in CCCV mode, and second is a charge of 0% to 100% at 1C in CCCV mode.

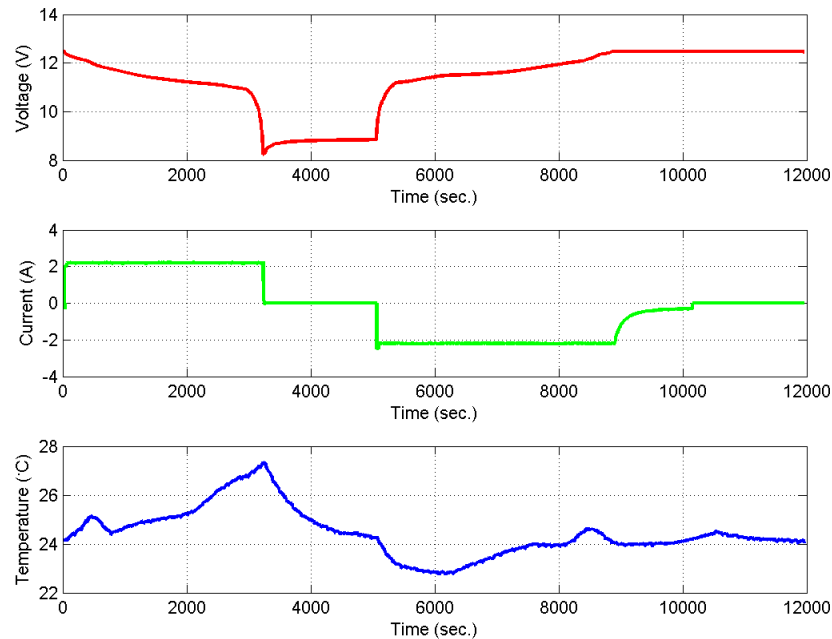


Figure 2.4:  $Q_i$  (characterization) test.

The capacity of the battery is obtained by summing the total charge removed during the complete discharge pulse. The  $Q_i$  test is a standardized true test to determine the actual capacity of a battery at any phase in its lifetime; Figure 2.4 illustrates a typical  $Q_i$  test. The capacity obtained from this test acts as the benchmark for true capacity for results in the sequel.

The main cyclic aging is caused by the implementation of the drive test. In our data generation endeavors, we have used two drive cycles; the first is a fairly simple one shown in Figure 2.5. The discharge portion of this test consists of three pulses, two at 10C and one at 20C. For the charge portion, there are again three pulses, two at 1C and one at 5C.

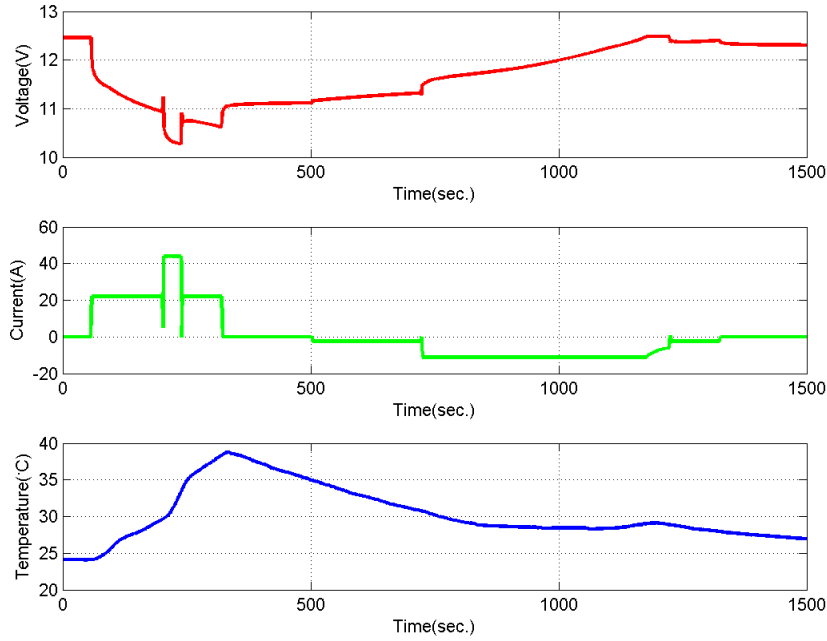


Figure 2.5: Representative “drive” test I.

A representation of the second drive cycle is highlighted in Figure 2.6, which consists of multiple pulses with C-rates varying between 0.2C and 15C at twenty different SoC points in the complete range of 0 to 100% SoC.

In the initial evaluations that were carried out, the  $Q_i$ , the mRPT and the first drive profile has been utilized in order to perform estimation of changes in the capacity of the pack. The reasoning for the use of the first drive cycle is due to simpler dynamics as compared to the second drive cycle.

The experimentation with the second, significantly more complicated, drive cycle, was a result of studying and finding key insights with the implementation of the first drive cycle as well as an in-depth look at common driving patterns EVs face in the real world. Some of the major considerations in designing the second drive cycle were:

1. The majority of the discharge pulses that battery packs in EVs experience are in the lower C-rate ranges.

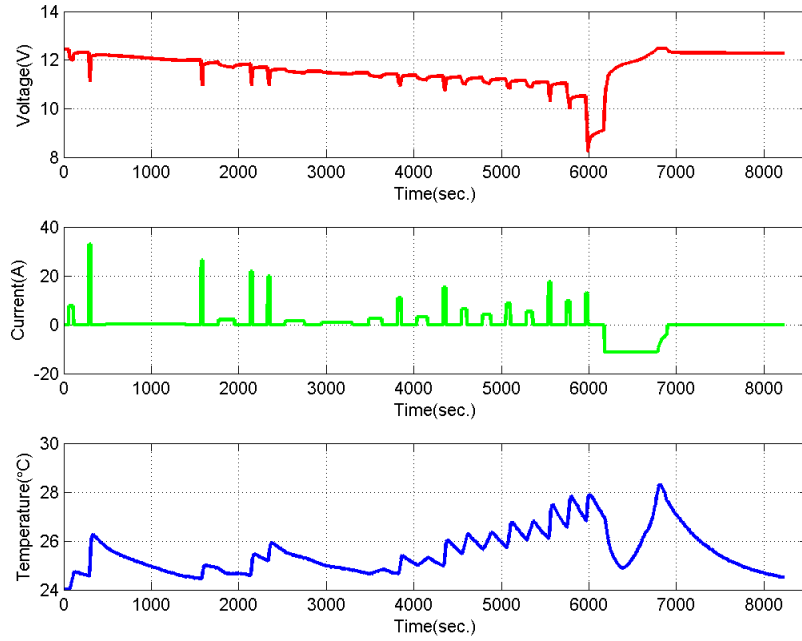


Figure 2.6: Representative “drive” test II.

2. High C-rate pulses can be relatively low in occurrence, but if present, they can be prolonged once, and cause higher degradation rates.
3. The repeated occurrence of high C-rate discharge pulses at particular SoC ranges can cause accelerated capacity fade.
4. Because EV battery packs face constant discharge pulses, whereas charge pulses usually occur with charging stations using a single charge pulse, which charges the battery, our focus has been towards studying the variations in discharge pulses.
5. The rest time after each pulse affects the behavior of the batteries during the next pulse, hence a variable range of rest times needs consideration.

Thus, keeping the above stated observations in mind, these drive cycle tests consist of multiple discharge pulses and a fixed as well as variable rest time between each pulse, and

were designed to mimic what a battery pack in an EV would experience under normal operation on the road (recognizing, of course, that the pack we are using is not automotive-grade in quality).

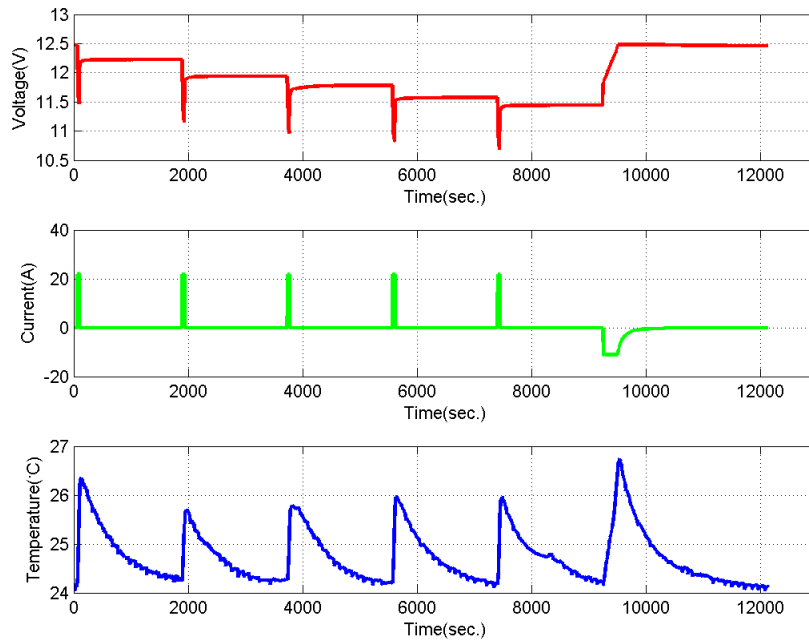


Figure 2.7: Mini-reference performance test (mRPT).

Our third test, the mRPT, was developed to provide data at intervals between the  $Q_i$  tests; such tests require less data and time, and in addition require 50% less depth of discharge than a typical  $Q_i$  characterization test. The mRPT consists of five 10C pulses which discharge the battery from 100% to 50% with a rest period of thirty minutes after each pulse. After the final rest period (fifth pulse), the charge pulse is initiated and charges the battery pack up to 100% in one pulse. A typical mRPT profile is shown in Figure 2.7.

## Observations

### 1. Packs Tested using Drive Cycle 1

Due to the repeated charging and discharging cycles being applied to the pack, aging occurs in an accelerated rate which results in a gradual decrease in the battery capacity. For our purposes, the threshold for end of life is considered to be approximately 60% of the pack's beginning of life capacity (as determined from the  $Q_0$  test).

The capacity fade patterns of a couple of battery packs that have been tested at ambient temperatures 50°C and 25°C, respectively, are summarized in Table 2.1. These two packs have been subjected to drive cycle 1.

Table 2.1: Capacity variation at different ambient temperatures (drive cycle 1 used).

Test No.	50°C	25°C
1	2.015	1.954
2	1.838	2.004
3	1.816	2.008
4	1.810	1.998
5	1.782	2.001
6	1.718	1.970
7	1.472	1.963
8	1.258	1.971
9	1.022	1.839
10	0.912	1.540
11	0.755	0.788

The graphical representation of the change in capacity over time for the two packs is highlighted in Figure 2.8, where it is evident that the capacity of the pack tested at 25°C loses its capacity rapidly only after  $Q_9$ , whereas the pack tested at 50°C starts losing its capacity rapidly after  $Q_6$ . This brings to our focus a couple of aspects, first, the well accepted fact that at a higher ambient temperature, the capacity fade patterns of a Li-ion battery shows an accelerated nature, and second, in the estimation of any parameter, temperature plays a significant role.

Outcome of such capacity fade patterns are also observed in the OCV behavior of the packs as depicted in Figure 2.9, in which, for both, the pack tested at 25°C and at 50°C, the

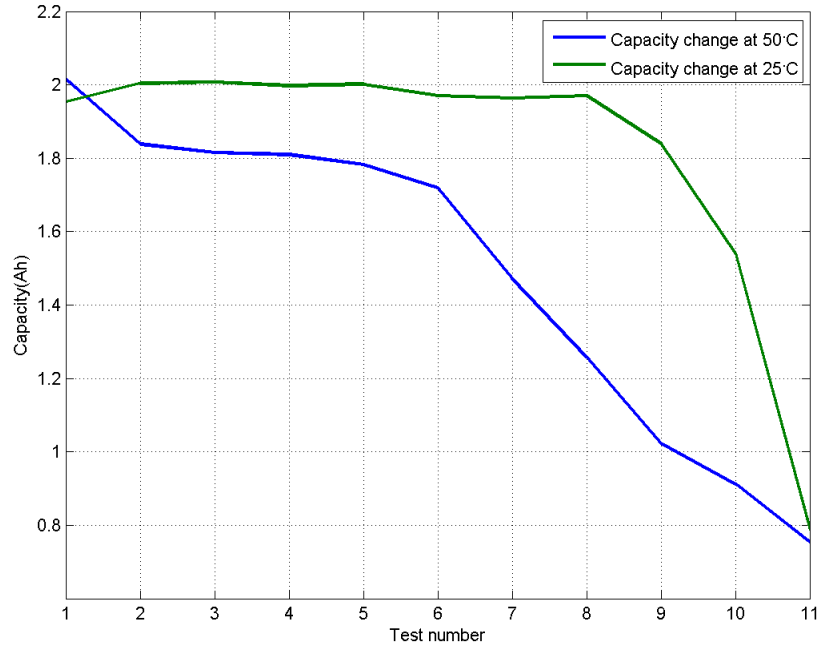
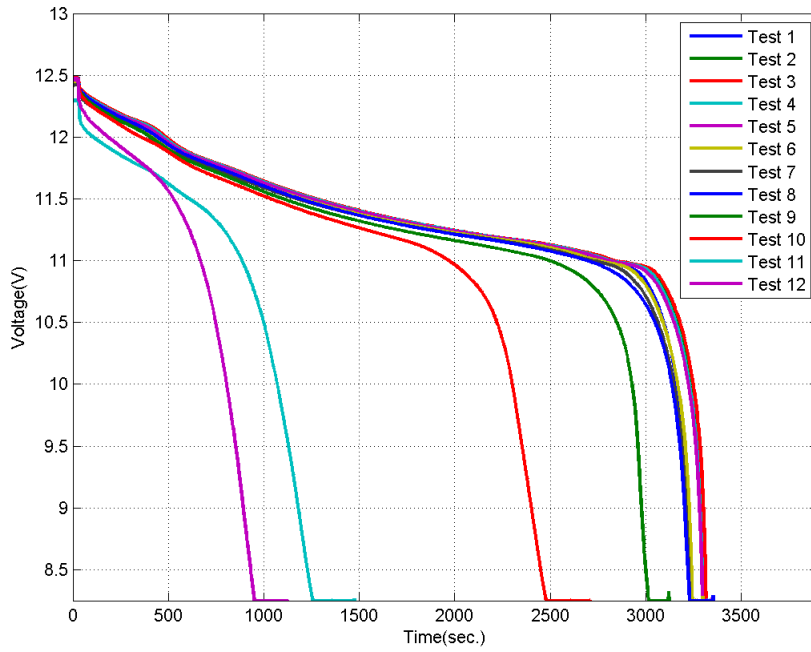


Figure 2.8: Graphical representation of capacity variation at different temperatures.

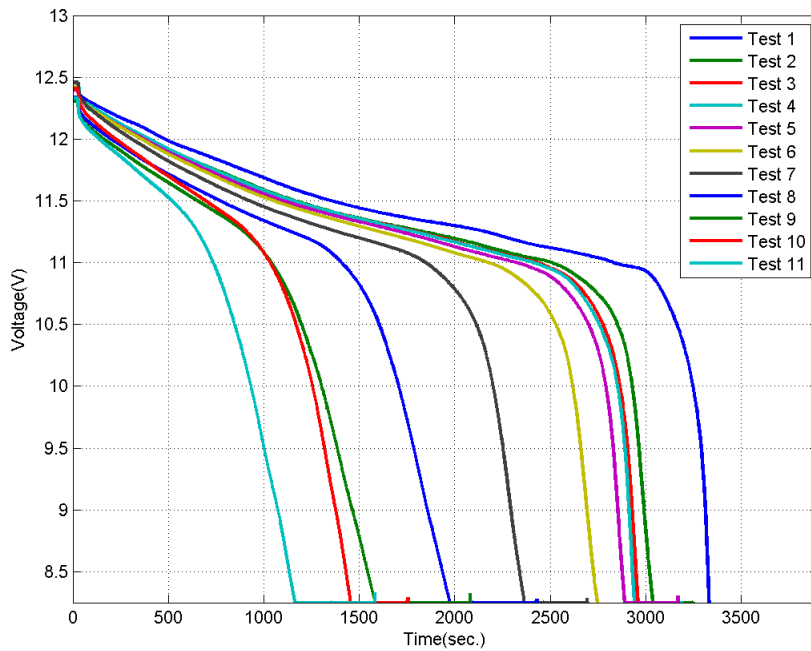
1C single pulse discharge from 100% to 0% SoC during the  $Q_i$  tests starts taking progressively lesser time than 3600 seconds.

These initial data sets have been used for preliminary development of algorithms. The details will be highlighted in subsequent chapters, but to be specific the data generated using the  $Q_i$  and mRPT tests have been used in developing a feature based capacity fade estimation algorithm which uses voltage and temperature data in order to predict trends in the loss of capacity of the pack. The data generated from the implementation of drive cycle 1 has been used to develop a “feature generator”, which predicts the feature behavior of mRPT tests after the battery has been trained on the drive cycle data. After the successful implementation of these algorithms, the subsequent drive cycle 2 was designed in order to address the short comings and also for further algorithmic development.

## 2. Pack Tested using Drive Cycle 2



(a) OCV from  $Q_i$  tests performed for the battery pack tested at 25°C.



(b) OCV from  $Q_i$  tests performed for the battery pack tested at 50°C.

Figure 2.9: Change in OCV voltage with prolonged testing at different temperatures.

Similar to the previous testing, another three cell pack has been subjected to cyclic charge-discharge testing in an environmental chamber at 25°C, with the difference being the use of a drive cycle 2 in place of drive Cycle 1. The test procedure consisted of exactly the same approach where three profiles were used, (i) a characterization profile ( $Q_i$ ,  $i$  indicating the number of the test) intended for determining the true capacity of the pack, (ii) a mini-reference performance test (mRPT), which is a scaled version of a stand RPT or HPPC test, and (iii) a representative operational drive profile consisting of multiple discharge profiles intended to replicate the discharge patterns that an EV experiences while in real-world operation. The details of the first two tests have been discussed comprehensively in the previous sections. The drive profile, as pointed out earlier, is different. First, this profile includes only discharge pulses ranging from 0.2 C to 15 C in the complete 100 to 0% SoC range, and second, a large number of discharge pulses of varying magnitude and duration have been used. The characteristics of the drive test can be seen in Figure 2.6.

The capacity fade pattern of the pack at 25°C is summarized in Table 2.2 and in Figure 2.10.

Table 2.2: Capacity variation at different ambient temperatures (drive cycle 2 used).

Test No.	Capacity (Ah)
1	1.976
2	1.953
3	1.943
4	2.057
5	1.938
6	1.906
7	1.913
8	1.895
9	1.857
10	1.754
11	1.576

Based on the capacity fade patterns shown in Table 2.1, it can be observed that there is no noticeable loss in capacity until the 9<sup>th</sup> capacity test. Based on this observation, the data

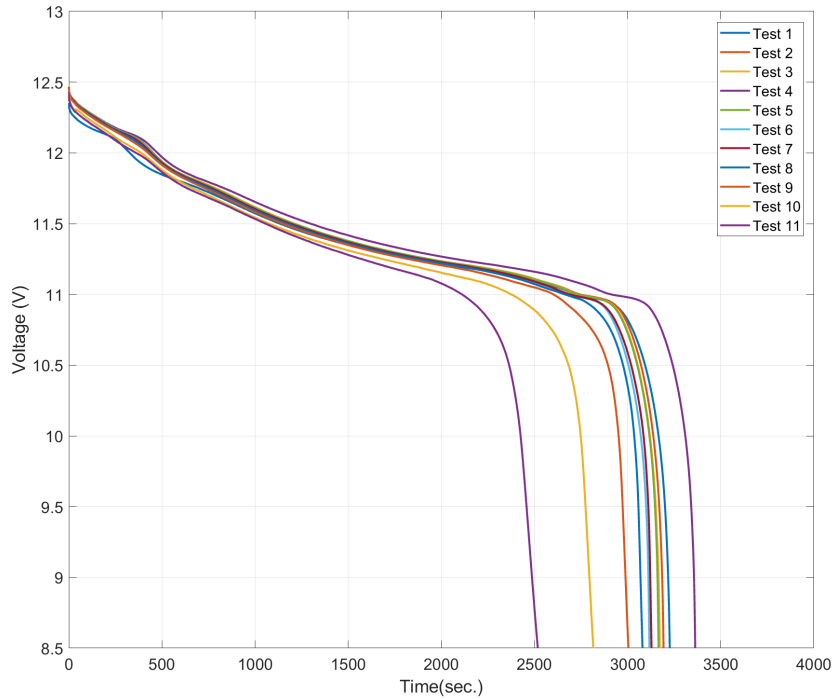


Figure 2.10: Voltage plots from  $Q_i$  characterization tests at 25°C.

generated with the implementation of drive cycle 2 up to the 9<sup>th</sup> characterization test has been used for the development (Chapter 6) of a synthetic battery data generations scheme which incorporates Markov chains that have developed using automotive grade battery data.

### 3. Electric Vehicle Data (Automotive Grade Batteries)

Two automotive data sets were obtained from a couple of different sources, first from Center for Automotive Research (CAR) at the Ohio State University and second from Renault Groupe, France.

The data set obtained from CAR is one that has been generated with repeated cyclic testing on automotive grade Li-ion batteries manufactured by LG Chem. This data set consisted of testing data generated from a of a total of 15 batteries, and the capacity behavior of 5 batteries from this data set, which showed maximum variation in capacity, shown in Table 2.3. In this table the test numbers correspond to capacity tests that have been per-

formed periodically over time to capture the fade in capacity, which has been brought about by a number of drive cycles that have been implemented on the batteries between consecutive capacity tests. In the following table, Table 2.4, the change in capacity is shown in percentages between Beginning-of-Life (BoL) and End-of-Life (EoL) as compared to a rated capacity of 15 Ahr.

Table 2.3: Capacity variation of 5 LG Chem batteries.

Test No.	Cell 1	Cell 2	Cell 3	Cell 4	Cell 5
1	14.227	14.375	14.597	14.629	14.331
2	14.133	14.225	14.428	14.505	14.255
3	13.782	13.953	14.118	14.339	13.865
4	13.645	13.761	13.894	14.112	13.974
5	13.503	13.803	13.667	13.958	13.384
6	13.251	13.517	13.429	13.873	12.9
7	13.16	13.389	13.452	13.772	13.07

Table 2.4: Capacity variation of 5 LG Chem batteries.

	Cell 1	Cell 2	Cell 3	Cell 4	Cell 5
BoL	95.18%	95.83%	97.31%	97.53%	95.54%
EoL	87.73%	89.26%	89.68%	91.81%	87.13%
% Change	7.45%	6.57%	7.6%	5.71%	8.41%

The behavior of the capacity tests is shown in Figure 2.11, which consists of first, a complete discharge from 100% to 0% SoC using a single pulse, followed by a rest phase and then a complete 0% to 100% charge with a single pulse. The discharge pulse is used for calculating the capacity of the battery. Second, after the complete charge and discharge pulses, a complete HPPC profile is executed, which consists of a total of 10 pulses at 1C each, each pulse discharging the battery 10% SoC and then followed by a rest phase.

Examples of drive cycles which have been implemented on the LG Chem batteries in-between consecutive capacity tests is depicted in Figure 2.12 and Figure 2.13. These drive cycles have been developed in order to create stresses at specific SoC ranges such that the the

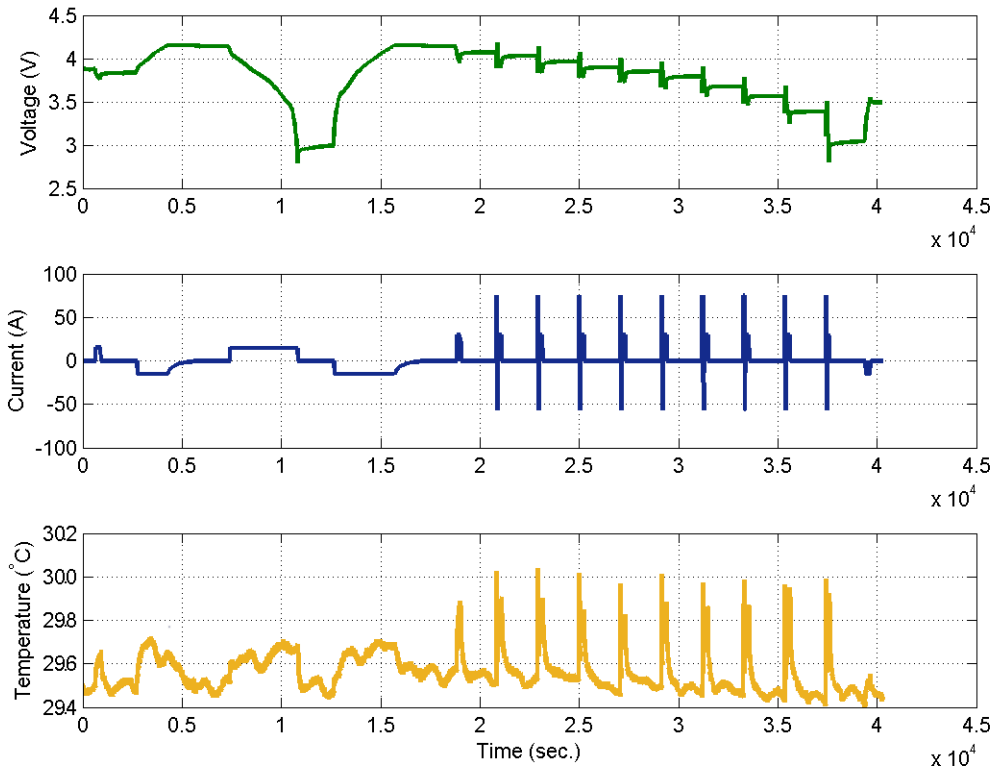


Figure 2.11: Capacity test performed on the automotive batteries.

battery performance can not only be observed in terms of the overall capacity but also observed as to how they hold up to specific C-rates at particular SoC ranges. The variation in the tests can be observed in the SoC plots, in Figure 2.12, multiple pulses are occurring in the range of 50% to 30% SoC, whereas in Figure 2.13, the pulses are covering a large range between 95% and 20% SoC. While the access to the drive cycle data is restricted, as a general rule, between each capacity test, the batteries have been subjected to roughly 3000 hours of testing with drive cycles.

Similar to such drive cycles, a number of other drive cycles have been used in order to bring about an accelerated aging. The ones shown here are the ones that have been used the most repeated number of times.

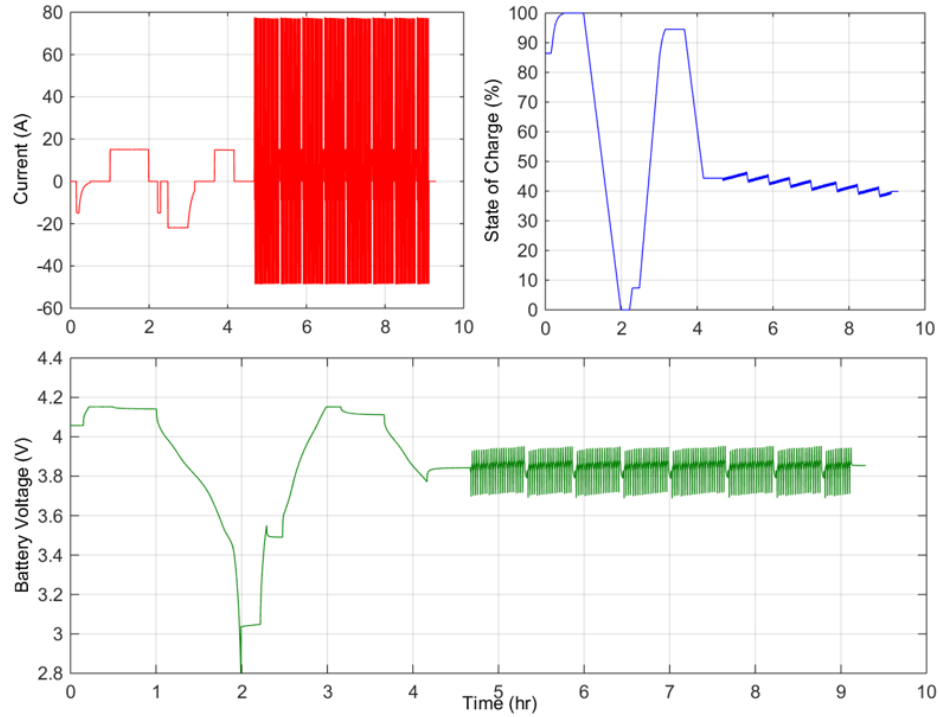


Figure 2.12: EV drive cycle (Example 1)

The voltage patterns during the single pulse complete discharge occurring in the capacity tests for Cell 1 is shown in Figure 2.14. If compared to Figure 2.10, the difference in how well the batteries hold their OCV characteristics can be observed. While both batteries have principally similar chemistry, the capability of withstanding prolonged stresses is much higher when it comes to the automotive grade batteries. This also goes on the back the standard life expectancy of such batteries, which is 10 years of approximately 150,000 miles of use. In this figure,  $Q_i$  indicates the number of the capacity test.

The second automotive data set used for our studies is obtained from the battery pack in a Renault Twizy consisting of 96 cells, from Groupe Renault, France. The main reason for our interest in this data set is primarily for the the fact that this data has been recorded from an EV which has been driven on public roads, hence this can be used as true drive cycle data. These data sets are is characterized by number of drive cycle data sets which contain multiple discharge pulses in chunks of a few hours. The limitation of this data set

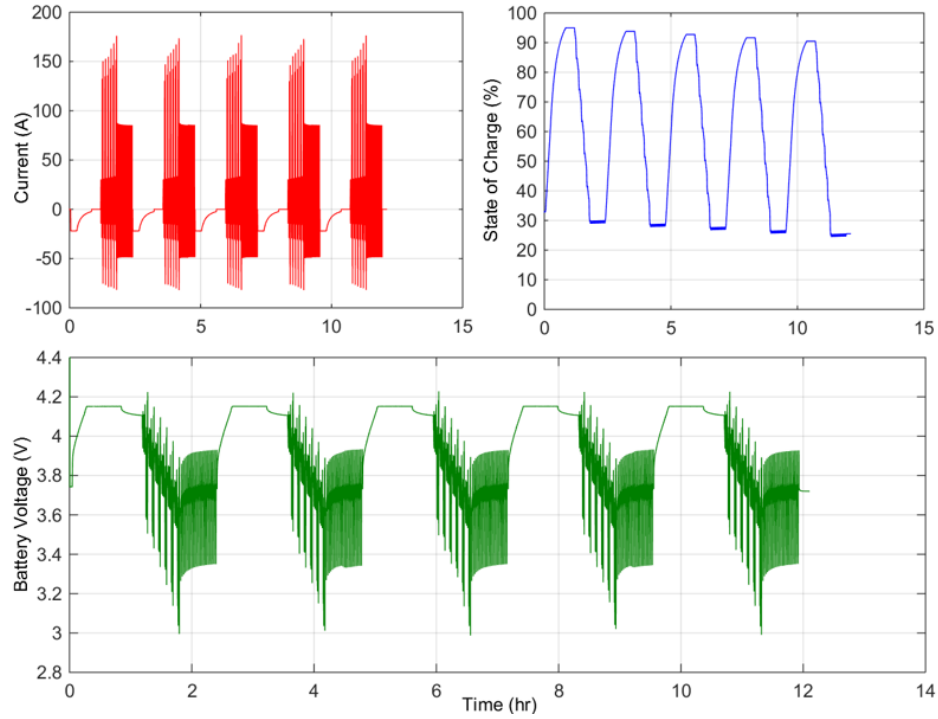


Figure 2.13: EV drive cycle (Example 2)

is that the capacity of the battery pack under observation has changed very little over the period under consideration (automotive grade packs typically exhibit long life). As a result, capacity fade analyses cannot be carried out on this data set. A representative visualization of this data set is presented in Figure 2.15.

In part (a) of Figure 2.15, the voltage and SoC response of the overall pack during one such drive cycle is highlighted. In this particular drive cycle, the pack has a max/min voltage of 398/348.5 V and discharges to an SoC of 60.44% from being fully charged.

Another view of a different drive cycle contained in this data set is provided in part (b) of Figure 2.15, where the voltage behavior of a single cell, which varies between 3.97 V and 3.75 V, is shown along with the SoC pattern of the pack from 65.84% to 49.52%.

All the data sets that have been presented in this section have been used in capacity fade evaluations in some manner except for the last one, which is the Renault Twizy data set. This set has been used in the generation of Transition Probability matrices for synthetic

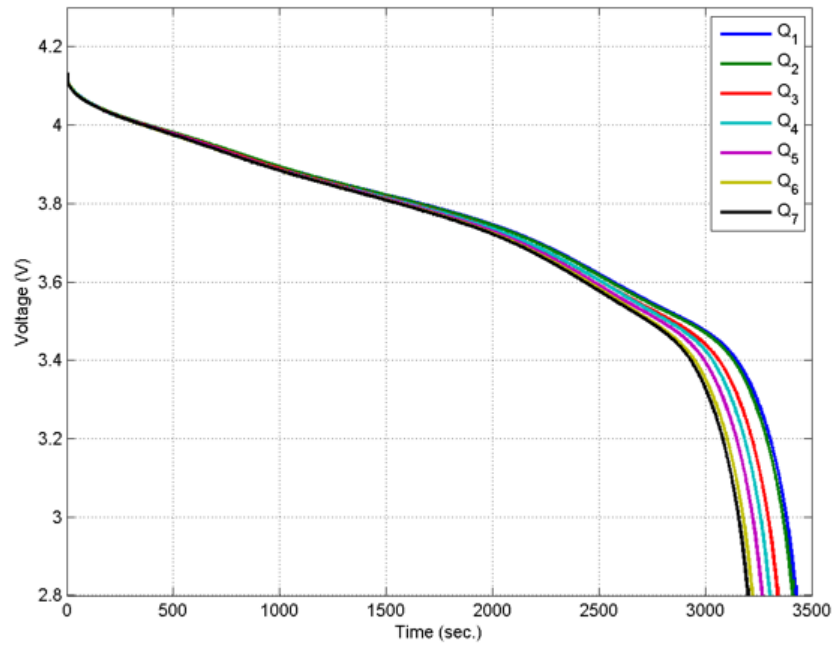
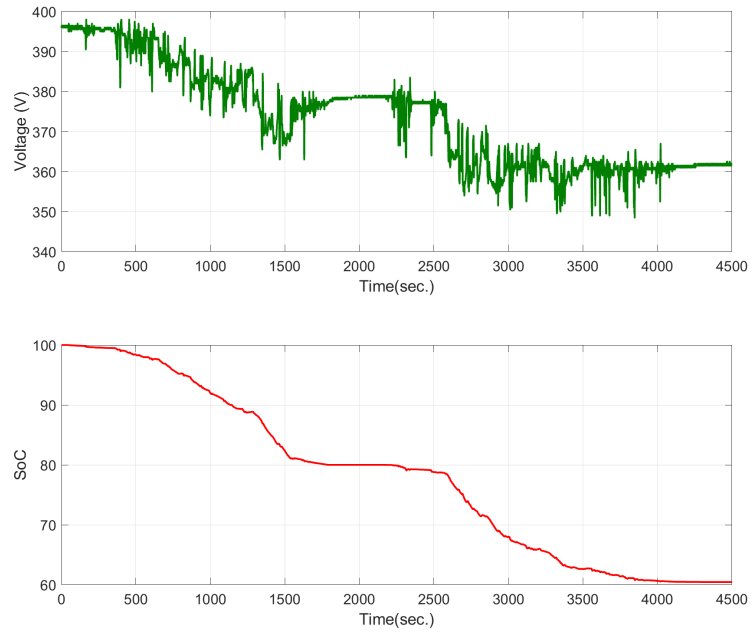
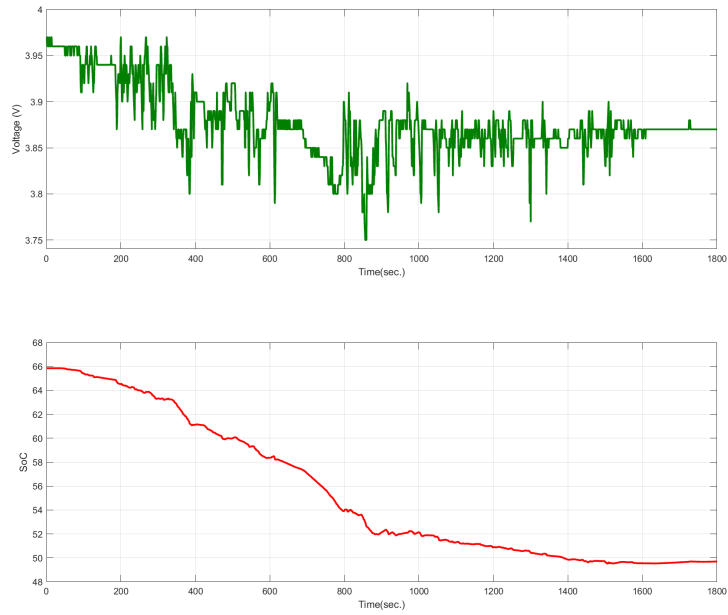


Figure 2.14: Voltage plots from capacity tests on the pack depicted as ‘Cell 1’ in Table 2.3.

data generation using Markov Chains. The specifics of how each data set has been used in estimation processes will be elaborated upon in step-wise detail in the following chapters.



(a) EV drive cycle (Example 1).



(b) EV drive cycle (Example 2).

Figure 2.15: Change in OCV voltage with prolonged testing at different temperatures.

## CHAPTER 3

### FEATURE ENGINEERING<sup>1</sup>

Simply stated, Machine Learning (ML) is the selection of a learning algorithm with training on an instance or modeled data. The two main challenges of such an approach are the use of a poor data set and incorrect algorithm for the problem at hand, discussed next (43).

In terms of data, a few examples of factors which can affect its effectiveness are:

1. Insufficient quantity of data: Even for simple problems, ML algorithms need thousands of data samples to effectively capture the particular traits. For more complex problems, examples can range in the millions of high and low dimensional data.
2. Non-representative training set: In order for the model to generalize well, it is crucial for the training data to be representative of the of the new cases or instances that need to be generalized. This is true for instance-based as well as model-based learning. This problem can get easily get complicated, that is, if the sample size is small, there can be sampling noise (non-representative data as a result of chance), or with large sample sets can have non-representation due to skewed sampling (sampling bias).
3. Poor quality: If the data set is full of errors, outliers and noise, it will be arduous for the system to detect the underlying patterns, hence reducing the likeliness for it to perform well.
4. Features: A critical part of any ML undertaking is coming up with a good set of features to train on. This process is called feature engineering, which involves:
  - Feature selection: selecting the most useful features to train among existing features.

---

<sup>1</sup>©2017 IEEE. Portions Adopted, with permission, from M. Pyne, B. J. Yurkovich, S. Yurkovich, “Capacity Fade Estimation Using Supervised Learning,” IEEE Conference on Control Technology and Applications (CCTA), August 2017.

- Feature Extraction: Combining existing features to produce useful ones (Principal Component Analysis and dimensionality reduction are examples of methods used for feature extraction).
5. Over-fitting: Complex models such as deep neural networks can detect subtle patterns in the data but if there is noise present, or the data set is too small, the model is likely to detect patterns in the noise itself. This can lead to faulty generalizing, known as over-fitting. To get around these, the models used need simplification, gathering of more training data or reduction of training data noise.
  6. Under-fitting: This is the opposite of over-fitting, where the model is too simplified to understand the underlying structure of the data.

While a detailed discussion of the data gathering procedure and the data sets that have been employed was presented in the previous chapter, and the specifics of the algorithmic approach will be described in the coming chapters, in this chapter we focus on extracting and engineering of “*features*” from the data sets in order to fulfil our larger objectives in this research.

Several research endeavors have utilized data-driven techniques. Chief among them, artificial neural network (ANN) based techniques are used to estimate the SoC and capacity fade in a battery. A common criticism concerns the amount of data required for training before the ANN can provide a desired performance.

Along these lines, our research endeavors to use established machine learning techniques in order to estimate the issue of capacity fade estimation. While trying this approach, our intention has always been on some of the inherent problems associated with data-driven approaches, primarily the limitation of memory available for computation and data storage, while having enough generalization in the data in order to accommodate effective learning by the models.

In battery research today, data can be obtained through different tests such as pulse or a constant current (dis)charge tests, various driving cycles, battery capacity measurement, and so on. With the rapid development of cloud based storage and computation services from the likes of Amazon and Google, application of data-driven algorithms are more manageable than ever. The only factor that governs the use of such cloud-based services is the cost associated with them. Hence, extraction of effective information from data, and storing only the useful bits, and thus paying for only what is necessary becomes a practical issue in need of resolving. In our research, extracting useful data from these data sets and reducing the computational stress has been given its due importance.

To be specific, in order to address this issue, we have broken up the unfiltered I-V-T data that is collected from the batteries into sections and features, followed by employing the K-means clustering approach, which reduces large pre-selected portions of the data down to multiple centroids, while still preserving the intrinsic trends in the raw data. In the following sections a discussion is presented on the features and K-means clustering.

### 3.1 K-Means Clustering

Clustering is the task of dividing the population or data points into a number of groups such that data points in the same groups are more similar to other data points in the same group and dissimilar to the data points in other groups. It is basically a collection of objects on the basis of similarity and dissimilarity between them. In our research, we have employed K-means clustering as a methodology to partition different sections of the test data followed by representing them by “*centroids*”.

The K-means algorithm is a method to automatically cluster similar data examples together. Given a training set  $\{x^{(1)}, \dots, x^{(m)}\}$ , where  $x^{(i)} \in \mathbb{R}$ , the concept is to group the data into a few cohesive “clusters”. The intuition behind K-means is an iterative procedure that starts by guessing the initial centroids, and then refines this guess by repeatedly assigning

examples to their closest centroids and then recomputing the centroids based on the assignments. The inner-loop of the algorithm repeatedly carries out two steps: (i) assigning each training example  $x^{(i)}$  to its closest centroid, and (ii) recomputing the mean of each centroid using the points assigned to it. The  $K$ -means algorithm will always converge to some final set of means for the centroids. Note that the converged solution may not always be ideal and depends on the initial setting of the centroids. Therefore, in practice the K-means algorithm is usually run a few times with different random initializations (44).

In the “cluster assignment” phase of the K-means algorithm, the algorithm assigns every training example  $x^{(i)}$  to its closest centroid, given the current positions of centroids. Specifically, for every example  $i$  we set

$$C^{(i)} := j \quad \text{that minimizes} \quad \|x^{(i)} - \eta_j\|^2, \quad (3.1)$$

where  $c^{(i)}$  is the index of the centroid that is closest to  $x^{(i)}$  and  $\eta_j$  is the position (value) of the  $j^{\text{th}}$  centroid.

Given assignments of every point to a centroid, the second phase of the algorithm recomputes, for each centroid, the mean of the points that were assigned to it. Specifically, for every centroid  $k$  we set

$$\eta_k := \frac{1}{|C_k|} \sum_{i \in C_k} x^{(i)}, \quad (3.2)$$

where  $C_k$  is the set of examples assigned to centroid  $k$ . When it comes to K-means clustering, there are a few potential drawbacks, namely,

- K-means assume the variance of the distribution of each attribute (variable) is spherical.
- all variables have the same variance.
- the prior probability for all  $K$  clusters are the same, i.e. each cluster has roughly equal number of observations.

If any one of these three assumptions are violated, then K-means will provide erroneous results.

In our research endeavor, the major problem with K-means has been the uneven distribution points in a cluster. In case the clusters are unequally distributed, the algorithm tends to let the small clusters end up far away from any center, while it uses those centers to “split up a much larger cluster. In order to work around this drawback, the pre-processing approach in the algorithms used in this research, attempts to keep an equal distribution of data points, and this is easily accomplished while the battery does not lose substantial percentages capacity between two consecutive iterations of capacity tests.

### 3.2 Features Set

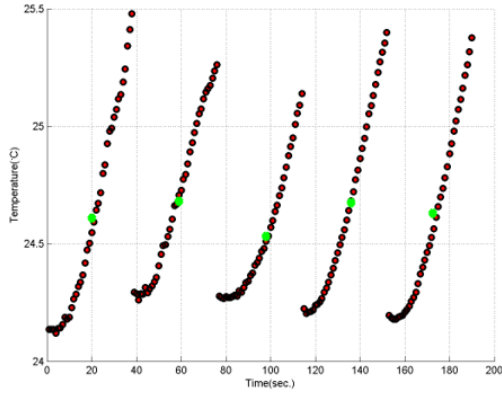
In our setup, we start by breaking up the mRPT and drive profiles into three sections: **Discharge**, **Charge** and **Rest**. In each of these sections we extract the features into individual components; these features are highlighted in Table 3.1, where rSoC1 is the SoC calculation based on Coulomb counting, rSoC2 is SoC calculated based on OCV-SoC look-up,  $R_0$  is ohmic resistance and  $\Delta$  represents the change in a parameter during a particular event such as a single discharge pulse or rest phase.

Table 3.1: Feature extraction.

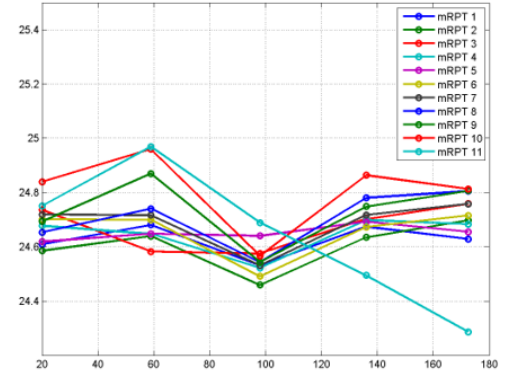
Period	Features
Discharge/Charge	$\Delta$ Temperature, $\Delta$ Voltage, $\Delta$ Current, Throughput, $\Delta$ rSoC1, $R_0$
Rest	Duration, $\Delta$ Temperature, $\Delta$ rSoC2, $\Delta$ Voltage

The behavior and subsequent extraction and clustering of these features is highlighted in Figures 3.1-3.6. For the depiction of these features, a similar approach of segregating the data sets, then clustering, followed by a representation of how they display trends over multiple test data sets is adopted.

Figure 3.1(a) illustrates data representing the change in surface temperature (as measured with a low-cost thermocouple device mounted on the pack surface) during the discharge pulses of the first mRPT on the battery pack (held at 25°C ambient); coinciding with the mRPT of Figure 2.7, there are five curves. In this figure the five green data-tips represent the centroids produced from the clustering algorithm.



(a) Surface temperature during first mRPT.



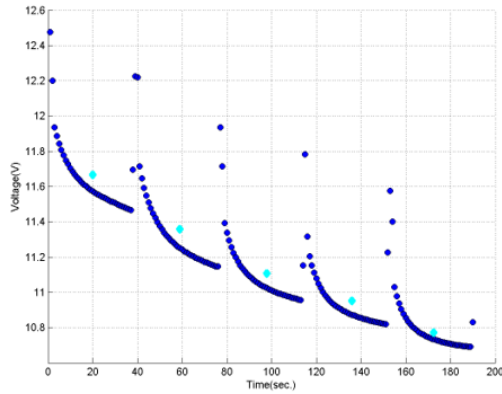
(b) Surface temperature centroids for all eleven mRPTs.

Figure 3.1: Behavior of  $\Delta$ Temperature.

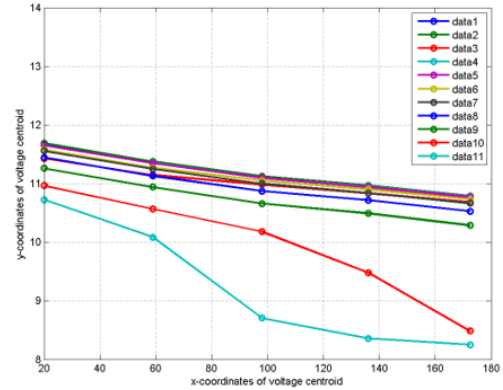
Notice that with mRPTs 1 through 9 the trends are grouped fairly closely (Figure 3.1(b)), whereas the 10<sup>th</sup> mRPT follows the trend but is further from the grouping. The mRPT result from test 11 deviates from the pattern, which coincides with the capacity values represented in Table 2.1, where we can observe that the pack begins to noticeably lose capacity after the 9<sup>th</sup> capacity test.

Similarly, the voltage variations during the five discharge pulses in the first mRPT along with the respective centroids are represented in Figure 3.2(a) for the pack held at ambient temperature 25°C. Similar to the pack surface temperature plots, clustering was applied to voltages corresponding to the five discharge pulses in all of the mRPTs, and the centroid trend results are shown in Figure 3.2(b). Similar to the temperature behavior, we can

observe that the pattern of voltage centroids is grouped closely until the battery begins to lose capacity. Upon reaching the 9<sup>th</sup> test, the centroids start deviating from the trend.



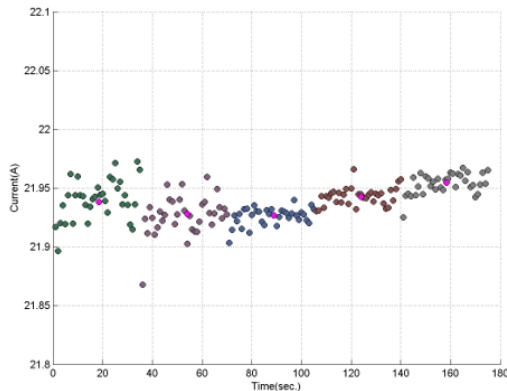
(a) Voltage plot of the first mRPT.



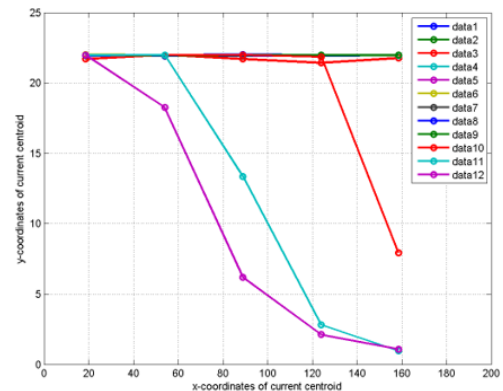
(b) Voltage centroids for all eleven mRPTs.

Figure 3.2: Behavior of  $\Delta$ Voltage.

Along comparable lines, the behavior of  $\Delta$ Current is shown in Figure 3.3. Notice that the current centroids stay grouped together until the battery pack starts to lose significant capacity retention ability and thus the current centroids start falling steeply as they start transitioning from CC to CV mode.



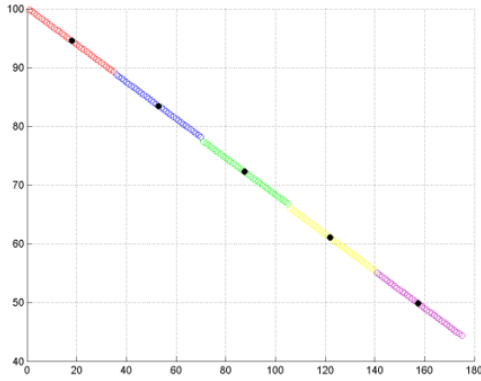
(a) Current pulse behavior during first mRPT.



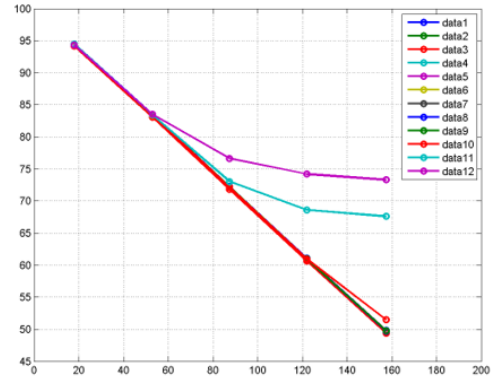
(b) Current centroids for all eleven mRPTs.

Figure 3.3: Behavior of  $\Delta$ Current.

For  $\Delta rSoC1$ , a very strong grouping is observed in the centroids in Figure 3.4, until the capacity starts falling and the battery has no charge remaining in the lower SoC levels, resulting in upwards movement of the centroids. It needs to be mentioned here that with the  $rSoC1$  based on Coulomb counting, as the battery loses capacity, the SoC changes relative to the capacity. But, in this analysis, the capacity term in the Coulomb counting equation has been kept constant at the initial capacity that was observed from the very first capacity test.



(a)  $rSoC1$  behavior during first mRPT.



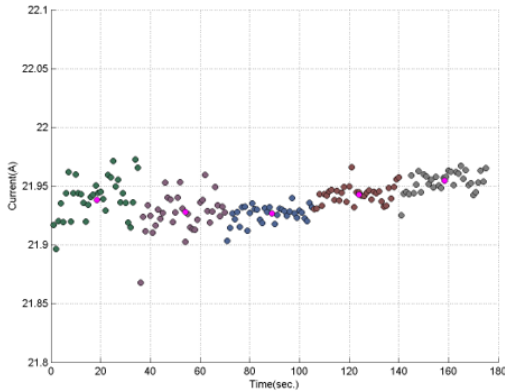
(b)  $rSoC1$  centroids for all eleven mRPTs.

Figure 3.4: Behavior of  $\Delta rSoC1$ .

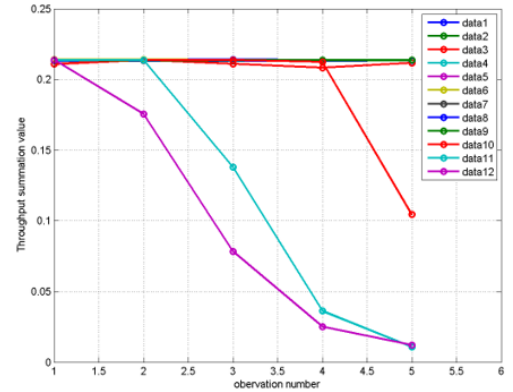
The trends in Throughput is shown in Figure 3.5, which is very similar in nature to  $\Delta Current$ . Throughput is defined as the change in energy level of the storage bank, measured after charging losses and before discharging losses.

Finally, the behavior of internal resistance ( $R_0$ ) is depicted in Figure 3.6, where it is evident that the internal resistance rises exponentially with fade in battery capacity.

These sets of centroids belonging to each mRPT can be accurately fitted with polynomials. Based on the requirement, those curve-fits are subsequently utilized as inputs to multiple deep neural net models for the purposes of estimating various parameters such as OCV characteristics and SoC behavior with data from readily-available data sets generated

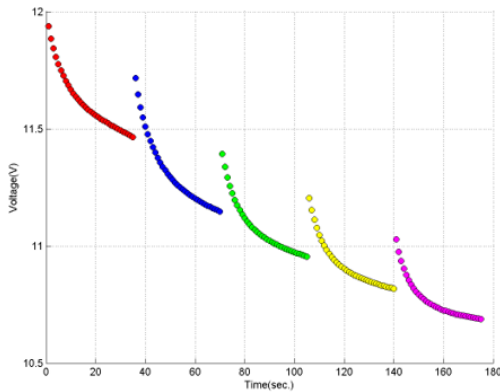


(a) Throughput behavior during first mRPT..

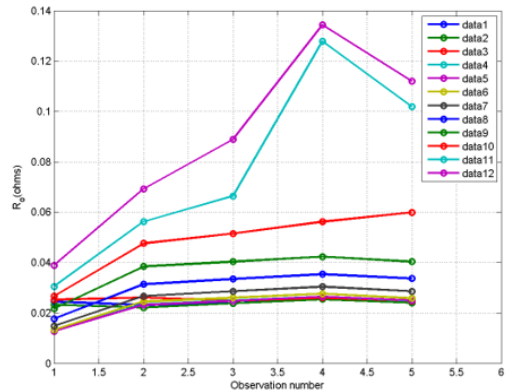


(b) Throughput centroids for all eleven mRPTs.

Figure 3.5: Behavior of Throughput.



(a)  $R_0$  behavior during first mRPT.



(b)  $R_0$  centroids for all eleven mRPTs.

Figure 3.6: Behavior of  $R_0$ .

from different batteries and packs. Those results can then be used in turn to estimate the capacity; details of this process follow in the next chapters.

Once the features were selected and had been extracted, we looked into executing a sensitivity analysis on the features with regard to the change in capacity as the battery pack ages. This enabled us to predict the behavior of a feature if a feature turned out to be different compared to the key prediction(s). The sensitivity relation employed in our analysis

is defined as

$$S = \frac{\partial V}{\partial C}, \quad (3.3)$$

where  $V$  represents the features that have been extracted and  $C$  is the capacity of the battery. It is to be noted here that high sensitivity means a close correlation between the two variables.

The sensitivity analysis is shown in Table 3.2, where the sensitivity coefficients for the five discharge pulses in the mRPT are shown separately for each of the features during the discharge phase. The comparison is made between the first mRPT features and ninth mRPT features.

Table 3.2: Sensitivity analysis.

	Pulse 1	Pulse 2	Pulse 3	Pulse 4	Pulse 5
$\Delta$ Voltage	3.571	3.584	3.530	3.821	4.065
$\Delta$ Temperature	0.669	1.651	0.176	0.558	1.394
$\Delta$ Current	0.284	0.332	0.437	0.270	0.159
Throughput	0.002	0.003	0.004	0.002	0.001
$\Delta$ rSoC1	0.113	0.263	0.488	0.667	0.803
$R_0$	0.025	0.133	0.144	0.142	0.135

From Table 3.2, we can see that the highest correlation is with voltage, whereas temperature is the second highest correlated feature. Also, comparing the pulses, it can be observed that  $R_0$  has the smallest change in correlation, whereas maximum change happens with temperature.

### 3.3 Feature Characterization

It is challenging to derive methodology that solves problems under highly non-linear conditions in a cluttered scene, such as recognizing a multi-dimensional object. Even with a good process defined, the resulting code might be extremely complicated. From a machine learning point-of-view, instead of writing a program for each specific task, a collection of examples

that specify the correct output for a given input can be used to generate a program which does the modeling of the complex relations between variables very effectively. The program produced by the learning algorithm may look very different from a standard hand-written program. But, if done effectively, the program works for new cases as well as the ones upon which it was trained. Also, such a process would afford the ability for the program itself to adjust with changing data by training on the new data. This flexibility of using data-driven learning based approaches has led us to use recurrent neural networks for the purposes of predicting the behavior of the internal resistance with changing C-rates as well as SoC.

In our application, we have used a closed-loop (recurrent) neural network with three layers, the input, hidden and output layers. For the purposes of training, the network uses a back propagation algorithm, which has  $n$  inputs  $x_i$  where  $i = 1, \dots, n$ . We have  $m$  outputs,  $s = 1, \dots, m$  with  $l$  neurons in the hidden layer. The outputs of the neurons in the hidden layer are  $z_j$ , where  $j = 1, \dots, l$ . The activation functions of the neurons in the hidden layer are  $f_j^h : \mathbb{R} \rightarrow \mathbb{R}$  and the activation for the neurons in the output layer are  $f_s^o : \mathbb{R} \rightarrow \mathbb{R}$ , where  $j = 1, \dots, l$  and  $s = 1, \dots, m$ . The weights from the inputs to the hidden layer are  $w_{ji}^h$  and those from the hidden to the output layer are  $w_{sj}^o$ . The output from the  $s^{th}$  neuron of the output layer is

$$y_s = f_s^o \left( \sum_{j=1}^l w_{sj}^o z_j \right). \quad (3.4)$$

Therefore the relation between the inputs  $x_i, i = 1, \dots, n$  and the  $s^{th}$  output  $y_s$  is given by

$$y_s = f_s^o \left( \sum_{j=1}^l w_{sj}^o \left( \sum_{i=1}^n w_{ji}^h x_i \right) \right) = F_s(x_1, \dots, x_n). \quad (3.5)$$

The network we have implemented consists of three layers: input, hidden and output, with the hidden layer having 10 neurons. The inputs that have been considered are true capacity, current and SoC, whereas the output is internal resistance.

### 3.4 Summary

In this chapter an overall picture of the available features from the battery data sets have been presented along with their quantification. These features will be used in the subsequent chapters to perform the desired estimations. In most of the estimations a total of two or three features have been used to varying degrees of success but a large scope for exploring these features still remains such as,

1. Exploring features which capture the internal functioning of the cell reactions in further detail.
2. Evaluating what is the minimum number of features that are relevant to a given estimation approach.
3. Exploring the feasibility and applicability of combined or inter-dependent features with methods such as Principal Component Analysis and Classification.

In this research, the approach has been to find a starting point into the use of supervised learning for capacity estimation, with a small subset of features. In the chapters that follow, these features are used extensively to predict the trends in capacity fade with using different data sets generated from the automotive as well as non-automotive battery packs.

## CHAPTER 4

### CAPACITY ESTIMATION USING STRUCTURED TESTS <sup>1</sup>

#### 4.1 Introduction

As was described in detail in Chapter 1 of this dissertation, the issue of estimating the fade in capacity in batteries is a one of the more convoluted problems in battery research and it is inherent with a number of fundamental drawbacks. Nevertheless, the estimation issue plays a vital role in any system level BMS application and/or real-world implementation of an energy storage system. With this in mind, the drawbacks that were highlighted have been addressed in a systematic manner where we have made progress in steps of increasing complexity in order to fulfil the objective of first, using less data for purposes of estimation and second, using drive cycle data, which is more accessible than capacity test data for the purposes of estimation. Here, the first step in Figure 1.5 is described and validated where we estimate capacity based on  $Q_i$ (characterization tests) and  $mRPT$  data sets.

Aimed at using a reduced amount of characterization data, while incorporating the impact of temperature, this chapter describes the results obtained from the initial steps taken in the investigation that addresses some of the issues in estimation of capacity fade, while giving attention to computational complexity. Although our ultimate goal is to transfer the methods developed here to automotive-grade batteries, the particular battery pack used in this preliminary work is not of such high quality; this facilitates general modeling and development of learning methodologies for capacity fade in a much shorter time frame. A clustering approach is presented to predict the characterization curve from a charge-discharge cycle. From this, along with inclusion of temperature effect, a recurrent neural network model is utilized to predict the capacity.

---

<sup>1</sup>©2017 IEEE. Portions Adopted, with permission, from M. Pyne, B. J. Yurkovich, S. Yurkovich, “Capacity Fade Estimation Using Supervised Learning,” IEEE Conference on Control Technology and Applications (CCTA), August 2017.

In the coming sections a brief overview of the particular data sets that have used are highlighted followed by a discussion of the working and structure of a neural network. The estimation is done in two parts with separate test profiles: the first part uses a the time series data from the  $Q_i$  tests, where the temperature and voltage behaviors are used as input and the SoC behavior is used as the target during the 1C discharge pulse in the  $Q_i$  test for training and testing a neural network. Second, the  $mRPT$  test profiles are used in much the same manner as the  $Q_i$  based modeling, but with the added step of segregating the voltage and temperature behaviors during the discharge pulses and clustering them for data reduction purposes. After clustering the obtained centroids are curve fitted with a 4<sup>th</sup> order polynomial, forming the input. For the targets, the SoC behavior of the discharge pulse of the  $Q_i$  test is used. The steps adopted for the estimation based on both types of testing profiles is highlighted in Figure 4.1.

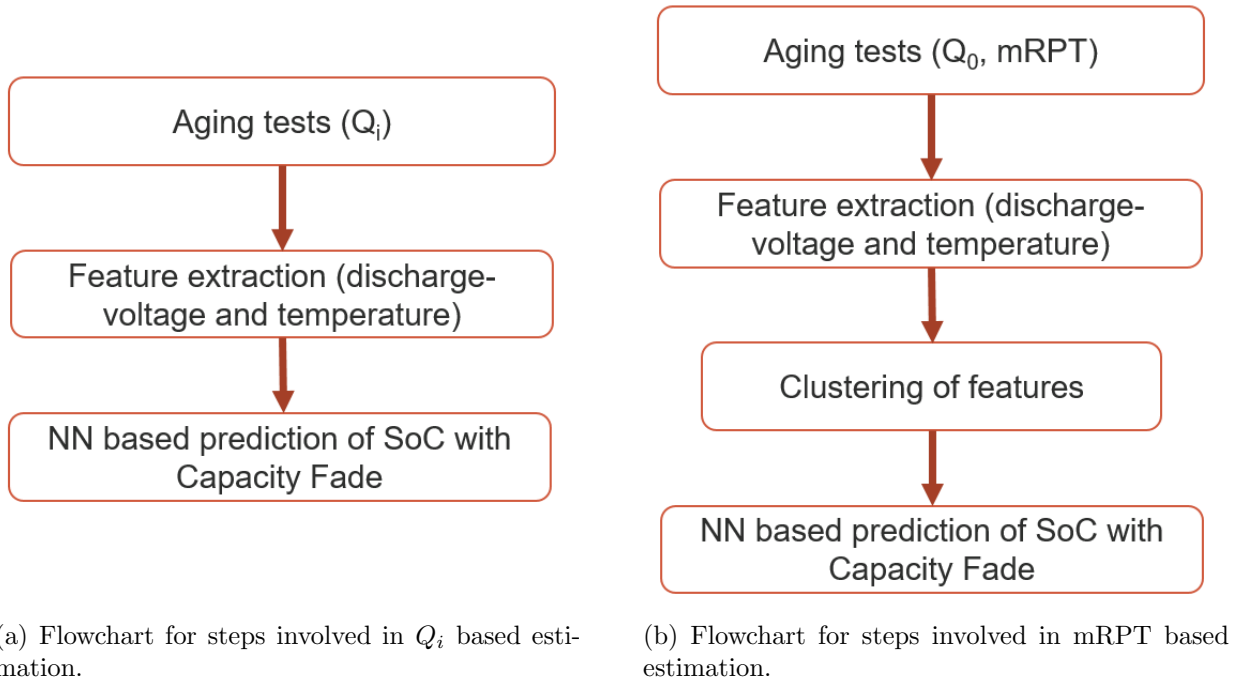


Figure 4.1: Estimation process flows.

## 4.2 Data Sets Under Consideration

In this chapter, the estimation of capacity is done on two different data sets, first is from a three cell Li-ion non-automotive pack, and the second is from a automotive grade Li-ion battery.

### 4.2.1 Three Cell Pack

In the first estimation process, only the  $Q_i$  test profiles generated from testing the Turnigy battery pack rated at 11.4 V/2200 mAh at 25°C are used. The details of the testing procedure undertaken and data generation achieved has been elaborated upon in Chapter 2.

To maintain clarity, the typical capacity or characterization test is referred to as  $Q_i$  where the initial test is named  $Q_0$  (Beginning-of-Life) and any capacity test that follows in the systematic testing approach is numbered  $i = 1, 2, \dots$  until the pack demonstrates a capacity below 70% of its initial rated value. In the testing of the battery pack under consideration, there were a total of eleven capacity tests. The behavior of a typical capacity test is shown in Figure 4.2 and the voltage and temperature behavior of the 1C 100% to 0% discharge pulse across all eleven of these tests are depicted in Figure 4.3.

For the second estimation approach, the data generated from running the mRPT profile has been used. It is to be mentioned here that in our testing procedure, an mRPT test is implemented directly after a  $Q_i$  test and there is no drive cycle run between these tests. Similar to the  $Q_i$  based estimation, there are eleven mRPTs that have been used in this approach.

As was briefly mentioned earlier, the voltage and temperature behaviors during the five discharge pulses are isolated and then K-means clustering is used to reduce these data sections to centroids. These centroids are then fitted with a fourth order polynomial and then used as inputs to the neural net used for estimation. The nature of an mRPT profile is depicted

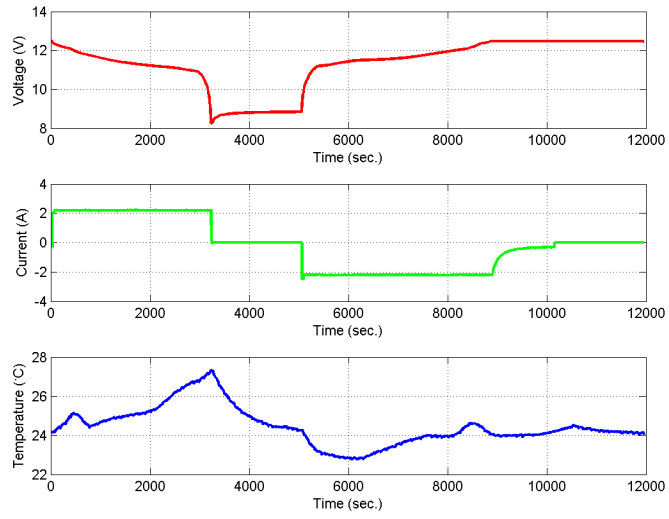
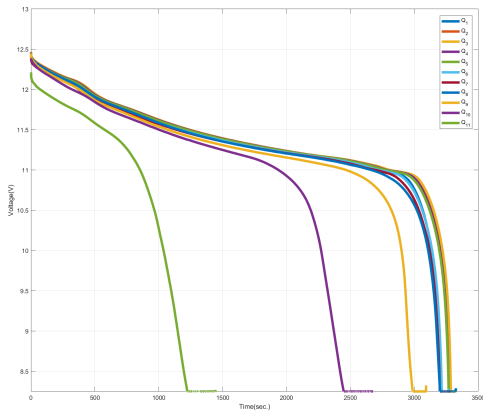
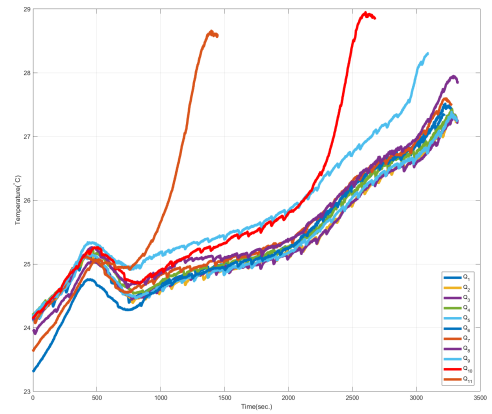


Figure 4.2:  $Q_i$  (characterization) test.



(a) Voltage behavior during  $Q_i$  tests.



(b) Temperature behavior during  $Q_i$  tests.

Figure 4.3: Behavior of variables.

in Figure 4.4 and the trends observed in all eleven mRPT voltage and temperature centroids during discharge are shown in Figure 4.5.

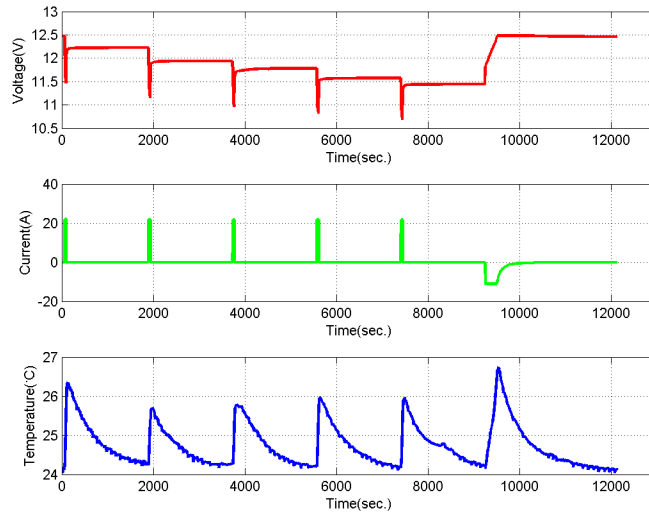
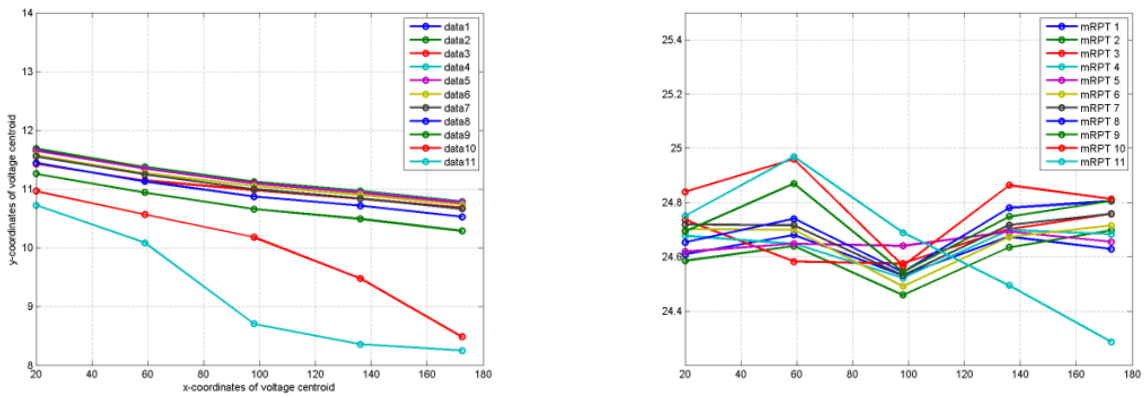


Figure 4.4: Mini-reference performance test (mRPT).



(a) Voltage centroids for all eleven mRPTs.

(b) Temperature centroids for all eleven mRPTs.

Figure 4.5: Behavior of variables.

### 4.2.2 Automotive Cell

For the estimation based on the automotive batteries, the data generated from a single Li-ion cell rated at 4.2v/ 15Ah at 30°C was used. The testing procedure was very similar to the one implemented on the three cell pack and the estimation approach was also along similar lines.

The behavior of the cell at seven distinct capacity tests is shown in Figure 4.6, where we observe a capacity change of 7.45% over the seven cycles of testing that had been implemented. It is to be noted that between each capacity test, there has been roughly 1400 hours of drive cycles that have been implemented on these cells.

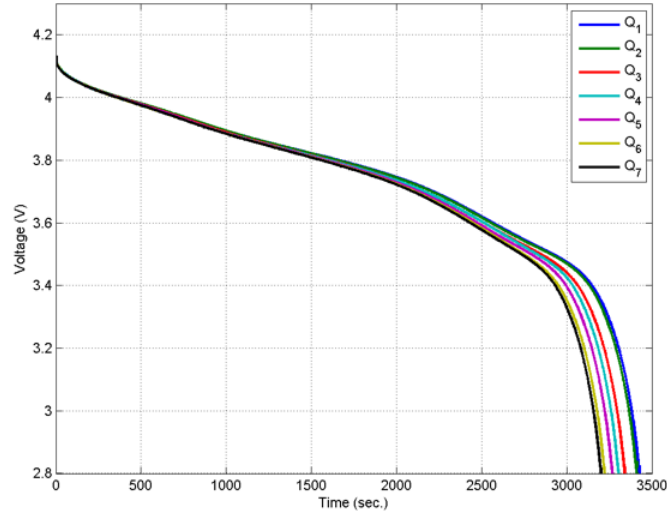


Figure 4.6: Voltage plots from capacity tests on the pack depicted as ‘Cell 1’ in Table 2.3.

The estimation approach that has been applied of this data set is along similar lines to what has been applied to the three cell pack, hence the test similar to an mRPT test, the HPPC test (Figure 4.7), is used for feature extraction and subsequent neural network training and estimation. The behavior of the centroids after clustering the discharge behavior of temperature and voltage are shown in Figure 4.8

The main difference from the three cell packs in the feature behaviors are firstly, there are nine discharge pulses in the HPPC tests in comparison to the mRPT tests and the clustering has been applied to all nine. Second, the capacity fade patterns are significantly lesser in this battery and hence the estimation is done in different ranges of SoC (will be elaborated upon later).

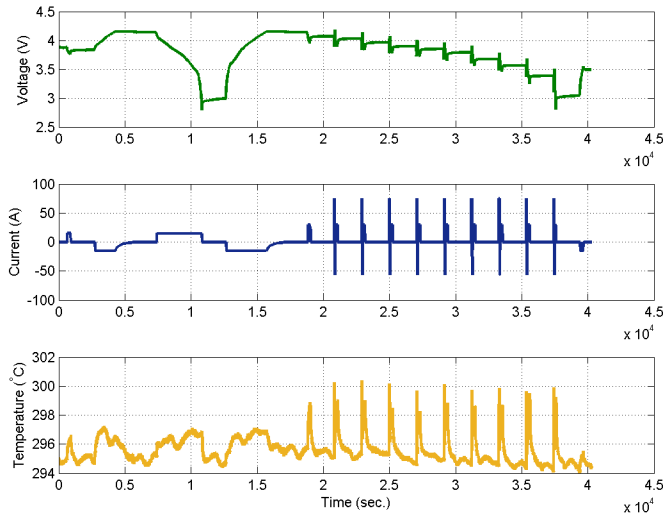
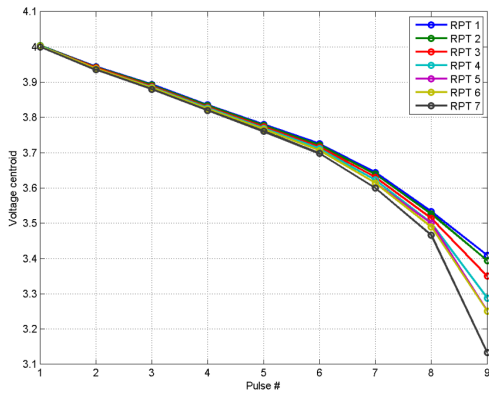
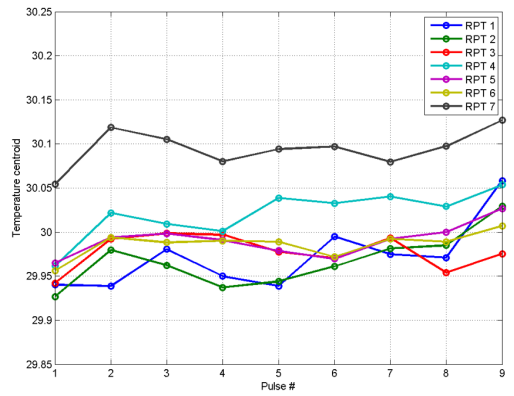


Figure 4.7: Capacity test performed on the automotive batteries.



(a) Voltage centroids for all seven mRPTs.



(b) Temperature centroids for all seven mRPTs.

Figure 4.8: Behavior of variables.

### 4.3 Neural Networks

In the final stage of both estimation approaches (1: using  $Q_i$ , 2: using  $mRPT$  data), we use a neural network for training and predicting the desired parameters in order to effectively obtain accurate capacity numbers.

Neural networks in principle are not new and have been around in concept for over 50 years now (1940s). The study of neural networks are motivated by the comparability they share in operation to biological nervous systems, which are complex systems, but are characterized by a large number of nerve cells working in parallel as well as the ability to *learn* (45), (46).

### 4.3.1 Definition of a Neural Network

By definition, a neural network is a sorted triple  $(N, V, w)$  with two sets  $N, V$  and a function  $w$ , where  $N$  is the set of *neurons* and  $V$  a set  $\{(i, j) | i, j \in N\}$  whose elements are called *connections* between neuron  $i$  and neuron  $j$ . The function  $w : V \rightarrow R$  defines the *weights*, where  $w_{i,j}$ , the weight of the connection between neuron  $i$  and neuron  $j$ , is shortened to  $w_{i,j}$ . Depending on the point of view it is either undefined or 0 for connections that do not exist in the network.

### 4.3.2 Data processing of a neuron

Data gets transferred between neurons through connections with the connecting weights being inhibitory or excitatory. Looking at a particular neuron  $j$ , it will usually have a lot of neurons with a connection to  $j$ , i.e., they transfer their output to  $j$ . For a neuron  $j$  (Figure 4.9), the *propagation function* receives the outputs  $o_1, o_2, \dots, o_n$  from other neurons  $i_1, i_2, \dots, i_n$ , which are connected to  $j$ , and transforms them in by multiplying them with the weights  $w_{i,j}$  and is further processed by the *activation function*. Thus the network input is the result of the propagation function. Hence the net input is:

$$net_j = \sum_i \in I(o_i \cdot w_{i,j}). \quad (4.1)$$

Based on the nature of the model, the reaction of the neuron to the inputs depends on the activation function and the activation state indicates the extent of the neuron's activation.

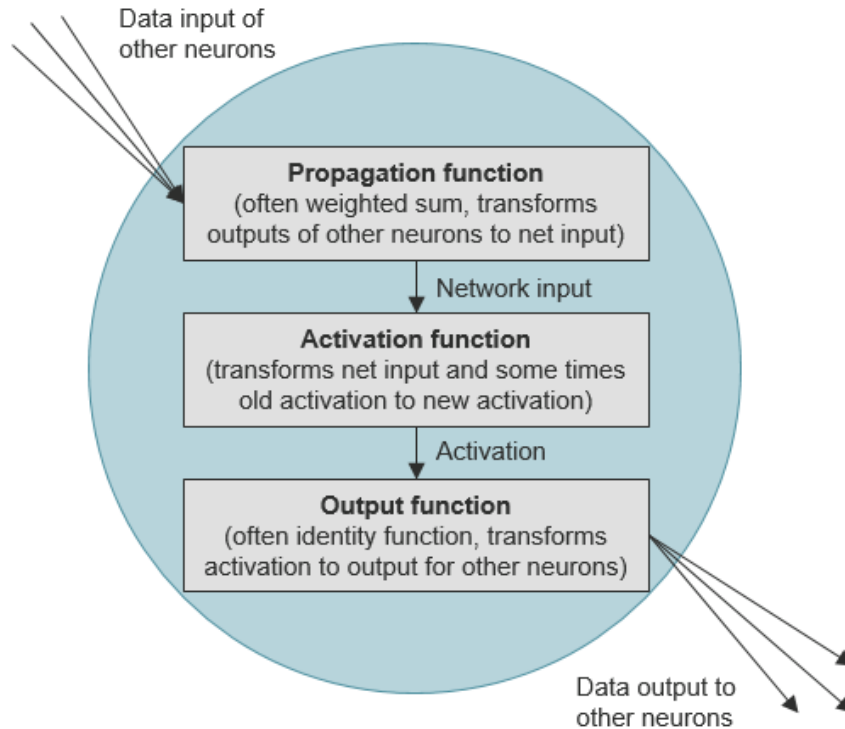


Figure 4.9: Neuron components.

This activation occurs near a threshold value, where the neuron is particularly sensitive. Some common activation functions that have been used in this research are:

**Linear function:**

$$f(x) = x \tag{4.2}$$

**Sigmoid function:** The main reason for the popularity of this function is because it exists between 0 and 1, hence well suited for probabilistic applications. It is differentiable and monotonic, hence allowing the slope to be calculated. A more generalized version of the sigmoid function is the *softmax function*.

$$\textit{Sigmoid} : f(x) = \frac{1}{1 + e^{-z}} \tag{4.3}$$

The sigmoid function suffers from “vanishing gradient” as it flattens out at both ends, resulting in very small changes in the weights during back propagation. This can make neural nets very slow in learning or even refuse to learn. A more generalized version of the sigmoid function is the *softmax function*.

**Rectified Linear Unit (ReLU):** The ReLU is the most used activation function in the literature, and is used in almost all the convolutional neural networks or deep learning. The function and its derivative both are monotonic:

$$ReLU : f(x) = \max(0, x), \quad f(x) \text{ is zero when } x < 0. \quad (4.4)$$

An issue is that all the negative values become zero immediately which decreases the ability of the model to fit or train from some types of data. That means any negative input given to the ReLU activation function turns the value into zero immediately in the graph, which in turns affects the resulting graph by not mapping the negative values appropriately.

Finally the output function of a neuron  $j$  calculates the values which are transferred to the other neurons connected to  $j$ .

### 4.3.3 Network Topologies

In this investigation into estimating capacity fade in Li-ion batteries, the initial steps are comprised of studying the behavior of the capacity in terms of uni- and multi-variable linear regression in order to understand and gain a general understanding the scale of complexity. Upon initial attempts at modeling, the transition to exploring more advanced data science approaches were explored for this research: feed forward and recurrent neural networks.

**Feed Forward:** The neuron layers of a feed forward network (Figure 4.10) are clearly separated: One input layer, one output layer and one or more processing layers which are invisible from the outside (also called hidden layers). Connections are only permitted to neurons of the following layer.

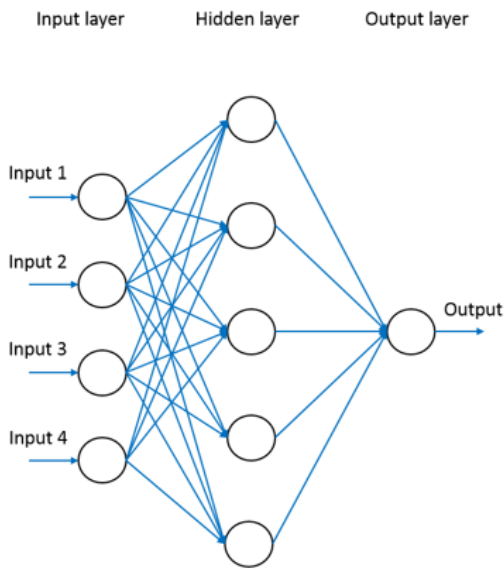


Figure 4.10: Feed forward neural network structure.

**Recurrent:** Recurrence is defined as the process of a neuron influencing itself by any means or by any connection. Recurrent networks do not always have explicitly defined input or output neurons and can have connections from one layer to any previous layer neuron (Figure 4.11).

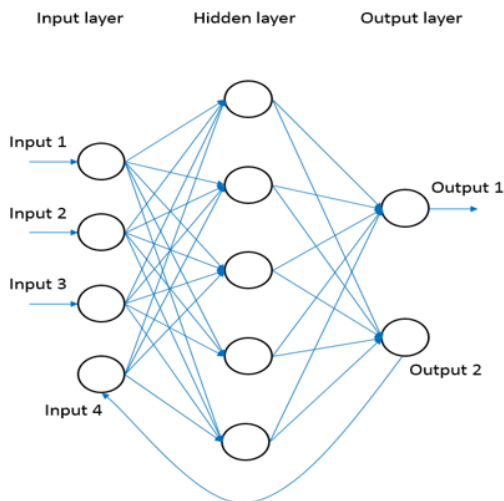


Figure 4.11: Recurrent neural network structure.

#### 4.3.4 Training of a Neural Network

As was discussed earlier, even though artificial neural networks (ANNs) are complicated structures, in essence, the building blocks of such networks are relatively simple. They process records one at a time, and “learn” by comparing their classification of the record (which, at the outset, is largely arbitrary) with the known actual classification of the record. The errors from the initial classification of the first record are fed back into the network, and used to modify the networks algorithm the second time around, and so on for many iterations. Roughly speaking, a neuron in an artificial neural network is,

1. A set of input values ( $x_i$ ) and associated weights  $w_{i,j}$ .
2. A function  $g$  that sums the weights and maps the results to an output  $y$ .

The input layer is composed not of full neurons, but rather consists simply of the values in a data record, that constitute inputs to the next layer of neurons. The next layer is called a hidden layer; there may be several hidden layers. The final layer is the output layer, where there is one node for each class. A single sweep forward through the network results in the assignment of a value to each output node, and the record is assigned to whichever class’s node had the highest value.

In the training phase, the correct class for each record is known (this is termed as supervised training), and the output nodes can therefore be assigned correct values for the node corresponding to the correct class. It is thus possible to compare the network’s calculated values for the output nodes to these “correct” values, and calculate an error term for each output (the “Delta’ rule”). These error terms are then used to adjust the weights in the hidden layers (back propagation, described later on in the chapter) so that in the next iteration, the output values will be closer to the “correct” values. This is one of the main benefits of neural nets where the network can self adjust the weights and biases.

### **The Iterative Learning Process:**

A key feature of neural networks is an iterative learning process in which data cases (rows) are presented to the network one at a time, and the weights associated with the input values are adjusted each time (through various optimization algorithms such as Gradient Descent, Bayesian regularization, ADAM Optimizer). After all cases are presented, the process often starts over again. During this learning phase, the network learns by adjusting the weights so as to be able to predict the correct class label of input samples. Neural network learning is also referred to as “connectionist learning”, due to connections between the units. Advantages of neural networks include their high tolerance to noisy data, as well as their ability to classify patterns on which they have not been trained. The most popular neural network algorithm is back-propagation algorithm proposed in the 1980’s.

Once a network has been structured for a particular application, that network is ready to be trained. To start this process, the initial weights are chosen randomly. Then the training, or learning, begins.

The network processes the records in the training data one at a time, using the weights and functions in the hidden layers, then compares the resulting outputs against the desired outputs. Errors are then propagated back through the system, causing the system to adjust the weights for application to the next record to be processed. This process occurs over and over as the weights are continually refined. During the training of a network the same set of data is processed many times as the connection weights are continually refined.

Note that some networks never learn. This could be because the input data do not contain the specific information from which the desired output is derived. Networks also do not converge if there is insufficient data to enable complete learning. Ideally, there should be enough data so that part of the data can be held back as a validation set.

### **Feed-forward, Back-Propagation:**

The feedforward, back-propagation architecture was developed in the early 1970’s. This independent co-development was the result of a proliferation of articles and talks at various

conferences which stimulated the entire industry. Currently, this synergistically developed back-propagation architecture is the most popular, effective, and easy-to-learn model for complex, multi-layered networks. Its greatest strength is in non-linear solutions to ill-defined problems. The typical back-propagation network has an input layer, an output layer, and at least one hidden layer. There is no theoretical limit on the number of hidden layers but in this research, there are just one or two at most. Some work has been done which indicates that a maximum of five layers (one input layer, three hidden layers and an output layer) are required to solve problems of any complexity. Each layer is fully connected to the succeeding layer.

As noted above, the training process normally uses some variant of the Delta Rule, which starts with the calculated difference between the actual outputs and the desired outputs. Using this error, connection weights are increased in proportion to the error times a scaling factor for global accuracy. Doing this for an individual node means that the inputs, the output, and the desired output all have to be present at the same processing element. The complex part of this learning mechanism is for the system to determine which input contributed the most to an incorrect output and how that element is changed to correct the error. An inactive node would not contribute to the error and would have no need to change its weights. To solve this problem, training inputs are applied to the input layer of the network, and desired outputs are compared at the output layer. During the learning process, a forward sweep is made through the network, and the output of each element is computed layer by layer. The difference between the output of the final layer and the desired output is back-propagated to the previous layer(s), usually modified by the derivative of the transfer function, and the connection weights are normally adjusted using an optimization algorithm. This process proceeds for the previous layer(s) until the input layer is reached.

If  $J(\theta)$  is the cost function associated with the network and  $\theta$  represents the vector of parameters associated with each node, then we must try to find the parameters which

minimize  $J(\theta)$ . In order to use gradient descent or any of the advanced optimizers, we need an algorithm which can take inputs as the parameters  $\theta$  and compute  $J(\theta)$  and the partial derivatives  $-\frac{\partial}{\partial \theta^{(l)ij}} J(\theta)$ .

Suppose we are given one training example  $(x, y)$  for a four layer network. The first step is to implement forward propagation:

$$a^{(1)} = x \tag{4.5}$$

$$z^{(2)} = \theta^{(1)} a^{(1)} \tag{4.6}$$

$$a^{(2)} = g(z^{(2)}) \text{ (add } a_0^{(2)}) \tag{4.7}$$

$$z^{(3)} = \theta^{(2)} a^{(2)} \tag{4.8}$$

$$a^{(3)} = g(z^{(3)}) \text{ (add } a_0^{(3)}) \tag{4.9}$$

$$z^{(4)} = \theta^{(3)} a^{(3)} \tag{4.10}$$

$$a^{(4)} = h_\theta(x) = g(z^{(4)}). \tag{4.11}$$

First we compute  $a^{(1)}$ , the activation of the first layer or the input layer of the network, which is set to  $x$ . Then we compute  $z^{(2)}$  and  $a^{(2)}$ , which is the sigmoid activation function applied to  $z^{(2)}$ . This gives us the activation values for the second layer. Similarly, we apply two more steps of this forward propagation to compute  $a^{(3)}$  and  $a^{(4)}$ , which is also the output of the overall net  $h_\theta(x)$ .

Next, back propagation is applied, where the intuition is that for each node, we are going to compute the error  $(\delta_j^{(l)})$  of node  $j$  in layer  $l$ . So building upon the previous example of a network with four layers,

$$\delta_j^{(4)} = a_j^{(4)} - y_j \tag{4.12}$$

First, we compute the output of layer four with  $\delta_j^{(4)}$ , which is equal to the activation of that unit  $a_j^{(4)}$  minus the actual output that was given in the training example  $y_j$ . Following this,

the  $\delta$  terms for the following layers are computed based on the equations,

$$\delta^{(3)} = (\theta^{(3)})^T \delta^{(4)} \cdot * g'(z^{(3)}), \quad (4.13)$$

$$\delta^{(2)} = (\theta^{(2)})^T \delta^{(3)} \cdot * g'(z^{(2)}). \quad (4.14)$$

Notice that there is no  $\delta^{(1)}$  term as first layer corresponds to the input layer.

### 4.3.5 Optimization Algorithms

The optimization algorithms that were used in this research are Gradient Descent and the ADAM optimizer. A brief background is discussed in this chapter.

**Gradient Descent:** Minimizing any function means finding the deepest valley in that function. The cost function is used to monitor the error in predictions of an ML model. So minimizing basically means getting to the lowest error value possible or increasing the accuracy of the model. The most common cost function is the mean square error:

$$j(\theta) = \frac{1}{m} \sum_{i=1}^m (h_{\theta}(x^{(i)}) - y^{(i)})^2. \quad (4.15)$$

The derivative of this equation with respect to any weight is the gradient computation.

The drawback of gradient descent however, arises with the learning rate. The update expression for each weight is

$$\theta_j \leftarrow \theta_j - \alpha \frac{\partial}{\partial \theta_j} j(\theta). \quad (4.16)$$

Here,  $\alpha$  is the learning rate. The computation of  $\partial J / \partial \theta_j$  (the gradient of weight  $\theta_j$ ) is done iteratively with a step size of  $\alpha$  in that direction, Hence, moving in the direction of the gradient. If  $\alpha$  is too large, the minimum might be overshoot or if  $\alpha$  is too small, the number of iterations might be large.

**ADAM Optimizer:** Adaptive Moment Estimation (ADAM), is a method that computes adaptive learning rates for each parameter. In addition to storing an exponentially decaying

average of past squared gradients, ADAM also keeps an exponentially decaying average of past gradients. We compute the decaying averages of past and past squared gradients  $m_t$  and  $v_t$  respectively as follows:

$$m_t = \beta_1 m_{t-1} + (1 - \beta_1) g_t, \quad (4.17)$$

$$v_t = \beta_2 v_{t-1} + (1 - \beta_2) g_t^2. \quad (4.18)$$

Here,  $m_t$  and  $v_t$  are estimates of the first moment (the mean) and the second moment (the uncentered variance) of the gradients respectively, hence the name of the method. As  $m_t$  and  $v_t$  are initialized as vectors of 0's, they are biased towards zero, especially during the initial time steps, and especially when the decay rates are small (i.e.  $\beta_1$  and  $\beta_2$  are close to 1). These biases are counteracted by computing bias-corrected first and second moment estimates:

$$\hat{m}_t = \frac{m_t}{1 - \beta_1^t}, \quad (4.19)$$

$$\hat{v}_t = \frac{v_t}{1 - \beta_2^t}. \quad (4.20)$$

These are then used to update the parameters yielding the ADAM update rule:

$$\theta_{t+1} = \theta_t - \frac{\eta}{\sqrt{\hat{v}_t} + \epsilon} \hat{m}_t. \quad (4.21)$$

### 4.3.6 Capacity Estimation in Three Cell Pack

In this section we elaborate on how the voltage and surface temperature centroids are used to estimate the OCV curve, using a neural network, and how the estimated OCV can then be used for capacity estimation. ANNs consist of inputs and outputs and are made of interconnected neurons. The weights between the nodes are determined during the training phase, and their values determine how the neural network will respond to a particular time

series of inputs (30). In our approach, we have used a closed-loop (recurrent) neural network. The output is given by

$$y(t) = f(x(t-1), \dots, x(t-d), y(t-1), \dots, y(t-d)), \quad (4.22)$$

where  $f(\cdot)$  represents the behavior of the system under consideration,  $x(t)$  indicates the input time series that consists of temperature and voltage data,  $y(t)$  is the predicted SoC (output), and  $d$  is a positive integer. From past experience we can know that recurrent networks are sufficiently capable of effectively handling many complex non-linearities. The weights in adaptive ANNs continuously adapt, in real time, to changes that occur after training, while non-adaptive ANNs have fixed weights that are determined in the training phase.

The development of the neural network model consists of first using the  $I$ - $V$ - $T$  (current, voltage, temperature) data from a  $Q_i$  test for developing a straight-forward model to predict capacity. Following this the smaller set of centroid data generated from mRPTs is used to facilitate the prediction of capacity without the need for additional  $Q_i$  tests beyond the initial  $Q_0$ .

### Using $Q_i$ Test Data

In this subsection we discuss how the  $Q_i$  test data is used with a neural network trained on  $I$ - $V$ - $T$  data as input and the SoC curve from  $Q_i$  tests as the target output. An SoC curve was generated using Coulomb counting in the manner

$$SoC(t) = SoC(t-1) + \frac{I(t)}{Q} \Delta t. \quad (4.23)$$

After the generation of these two curves, a mean square error reduction step was used to adjust the capacity value  $Q$  in the SoC calculation using Coulomb counting. This step was repeated until the error difference between the two curves was less than 0.05. The capacity value corresponding to the last iteration is the estimated capacity of the battery pack.

The first iteration using this network was carried out using data collected from the tests conducted at ambient temperature 25°C. For training this network, we used the beginning of life characterization test (from  $Q_0$ ), that is, the discharge portion of the first characterization test. After training this network, the voltage and temperature data were fed to the network from the second, fourth, sixth and tenth  $Q_i$  tests to produce the SoC curves. The results of this SoC prediction process are shown in Figure 4.12.

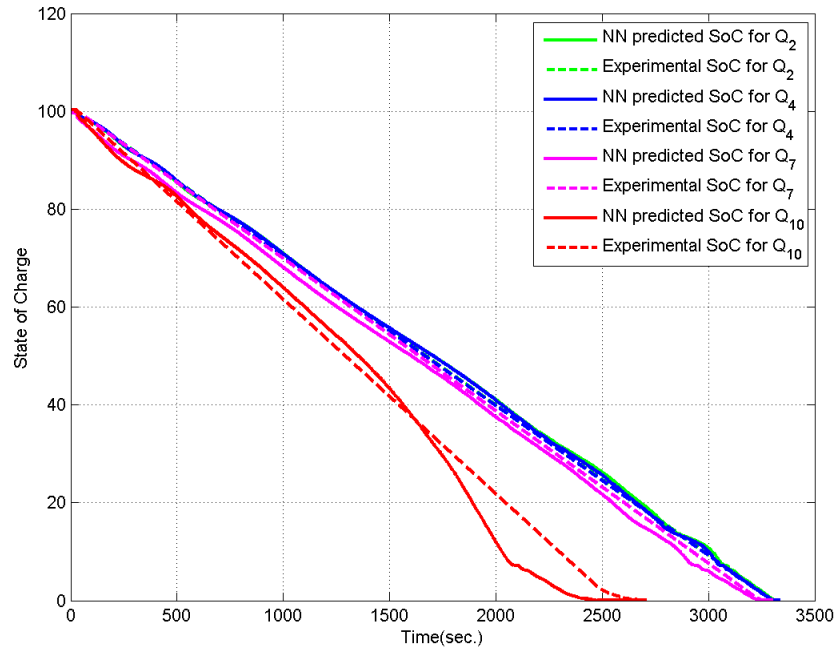


Figure 4.12: Comparison of experimental (“true”) and predicted SoC using full data from  $Q_i$  tests 2, 4, 7, 10.

To generate the second SoC curve we use the equation

$$C = C_{t_1, t_2} = \frac{\int_{t_1}^{t_2} I_{pack}(t) dt}{SoC(t_1) - SoC(t_2)}, \quad (4.24)$$

where  $C$  refers to the capacity of the pack and the interval  $t_1 - t_2$  is the sampling interval in our data acquisition for a frequency of 1 Hz. Once again, to obtain the capacity value, the following mean square error calculation is used iteratively on the two curves until the 0.05

threshold is passed,

$$\frac{1}{n} \sum_{i,j=1}^n (SoC_{NN}(i) - SoC_{CC}(j)), \quad (4.25)$$

where  $SoC_{NN}$  is the SoC curve predicted by the neural network and  $SoC_{CC}$  is the SoC curve obtained using Coulomb counting. The resulting capacities obtained in this process are summarized in Table 3.2.

Table 4.1: Capacity estimation results using full  $Q_i$  test data.

Test No.	Estimated Capacity	True Capacity
2	1.984	2.004
4	1.996	1.998
7	1.963	1.970
10	1.520	1.540

### Using mRPT Data

The results of the previous subsection required full data from  $Q_i$  tests for training, SoC prediction and capacity prediction. As explained previously, our motivation lies in typical run scenarios for electric propulsion systems, because of the relative ease in obtaining short duration charge or discharge pulses of current from the data recorded in normal use on a day-to-day basis. Thus, the process developed above has brought us to the point whereby in this subsection we use data from the initial  $Q_0$  test to generate an SoC output target for training only, and data generated from the clustered mRPTs for training and prediction. To do this, functional values from the fourth-order polynomial fit on the cluster centroids of surface temperature and voltage are used as inputs to the neural network to predict SoC curves, using the SoC curve from  $Q_0$  test as a target output.

The calculations from this process are shown in Figure 4.13, where we see a comparison of the experimental results (SoC plots obtained from the  $Q_i$  tests) and SoC plots that have been predicted by the neural network from the clustered temperature and voltage mRPT

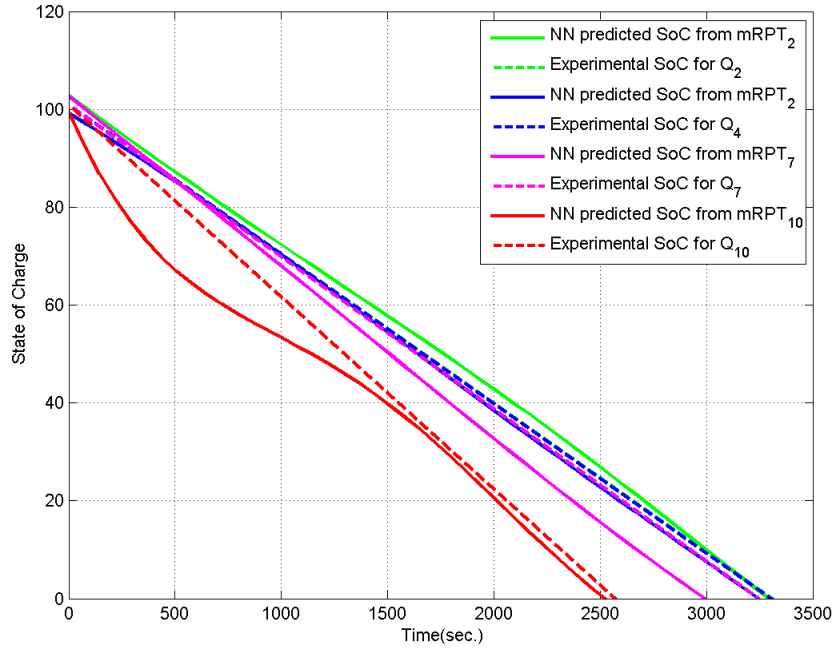


Figure 4.13: Comparison of experimental (“true”) and predicted SoC using mRPT tests 2, 4, 7, 10.

data. It is worth mentioning here that as long as the pack holds its capacity within 70% of its initial value, we obtain reasonably accurate capacity predictions. Once the capacity drops below 70%, the trends in the voltage and temperature clusters start deviating and as a result the neural network predictions produce larger errors.

Finally the capacities obtained using the mean square error criteria mentioned earlier are presented in Table 4.2. A comparison with the results using the full  $Q_i$  tests for training, SoC prediction and capacity prediction (see Table 4.1) reveal that the methodology comprised in the supervised learning with data clustering for the mRPT data performs reasonably well.

### 4.3.7 Capacity Estimation in Automotive Grade Battery

As is evident from Figure 4.6, the capacity fade patterns are much more pronounced in the lower SoC ranges. Hence, keeping in view the aim of reducing the volume of data utilized

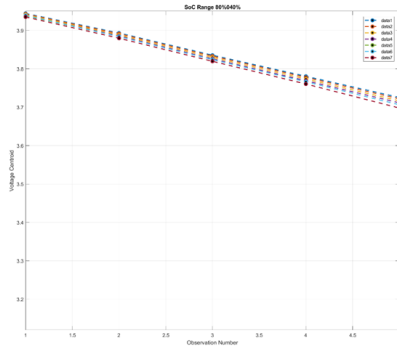
Table 4.2: Capacity estimation results using mRPT data.

Test No.	Estimated Capacity	True Capacity
2	2.011	2.004
4	1.981	1.998
7	1.949	1.970
10	1.522	1.540

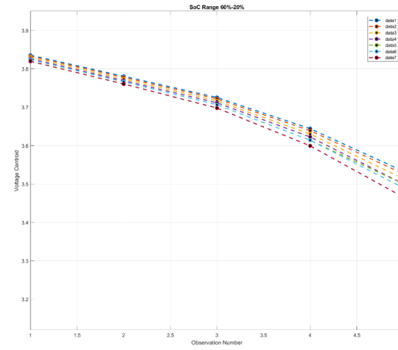
in estimation of capacity fade, the same procedure outlined for the three cell pack utilizing the mRPT data is applied to this automotive data set with the only difference being that the algorithm was applied to different ranges of SoC rather than to only one range of 100% to 50% SoC. The ranges that have been considered are 80% to 40%, 60% to 20% and 50% to 10%.

From the observations that were made on the three cell pack, it was evident that more features needed to be incorporated into the estimation approach so as to pick up on the minute changes in capacity fade trends. Hence three features were considered, voltage, temperature and internal resistance ( $R_0$ ). The behavior of these features in the different ranges is highlighted in Figures 4.14, 4.15 and 4.16. In the case of the voltage centroids, in any SoC range, it is evident that the centroids show expected variations with the drop in capacity, i.e., the lower SoC ranges show a higher drop with the same current pulses. The temperature centroids have a consistent behavior throughout. Temperature rises slightly in the lower SoC ranges, but does not show large variations with capacity. In  $R_0$ , in the highest SoC range, there is no visible change in  $R_0$ , but with mid range and lower range of SoC, we start seeing significant changes in  $R_0$ . This observation helped in making the decision to include  $R_0$  as a feature for the estimation using the automotive data set.

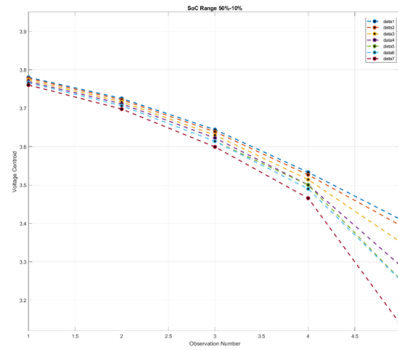
In the estimation approach using the neural net, similar to what was done in the case of the three cell pack, the net was trained in the beginning of life data with the centroids being curve fitted with a fourth order polynomial with the voltage and temperature centroids along with  $R_0$  are the inputs in this case and the SoC curve corresponding to the  $Q_i$  test, implemented directly before the HPPC test are used as the targets.



(a) Voltage centroids in the range of 80%-40%.



(b) Voltage centroids in the range of 60%-20%.



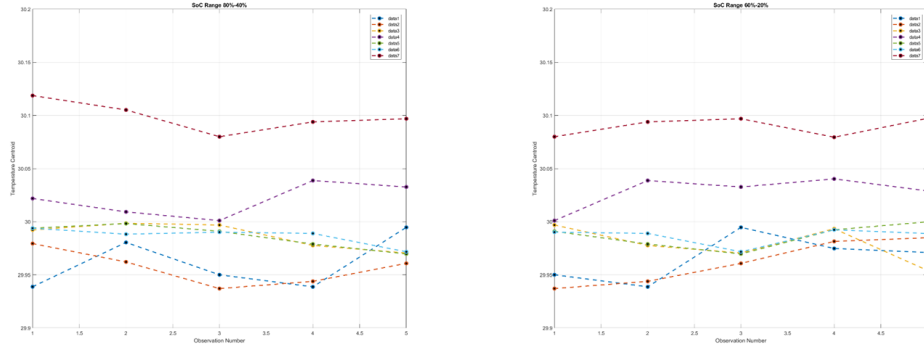
(c) Voltage centroids in the range of 50%-10%.

Figure 4.14: Behavior of Voltage centroids.

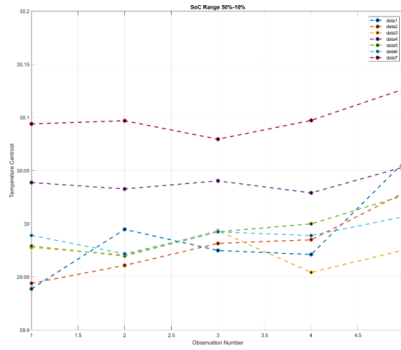
As a final step, the capacities obtained using the mean square error criteria using the three cell pack are used for the automotive cell as well and comparison of results of capacity estimation at different SoC ranges is shown in Tables 4.3, 4.4 and 4.5. This is followed by a brief discussion on how these SoC ranges can be used for estimation in different stages.

Table 4.3: Capacity estimation results in the SoC range 80% to 40%.

Test No.	Estimated Capacity	True Capacity	% Error
2	14.201	14.133	0.48
4	14.024	13.645	2.77
7	13.587	13.16	3.24



(a) Temperature centroids in the range of 80%-40%. (b) Temperature centroids in the range of 60%-20%.



(c) Temperature centroids in the range of 50%-10%.

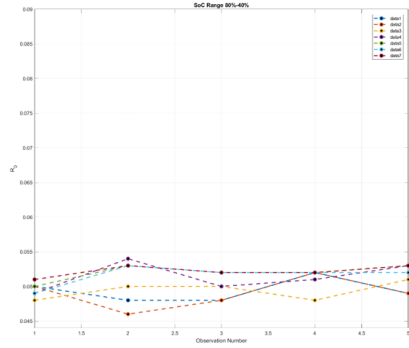
Figure 4.15: Behavior of Temperature centroids.

Table 4.4: Capacity estimation results in the SoC range 60% to 20%.

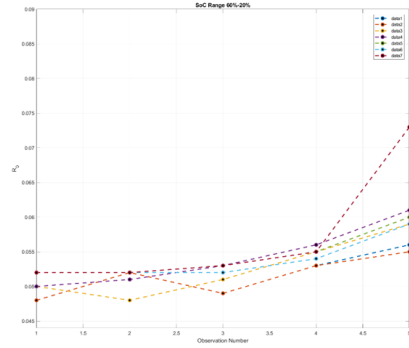
Test No.	Estimated Capacity	True Capacity	% Error
2	14.191	14.133	0.41
4	13.919	13.645	2.08
7	13.42	13.16	2.01

From the Tables 4.3, 4.4 and 4.5, the main observations are:

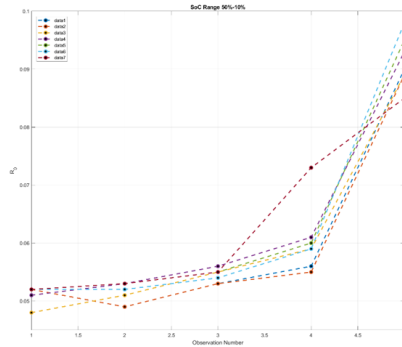
1. In the highest SoC range the initial prediction is acceptable but as the battery loses capacity the error margin increases.
2. In the second SoC range, the error margins are similar throughout.



(a)  $R_0$  in the range of 80%-40%.



(b)  $R_0$  centroids in the range of 60%-20%.



(c)  $R_0$  centroids in the range of 50%-10%.

Figure 4.16: Behavior of Internal Resistance  $R_0$ .

Table 4.5: Capacity estimation results in the SoC range 50% to 10%.

Test No.	Estimated Capacity	True Capacity	% Error
2	14.185	14.133	0.367
4	13.896	13.645	1.84
7	12.851	13.16	2.34

- In the lowest range, accuracy is good but as the battery loses capacity, we have one pulse in the HPPC test which goes into CV mode hence deviating from the trend and hence the error increases.
- This comparison shows that the use of data from different SoC ranges can give good prediction accuracy depending upon which stage the battery is in its life-cycle.

5. The clarity and accuracy in the data plays a factor as is evident from the accurate estimation using the automotive data compared to the non-automotive data.

#### 4.4 On-Board Estimation

Attributed to the growing interest in using real-time estimation of capacity fade (48; 49), as a next step in the evolution of using supervised estimation using  $Q_i$  and mRPT data sets, in this section we investigate implementation of our estimation concepts on an embedded microcontroller. The focus of this step is to take the approaches to the next level by demonstrating feasibility of implementation on a readily-available single-board computing environment (Raspberry Pi). The data sets used are the  $Q_i$  and mRPT sets generated on the non-automotive Turnigy pack at 25°C. This development provides the next step in the evolution toward the ultimate goal of using cloud based monitoring and computing for effective real-time capacity estimation in EVs while fulfilling the requirement of reduced memory and data loads (50).

##### 4.4.1 Proposed Embedded System

Because the microcontroller chosen will ultimately be required to coexist within a vehicular system to estimate capacity using data-driven models, it must possess a few vital characteristics. For example, it must interface easily with the vehicle communication network, and it must consume the least amount of power as possible. What's more, it must be able to run supervised learning algorithms adequately. The Raspberry Pi addresses all these characteristics as well as being cost effective and readily available, and even supports machine learning frameworks and libraries such as TensorFlow and Keras, making it the one of the most favorable for the intended application. Important specifications of Raspberry Pi 3 Model B relevant to this purpose are: quad core 1.2GHz 64-bit processor; 1GB RAM; on

board Wireless LAN and Ethernet; multithreading support; and, Micro SD port for data storage.

This single-board computing system also runs the Raspbian Operating System (OS), which is a debian based OS that is optimized specifically for the Raspberry Pi. The system supports a wide range of packages that provides easy interfacing with additional hardware.

#### 4.4.2 Algorithm Implementation

Implementation on the single-board microcontroller for this work requires a streamlined version of algorithms described in the previous sections of this chapter, with reconfiguration using TensorFlow and Keras. This approach basically takes simple and uncomplicated methods from the domain of supervised learning and uses them to extract relevant information from characterization and reference performance tests in order to reduce the computational and memory stresses, all the while maintaining prediction standards. The features focused upon here are the voltage and temperature centroids during discharge.

Estimating capacity through characterization ( $Q_i$ ) and mRPT data sets, deep neural networks were developed on Keras with TensorFlow back-end. These networks were provided with two inputs consisting of the curve fitted clustered voltage and temperature data, whereas targets were the 100% to 0% SoC data corresponding to the specific  $Q_i$  test.

The algorithmic steps adopted here are identical to the steps outlined previously, with adjustments for real-time implementation. Two estimations are carried out in the proof-of-concept implementation: the first was done on the  $Q_i$  data set with the application of the neural nets, then the second was done on the mRPT data set with data pre-processing through K-means clustering, followed by neural net based regression for prediction.

The specifics and details pertaining to the networks used as implemented on the single-board computer for this application are described in the following subsections.

### 4.4.3 Estimation Results

**Using  $Q_i$  Test Data:** Nominally, for use with the full set of  $Q_i$  test data, the feedforward network implemented consists of two hidden layers of 10 and 4 neurons, respectively, followed by an output layer of a single neuron. For the training of the network, only the initial  $Q_i$  test data is utilized, providing the “beginning-of-life” capacity of the pack. Thus, only the initial set is used in training whereas estimation for capacity following that initial test is carried out with a stream of input data from the second  $Q_i$  test through to test 11. To mimic real-time implementation, as for example will be done on the targeted electric vehicle for this project, data is input to the network in a continuous fashion using a set sample time.

After training, real-time data flows into the network and the outputs consisting of a predicted stream of continuous values are curve fitted for the SoC values to range between  $[0, 100]$ . Because the SoC curve corresponds to the 1C discharge rate, the total time taken for discharge is used to calculate the battery capacity. In other words, the capacity of the battery pack is estimated by summing the currents from the entire discharge cycle.

The estimated capacity numbers and the total time taken for the discharge are given in Table 4.6. The % Error is computed between estimated ( $C_e$ ) and true capacity ( $C_t$ ) values.

Table 4.6: Capacity estimation results using  $Q_i$  data.

Test No.	Discharge time for $C_e$ (s)	Estimated Capacity ( $C_e$ ) (Ahr)	Discharge time for $C_t$ (s)	True Capacity ( $C_t$ ) (Ahr)	% Error
2	3328	2.033	3250	1.986	2.39
3	3290	2.010	3310	2.022	0.60
4	3300	2.016	3323	2.030	0.69
5	3176	1.940	3275	2.001	3.02
6	3213	1.963	3281	2.005	2.07
7	3214	1.964	3332	2.036	3.54

**Using mRPT Data:** To perform the SoC estimation with reduced data (mRPT), a two step process is followed: (i) The reduced set of data points are reduced further to centroids

using standard K-means clustering technique, and (ii) the centroids are then used with a curve fitting approach to form an input to the network to estimate the SoC values.

After clustering, the neural network is employed to predict SoC values from the reduced mRPT data represented by centroid curves. In contrast to the network used for prediction using the  $Q_i$  data, a deeper and wider neural network is utilized for the clustered data by adding an additional layer and more neurons at each layer, resulting in better extraction of features from the reduced data fed to the network for training. The network has three hidden dense layers with 10, 60 and 10 neurons, respectively, followed by a single neuron output layer.

Data obtained from fitting the fourth order polynomial on voltage and temperature centroids are fed as input to the neural network and SoC curves obtained from corresponding  $Q_i$  tests are set as targets.

As with the full set of data, for training only data from the initial test cycle is used. That is, in this case the centroids generated from the first mRPT are taken in training, whereas prediction after that the centroids generated from the subsequent mRPTs are used. The output values generated by the network are curve fitted to range between  $[0, 100]$  to generate the predicted SoC curve. The results are summarized in Table 4.7, representing the estimated and true SoC curves, while the corresponding percentage errors are calculated in a fashion similar to Table 4.6.

Table 4.7: Capacity estimation results using mRPT data.

Test No.	Discharge time for $C_e$ (s)	Estimated Capacity ( $C_e$ ) (Ahr)	Discharge time for $C_t$ (s)	True Capacity ( $C_t$ ) (Ahr)	% Error
2	3175	1.940	3250	1.986	2.30
3	3376	2.063	3310	2.022	1.99
4	3373	2.061	3323	2.030	1.50
5	3293	2.012	3275	2.001	0.54
6	3240	1.980	3281	2.005	1.24
7	3205	1.958	3332	2.036	3.81

#### 4.4.4 Discussion

In the evolution of this capacity fade prediction research of the authors, this subsection focuses on a streamlined implementation intended ultimately for on-board real-time application of algorithms and approaches established earlier. Thus, a few points of comparison should be highlighted:

1. Actual computing times on the Raspberry Pi for prediction of the battery pack capacity on  $Q_i$  and mRPT data sets are approximately 0.22 seconds and 0.38 seconds, respectively.
2. It can be observed that the percentage error in capacity estimation remains reasonably good until the 6th test cycle. Note that after this point, the SoC prediction curves begin to drift from the true SoC, coinciding with increased errors in capacity estimation. Nonetheless, an argument can be made that this on-board application provides favorable results within permissible limits that would be experienced in normal operation.

#### 4.4.5 Memory Considerations

An important factor to be considered in designing of neural nets for embedded platforms is their limited memory availability. Raspberry Pi model B has a maximum of 927 MB of memory available for user processes (out of 1 GB total). Keeping this in mind, the neural nets developed for capacity estimation using  $Q_i$  and mRPT tests were designed to have a lower memory footprint. The memory consumption patterns are summarized in Table 4.8, in which the second column gives the percentage of the total available memory occupied by the untrained network, whereas the third column gives the percentage memory occupation after training is completed. Finally, the fourth column gives the percentage change in memory consumption prior to training and after training.

Table 4.8: Memory Consumption.

Test	Memory Before Training (%)	Memory After Training (%)	Change (%)
$Q_i$	12.72	21.35	67.79
mRPT	12.72	21.57	69.49

#### 4.4.6 Future Scope

With the satisfactory on-board application of the data-driven capacity estimation approach, a number of possibilities are facilitated for the next steps in the evolution of the work. The real time capability of the prediction algorithm and the ability of a single-board computing system as simple as the Raspberry Pi to implement complicated training and prediction algorithms points to the next step: receive data from a vehicle Controller Area Network (CAN) through the Serial Peripheral Interface (SPI). Therefore, this platform is well-suited for deployment inside an electric vehicle for capacity estimation. With this capability in hand, the next step for the group at UT Dallas is to utilize this platform in an actual on-board application for a Polaris GEM e4 electric vehicle. The effective battery management capabilities of this work will contribute to the broader goals of the ongoing GEM e4 vehicle project, which include autonomy and sensor fusion.

Another element in the future scope of this work is the introduction of on-board cloud connectivity. Training the neural networks nominally requires approximately 650 seconds and 940 seconds for  $Q_i$  and mRPT test data, respectively. Therefore, by leveraging the Raspberry Pis Wireless Fidelity (WiFi) (BCM43438 WiFi/Bluetooth up to 72.2 Mbps net throughput) capability, real time data obtained from the vehicles CAN may be transmitted to the cloud wherein data may be stored, and with cloud computing the network models may be tuned and even trained. Fine-tuned models can then be exported back to the on-board computing system, facilitating further computation in the cloud for improved prediction based on live incoming battery data. Because most microcontrollers rely on external data storage such as

SD cards, such a distributed process would reduce the burden on the microcontroller both in terms of computation as well as memory requirements.

## 4.5 Summary

Prediction and estimation of capacity fade in batteries and battery packs is a challenging problem due to the complexity of the relationship between many characteristics and features present in the battery pack system. Moreover, the amount of aging data required over long time intervals complicates the problem further, particularly because of the expensive and reliable testing environments required. The first step of this research reported in this chapter has shown very promising results for a methodology whereby simple ideas from machine learning are used to not only reduce the amount of data required in prediction of capacity fade, but also to shift reliance to more accessible data in typical battery pack operation scenarios. Such methodologies readily facilitate the incorporation of pack temperature data, a factor not seen in typical studies of this nature.

The research following this work is focused on several important off-shoots where the ultimate goal in capacity fade estimation, and prediction of general state of health for battery packs, is to be able to use typical drive cycle data for learning and prediction.

Therefore, with this goal in mind, we focus on the use of data types gleaned from typical drive cycles or data which can be easily generated during operation of a battery pack in a normal day of use and charging. To do this, we feel that further training data with relevant information will be needed along with larger or more complicated networks incorporated into the machine learning environment. Of course, our primary application for these ideas lies in vehicle propulsion systems, so the aim throughout will be to evolve this effort to investigate data from automotive-quality batteries and packs in terms of drive cycles. Hence in the next chapter, a discussion is presented upon the efforts that were made into using drive cycle data for capacity estimation, and ultimately to explore the idea of synthetic data generation.

## CHAPTER 5

### CAPACITY ESTIMATION USING DRIVE CYCLES <sup>1</sup>

#### 5.1 Introduction

From a model based estimation point-of-view, as highlighted earlier, the chemical reactions are numerous in number, which in turn makes simulating them computationally cumbersome and convoluted. Model based techniques such as equivalent circuits as well as other analytical techniques have been explored extensively in the literature (19)-(20). A discussion of these approaches has been presented in Chapter 4, upon which this work evolved. Along with having restrictions of accuracy during varied current pulses and over emphasis on the OCV measurements, a troublesome drawback of such approaches is the trade-off between model accuracy versus computational complexity. Data-driven estimation approaches such as neural networks have gained popularity in recent times (26), (52), (53), (54) and have been able to make progress on the issue of having to consider many factors to effectively provide estimation in a timely fashion. The most significant drawback with supervised learning approaches is the variety and volume of data required for training, in turn leading to a cascading issue of requiring round the clock testing for generating reliable data. As was highlighted previously, the expenditures in terms of equipment, man-hours and time serve as the major deterrents to advancement in such estimation approaches.

As a logical next-step in this investigation into using supervised learning approaches in determining capacity fade in battery packs, this chapter addresses the issue of the quantity and characterization of data needed for capacity fade estimation. In the approach adopted for estimating capacity fade in the last chapter, features are reduced to centroids and trends among these centroids are used to estimate capacity. With the capability of reducing features

---

<sup>1</sup>©2018 IEEE. Portions Adopted, with permission, from M. Pyne, B. J. Yurkovich, S. Yurkovich, "Toward the Use of Operational Cycle Data for Capacity Estimation," IEEE Conference on Control Technology and Applications (CCTA), August 2018.

to individual points, the ability of analyzing large volumes of data without the need for large volumes of computational memory has become a reality. This has moved the analysis toward using operational data for training of “feature generators”, thereby reducing the quantity of experimental data used and moving toward the goal of eliminating the requirement for additional characteristic capacity determination tests in the process.

In what follows, we first discuss the test data used, followed by a brief summary of the process for generating features (voltage, temperature and  $R_0$ ) for a reference performance test using a simple rule-based machine learning methodology for constructing feature generators. This is followed by results of capacity fade estimation using a neural net based SoC curve estimation, following in the evolution of the prediction philosophy presented in (51).

For the study presented in Chapter 4, emphasis was placed on extracting useful and effective information in terms of features from operational data as well as specific reference performance tests, with a focus on reducing the total amount of data required and computational stress. This was achieved through  $K$ -means clustering of the data, whereas two features were considered, namely, voltage and temperature change during discharge.

While providing promising results, Chapter 4 relied on feature extraction from the mRPT tests. These mRPT tests consisted of more dynamics than a capacity test, although shorter in duration, and resembled a formal structured HPPC test. In this chapter we shift our attention to the use of data from typical operational cycles, with no particular conformity to standardized tests, while using the same methodology. That is, the data used will represent a variety of current pulses and responses over typical operational envelopes. A machine learning model is proposed which utilizes a rule-based selection structure to segment the training data for training of several neural networks (feature generators). The motivation for segmenting the data and moving to multiple nets is to avoid over-fitting and to make predictions within bounds by restricting the regions of the training set. While such a segmentation allows better resolution in the modeling for different regions in the operational

range of the battery, some added complexity results with simple rules and multiple neural nets. However, the feature generators (multiple nets) are smaller in size than an overall net for the entire region, where each net is focused on a training set from specific regions in the operational data. Added benefits are that memory requirements can be segregated, and over-fitting sometimes seen in the use of deep neural networks is avoided as much as possible.

### 5.1.1 Feature Generation

The process for generating features consists of two components cascaded together. The first part employs a rule base whereas the second employs machine learning through a set of multiple neural nets.

#### Rule-Based Selector

In implementing a rule-based strategy, fuzzy logic provides the ability to methodologically express and exercise heuristic knowledge of how a system responds to perturbation. The fuzzy rule-based selector strategy here uses two inputs: (i) the capacity of the battery when training data is collected, and (ii) the state of charge (SoC) at which each of the pulses in the training set begins. To accomplish this, we have segmented the capacity of the battery pack into three ranges: 0.5 to 1.6 Ah, 1.6 to 1.8 Ah and 1.8-2.2 Ah. Also, the complete SoC range of 0 to 100% has been divided into four equal ranges of 25%. With combinations of inputs over these ranges through rules such as “If capacity is low (0.5 to 1.6 Ah range) and SoC is low (in 0-25%), then select net  $M$ ,” a total of twelve artificial neural networks are created, which are trained (based on the inputs to the rule-based selector) on different segments of the training data.

The membership functions used for both inputs are Gaussian and the ones used for the output are triangular. That is, a typical Gaussian membership function  $M_G$  is expressed by

$$M_G(x; c, \phi) = e^{-\frac{1}{2}\left(\frac{x-c}{\phi}\right)^2}, \quad (5.1)$$

where  $c$  represents the center and  $\phi$  the width of the membership function, respectively. A typical triangular output membership function  $M_T$  can be implemented with

$$M_T(x; a, b, c) = \max\left(\min\left(\frac{x-a}{b-a}, \frac{c-x}{c-b}\right), 0\right) \quad (5.2)$$

where  $a < b < c$  determine the x-coordinates of the three corners of the underlying membership functions.

### Feature Generators

It is challenging to derive methodology that solves problems under highly non-linear conditions in a cluttered scene, such as recognizing a multi-dimensional object (55). Even with a good process defined, the resulting code might be extremely complicated. From a machine learning point-of-view, instead of writing a program for each specific task, a collection of examples that specify the correct output for a given input can be used to generate a program which can effectively model complex relations between variables. The program produced by the learning algorithm may look very different from a standard hand-written program. But, if done effectively, the program applies to new cases as well as the ones upon which it was trained. Also, such a process would afford the ability for the program itself to adjust with changing data by training on new data. This flexibility of using data-driven learning based approaches has led us to using recurrent neural networks for the purposes of predicting behavior through features with changing C-rates such as the internal resistance and SoC.

In this study we propose the use of twelve closed-loop (recurrent) neural networks as feature generators, each with three layers (input, hidden and output layers). For the purposes of training, the network uses the Bayesian regularization back-propagation algorithm, which has  $n$  inputs  $x_i$ ,  $i = 1, \dots, n$ ,  $m$  outputs,  $s = 1, \dots, m$ , and  $l$  neurons in the hidden layer. The outputs of the neurons in the hidden layer are  $z_j$ ,  $j = 1, \dots, l$ . The activation functions of the neurons in the hidden layer are  $f_j^h : \mathbb{R} \rightarrow \mathbb{R}$  and the activation for the neurons in the output

layer are  $f_s^o : \mathbb{R} \rightarrow \mathbb{R}$ , where  $j = 1, \dots, l$  and  $s = 1, \dots, m$ . The weights from the inputs to the hidden layer are  $w_{ji}^h$  and those from the hidden to the output layer are  $w_{sj}^o$ . The output from the  $s^{th}$  neuron of the output layer is

$$y_s = f_s^o \left( \sum_{j=1}^l w_{sj}^o z_j \right). \quad (5.3)$$

Therefore the relationship between the inputs  $x_i, i = 1, \dots, n$ , and the  $s^{th}$  output  $y_s$  is given by

$$y_s = f_s^o \left( \sum_{j=1}^l w_{sj}^o \left( \sum_{i=1}^n w_{ji}^h x_i \right) \right) = F_s(x_1, \dots, x_n). \quad (5.4)$$

The networks implemented consist of three layers: input, hidden and output, with the hidden layer having 10 neurons. The inputs and targets of the complete model are summarized in Table 5.1.

Table 5.1: Features

Input	SoC starting point of each discharge pulse C-rate of discharge pulse
Target	Voltage and Temperature centroids, and $R_0$

The overall training set for the model is the complete set of all the drive cycles that were implemented during the complete life the battery pack, where the concept is to emulate continuous training during normal operation. The number of drive cycles in each of the capacity ranges (input 1) are shown in Table 5.2.

Table 5.2: Training data

0.5 to 1.6 Ah	20 drive cycles
1.6 to 1.8 Ah	10 drive cycles
1.8 to 2.2 Ah	80 drive cycles

In order to reduce the data load further, we have used the voltage ( $\Delta V_c$ ) and temperature ( $\Delta T_c$ ) centroids and the calculated internal resistance ( $R_0$ ); these represent outputs of the

feature generators. The centroids are calculated using K-means clustering as described in Chapter 4. This clustering algorithm separates data into the best suited groups based on the information available. Data is separated in different clusters, which are usually chosen to be far enough apart from each other spatially, in Euclidean distance, to be able to produce effective data mining results. Each cluster has a center, called the centroid, and a data point is clustered into a certain cluster based on how close the features are to the centroid.

The objective function for the K-means clustering algorithm is

$$J = \sum_{i=1}^k \sum_{j=1}^n (||x_i - v_j||)^2 = 1 \quad (5.5)$$

where  $||x_i - v_j||$  is the Euclidean distance between a point  $x_i$  and a centroid  $v_j$ , iterated over all  $k$  points in the  $i^{th}$  cluster, for all  $n$  clusters.

For calculating the internal resistance  $R_0$  we employ the widely-used Randles first order model (56). It consists of an ideal voltage source represented by open circuit voltage ( $V_{OCV}$ ), ohmic internal resistance ( $R_0$ ) (57) which is in series with a parallel resistor-capacitor ( $R_1 - C_1$ ) branch. The single resistor ( $R_0$ ) models an instantaneous response (instant voltage drop) while the parallel R-C branch ( $R_1, C_1$ ) accounts for the transient response (an exponential voltage decay). For calculating the  $R_0$  values, we considered the range between the beginning of the pulse and four data points after the pulse started.

The terminal voltage is given by

$$V(t) = V_{OCV}(t) - R_0 I(t) - V_{RC} = R_1(1 - e^{(t/R_1 C_1)}) . \quad (5.6)$$

For validation of the feature generators, we will use a selected set of mRPT tests at different stages of the life cycle of the battery pack. The details of this training-testing are discussed in the next sections.

## 5.2 Validation

In order to predict the behavior of  $\Delta V_c$ ,  $\Delta T_c$  and  $R_0$ , we trained the feature generators using a training data set of 110 drive cycles with capacity, current C-rate and SoC as the inputs, and  $\Delta V_c$ ,  $\Delta T_c$  and  $R_0$  as the target outputs. For validation, we picked four out of the five discharge pulses from the mRPT tests performed after the 2nd, 4th, 7th and the 10th  $Q_i$  tests, thus giving us a good range of capacity degradation. The comparison between the predicted and experimental targets are shown in Figures 5.1, 5.2 and 5.3.

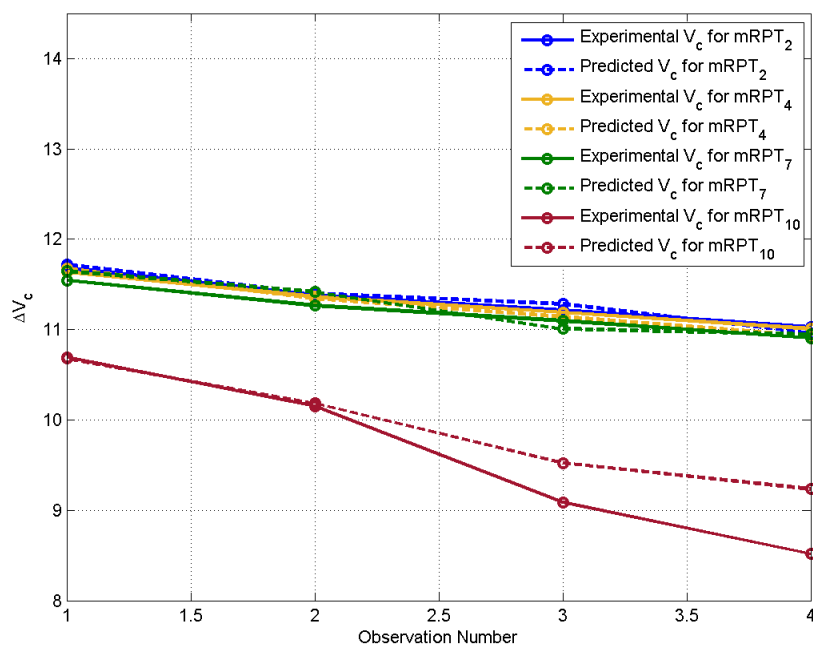


Figure 5.1: Comparison of predicted (dashed) and experimental  $\Delta V_c$ .

## 5.3 Capacity Estimation Results

For estimating the capacity of the battery pack we employ here the methodology introduced in Chapter 4. We have used  $\Delta V_c$  and  $\Delta T_c$  along with  $R_0$  to estimate the SoC curve of the  $Q_i$  test as the target. In the previous work we had used  $\Delta V_c$  and  $\Delta T_c$ , and suggested the

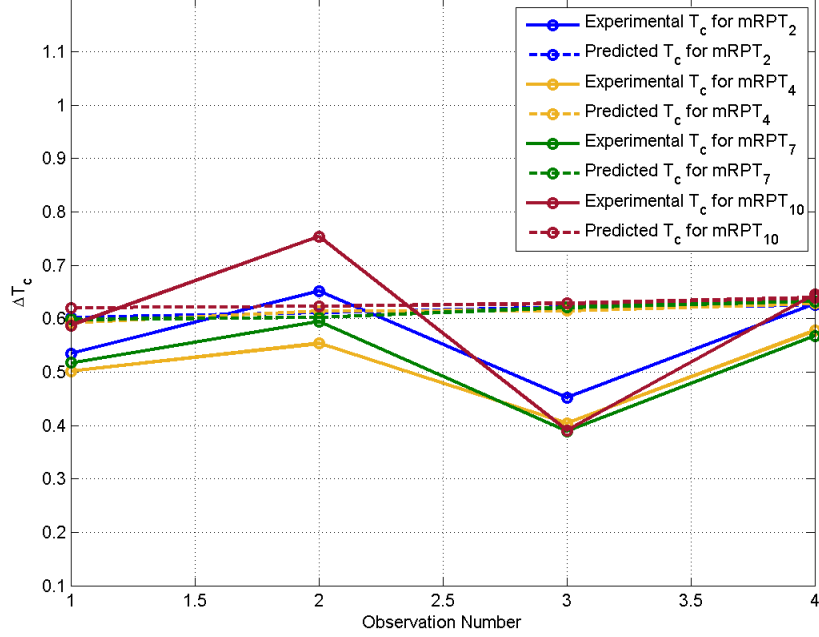


Figure 5.2: Comparison of predicted (dashed) and experimental  $\Delta T_c$ .

possibility of exploring other features. In this regard, for this chapter we introduce  $R_0$  as an additional feature along with SoC starting points and C-rates.

To determine the capacity, another RNN is trained using as inputs the functional values of a third-order polynomial fit on the centroids predicted by the feature generators. The target (model output) is the SoC curve of the  $Q_1$  test, which was the first capacity test done in order to determine beginning-of-life capacity. We generate a second SoC curve by using the Coulomb counting equation for a current pulse of 1C 100 to 0% SoC single discharge,

$$SoC(t) = SoC(t-1) + \frac{I(t)}{Q} \Delta t, \quad (5.7)$$

and iteratively change the capacity term in the equation until the mean square error between the two curves,

$$\frac{1}{n} \sum_{i,j=1}^n (SoC_{NN}(i) - SoC_{CC}(j))^2, \quad (5.8)$$

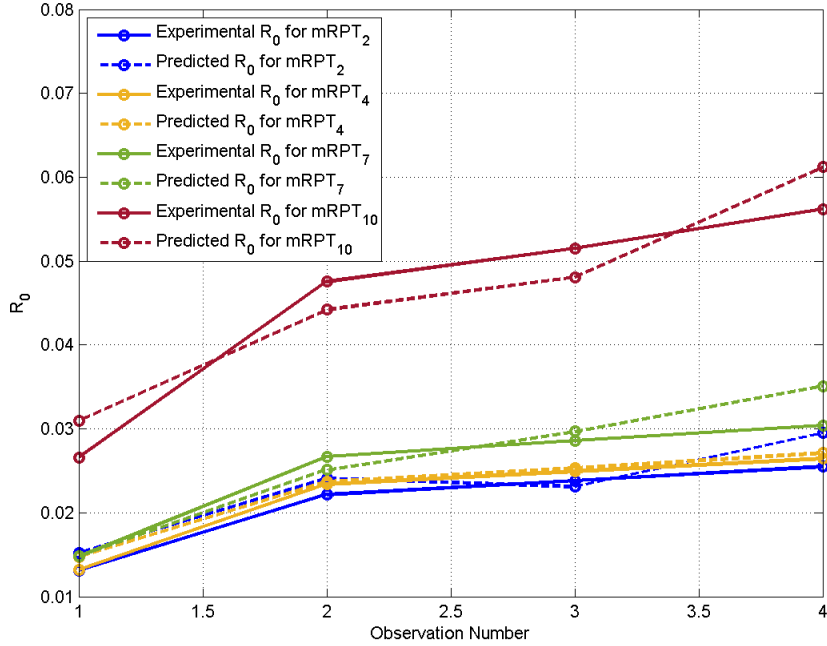


Figure 5.3: Comparison of predicted (dashed) and experimental  $R_0$ .

is below a threshold of 0.05, where  $SoC_{NN}$  is the SoC curve predicted by the neural network and  $SoC_{CC}$  is the SoC curve obtained using Coulomb counting.

To estimate capacity with this model (additional RNN trained in the fashion described above), outputs of the feature generators corresponding to the mRPTs 2, 4, 7, 10 are used as inputs. The predicted SoC curve from this exercise is compared with the SoC curve from the Coulomb counting method as in (5.8) to obtain a capacity value.

The results from this process are shown in Figure 5.4, where we see a comparison of the experimental results (SoC plots obtained from the  $Q_i$  tests) and SoC plots that have been predicted by the neural network from the clustered  $\Delta V_c$ ,  $\Delta T_c$  and  $R_0$  data. The supervised machine learning procedure relies heavily on the accuracy of data. Hence, pre-processing the data and ensuring the inputs to the models are free of noise and outliers is an important step. To eliminate such issues, a fixed initial upper voltage level of 12.48V is used, which is taken to be 100% SOC.

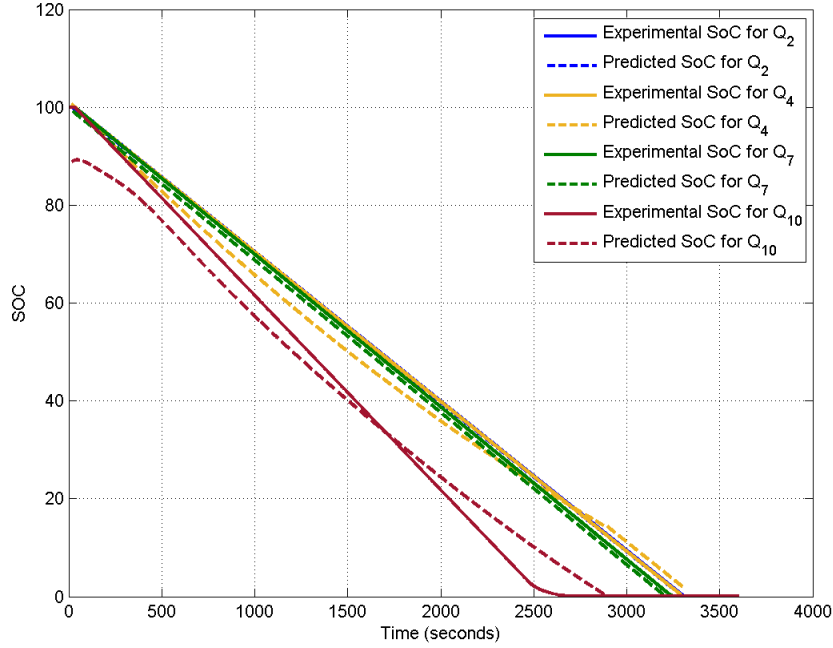


Figure 5.4: Comparison of predicted (dashed) and experimental SoC.

Results and comparison for the capacity estimation approaches of this work and that of Chapter 4 are tabulated in Table 5.3. In the table, three figures are presented, the true capacity obtained from the  $Q_i$  tests, the estimated capacity obtained from the mRPT feature based estimation, and the estimated capacity obtained using the drive cycles.

Table 5.3: Comparison of capacity estimation results using drive data.

Test No.	True Capacity ( $Q_i$ )	Est. Capacity (mRPT)	Est. Capacity (Drive cycle)
2	2.004	2.011	2.036
4	1.998	1.981	1.967
7	1.970	1.949	1.961
10	1.540	1.522	1.667

As seen in the table, results of this approach compare favorably to the true capacity results as well as to the results of Chapter 4. Once a significant degradation has occurred (for example, when the battery enters a state of failure), estimation of capacity is challenging

because features tend to become unruly and deviate in unpredictable ways from typical trends. Because our goal was to investigate the concept of limited amounts of data from profiles that resemble typical drive cycles, we conclude from these results that the approach is effective.

## 5.4 Summary

In this chapter we presented the next step in the study of capacity estimation in Li-ion battery packs. Our focus in this evolution has been on managing the amount of data required to predict capacity fade. Relying on experimental data from a commercially available, low power battery pack, we have employed machine learning techniques with the intent of continuously learning battery characteristics through available features and typical measurements. For this study, we were able to achieve proof of concept for an estimation and modeling approach that essentially uses operational data (“drive cycles” for our experimental pack). The trade-off in complexity to achieve this was to segment the data through a rule-based control scheme, for training of multiple neural nets, although the size of the individual nets in each case was maintained to be reasonably small. Results obtained compared favorably to our previous results using data from specially designed reference performance test profiles.

In the next chapter, a description is presented of how we handle the issue of shortage of data with the help of synthetic methods of data generation.

## CHAPTER 6

### SYNTHETIC DATA GENERATION

#### 6.1 Introduction

In the dissertation to this point we have made the case that monitoring the state of health for modern battery pack systems, particularly for Electric Vehicles (EV), presents several unique challenges. Foremost among these is that, the sheer volume of data required for accurate prediction of capacity fade in a pack is daunting, and the types of tests required for data generation can be time and labor intensive. Ideally, a battery management system (BMS) would be able to utilize strictly operational data for health monitoring and control, in lieu of expensive data sets. However, it is obvious that one cannot avoid the need for rich data sets based on actual battery pack measurements. The focus of this chapter is on the feasibility of ideas addressing these challenges.

The fact remains that, out of all the components in an EV which are prone to failure, the battery pack is the most significant and hence the Li-ion batteries that are the main building blocks of such packs need to be robust more than ever. Similar is the case with stationary energy storage as well as smaller portable electronics.

The primary issue concerned with the effective use of Li-ion batteries is the nature of capacity fade and the nature in which capacity degrades in normal operational use. As topics for ongoing research, battery pack life expectancy and failure modes have received significant interest from investigators (58). When it comes to consumer electronics such as smartphones and laptops, a life cycle lasting about three years is generally accepted, but when it comes to an EV battery pack, the standardized range of 150,000 to 300,000 km life, which roughly equals about eight years worth of normal usage, appears acceptable. Nonetheless, for an average consumer who owns an EV for a period of more than eight years (59), the prospect of having to replace a battery pack is undesirable.

We have seen that extensive testing and deep discharge cycling of Li-ion batteries can be effective in estimating capacity fade. Along with cycling, subjecting such batteries to high C-rates and large variations in ambient temperature have other effects such as mechanical abrasion of the electrodes, electrolyte oxidation and Lithium-plating on the surface of the anode. All these effects are cumulatively observed as loss in capacity of the battery. Nonetheless, from a modeling perspective, having access to effective aging data, in which the battery gradually loses capacity while being subjected to a multitude of charge and discharge pulses with varying C-rates is highly desirable. One promising approach at this requirement is the creation of data-driven synthetic data for these studies.

Typical analyses for state-of-health in battery pack systems are based on historical data collections and testing done at various facilities, often under proprietary restrictions; as a result, only a limited number of measurement databases are available to investigators. The novel idea of using a limited experimental data set to generate iterative synthetic drive cycles and study the technical performance of a BMS has been explored in (33). Moreover, the concept of utilizing synthetic data has been used extensively in renewable energy studies (34) and health-care systems (35), where in both cases the quality of data is vital. In the domain of energy systems, synthetic data has found applications in modeling as well as large scale and domestic power consumption simulations. In (36), physics based modeling of batteries was presented, where computational challenges are tackled with particle Markov Chain Monte Carlo methods, with an implementation specifically designed for the non-Markovian setting. In large scale power systems (37), synthetic PV and load demands are used to validate control algorithms. In (38), a prototype demand-side load controller is validated using synthetically generated load data. It is evident in these examples that use of synthetic data as a validation tool is a well established practice in the research community.

In light of the need for validation of estimation schemes on diverse test data, and based on trends in the literature, we investigate the idea of generation of synthetic battery data

using Markov chains while exploiting actual experimental data. The primary motivation for this work is multifaceted, focused on using limited experimental data to synthetically generate data to fill gaps in data records based on trends in the actual data. In so doing, it becomes possible to predict battery pack characteristics such as open circuit voltage (OCV) relationships and even capacity and capacity fade. Moreover, having such mechanisms would easily allow one to statistically perturb the total data set in ways otherwise impractical (perhaps impossible) with the actual system in experimentation. As new experimental data becomes available through normal operation and through evolution of a machine learning process, portions of synthetic data could be judiciously dropped in favor of actual data.

In the evolution of capacity fade estimation studies using supervised learning algorithms for Li-ion packs in this dissertation, this chapter takes the next step in exploring avenues of extrapolating and generating “feature” based data from pre-existing data sets for facilitating improved learning and subsequent prediction of capacity by learning based algorithms. In previous chapters, sections of voltage, current and temperature data are reduced to centroids and how these centroids behave over time are used to determine capacity. In this chapter we provide a methodology to generate these centroids synthetically by combining multiple drive cycle or operational data.

Our previous analysis of features used for capacity estimation has indicated that by comparing an expected and experimental behavior of features, a reasonably accurate determination of battery pack capacity can be obtained. This not only plays a vital role from a BMS application point-of-view but also gives us the ability to eliminate the necessity for specific capacity determination tests, which themselves are detrimental to the batteries. Hence, armed with necessary tools for effectively analyzing large volumes of data, in this chapter a novel approach is presented of how multiple pulses can be managed in a probabilistic manner, such that the data generated is true in nature to the experimental data upon which it is based, while incorporating an increased number of pulses or features. We provide validation by highlighting a case study for prediction using synthetic data.

In the following sections, first an overview of the test data used is presented, followed by a concise description of the process for synthetic data generation using Markov Chains. This is followed by results of generating synthetic data using data from two battery packs, leading to a case study using simple machine learning, with the goal of providing data streams for the prediction philosophy presented thus far in this dissertation.

## 6.2 Data Sets Under Consideration

In this chapter, the generation of synthetic data is carried out with the generation of current and voltage profiles separately. For voltage generation, the data set generated on testing the three cell pack at 25°C using Drive Cycle 2 is used (Figure 6.1).

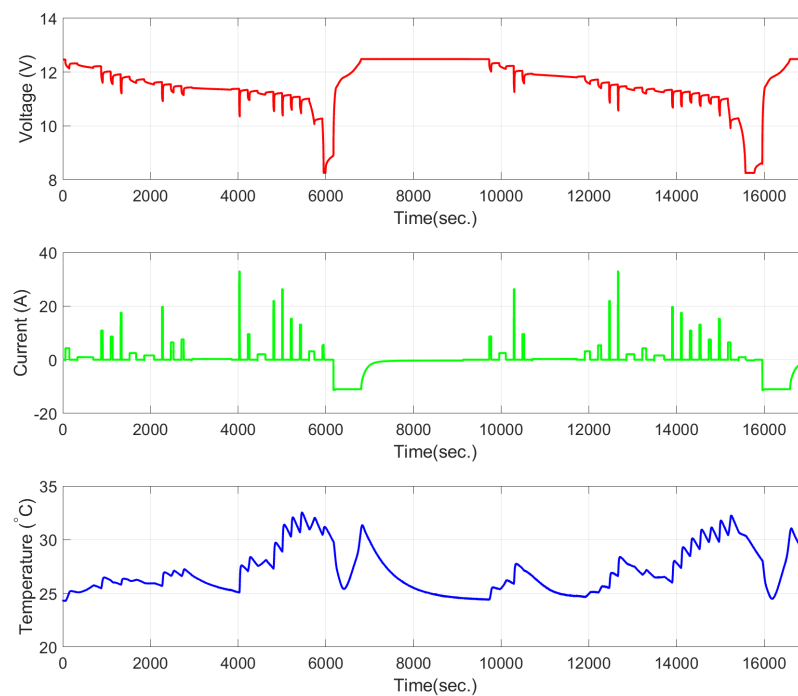


Figure 6.1: Representative “drive” test II.

For the current profile generation, multiple profiles obtained from the second automotive data set available for our studies is utilized. This was obtained from the battery pack in a

Renault Twizy consisting of 96 cells, from Groupe Renault, France. A representative drive profile is shown in Figure 6.2.

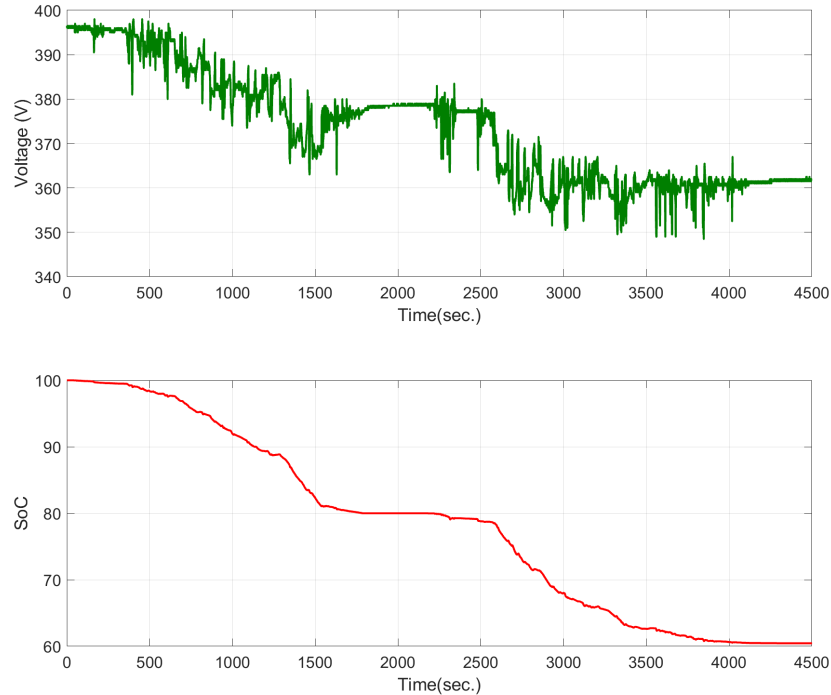


Figure 6.2: Sample Renault Twizy drive profile..

### 6.3 Synthetic Data Generation Methodology

The generation of synthetic data basically involves two primary steps:

1. Use the EV data set to generate transition probability matrices, based on which new current profiles can be generated using the concept of Markov chain propagation.
2. Use the generated current profile in the first step, along with a specified capacity profile, as inputs to a neural net structure which is trained on the three-cell pack data. The output of this model gives the voltage behavior of the synthetic data in terms of centroids of clusters.

### 6.3.1 Current Profile Generation

Because obtaining continuous drive data for a battery in order to show capacity fade presents a difficult challenge from a time and resource perspective, we employ stochastic models to generate useful data based on realistic scenarios and actual testing. Among methods based on stochastic models, of the most recognized are those using Markov chains. Markov chain based stochastic models afford the ability to generate time series drive data time possessing identical statistical parameters, with the added flexibility of different dimensions for the transition matrix (47).

Markov chains are useful for cases where current states are dictated by previous states. EV drive cycle data could be considered as a stochastic process in the sense that as the current drawn from the battery pack is a continuous process, the current drawn at the present state depends on the previous state. Based on a set of experimental drive data, a transition probability matrix of current transition can be set up in the following manner:

$$\begin{bmatrix} a_{1,1} & a_{1,2} & \dots & \dots & \dots & a_{1,j-1} & a_{1,j} \\ a_{2,1} & a_{2,2} & \dots & \dots & \dots & a_{2,j-1} & a_{2,j} \\ \vdots & \vdots & \ddots & & & \vdots & \vdots \\ \vdots & \vdots & & \ddots & & \vdots & \vdots \\ \vdots & \vdots & & & \ddots & \vdots & \vdots \\ a_{i-1,1} & a_{i-1,2} & \dots & \dots & \dots & a_{i-1,j-1} & a_{i-1,j} \\ a_{i,1} & a_{i,2} & \dots & \dots & \dots & a_{i,j-1} & a_{i,j} \end{bmatrix}, \quad (6.1)$$

where  $a_{i,j}$  represents the number of times the current changes from state  $i$  to state  $j$  in the experimental data.

In the EV data set, the maximum discharge current is 193.4 A, the minimum is 0.2 A and the average discharge current is 3.25 A. Based on these observations a total of 50 states have been chosen between 0 and 200 A.

The summation of each row in (6.1) represents the total number of times that previous current states are associated with state  $i$ . Elements of a related matrix can be obtained using

$$b_{i,j} = \frac{a_{i,j}}{\sum_{k=1}^n a_{i,k}} \quad , \quad (6.2)$$

where  $b_{i,j}$  represents the transition probability from state  $i$  to state  $j$ .

A uniformly distributed random number  $R$  between 0 and 1 can then be used to generate current time series data based on (6.2). To facilitate this, a new probability matrix  $C$  can be obtained with elements

$$c_{i,j} = \sum_{k=1}^j b_{i,k} \quad , \quad (6.3)$$

where  $c_{i,j}$  represents the summation of transition probabilities from state 1 to state  $j$  in row  $i$  of (6.2).

Once the matrix  $C$  is generated using experimental data, the random number  $R$  is used to generate the synthetic data. Comparing  $R$  with the elements in  $c_{i,j}$  ( $j = 1, 2, 3, \dots, n$ ), if  $R$  is smaller than  $c_{i,j}$ , the next current pulse belongs to state  $j$ . In this manner a current profile with unlimited length could be generated from an experimental data set.

Apart from generating the transition probability matrix, a few other considerations have been taken into account while generating the synthetic current profiles, namely:

1. Duration of each discharge pulse and the rest time after each pulse has been set to vary randomly between 1 and 5 minutes.
2. There are conditions encountered while running the generation process where the same state transition is repeated several times. In order to eliminate the effect of this, if a state transition gets repeated more than three times in a sequence, these three steps are eliminated and the matrix is re-initiated.
3. If the battery pack reaches 0% SoC, the process is terminated.

The above are essentially user-specific criteria and can easily be modified based on requirements or limitations of the estimation algorithm or data set.

### 6.3.2 Voltage Profile Generation

Because reducing data loads is one of the pivotal objectives of this work, we have used voltage clusters as the intended targets for the neural net structure employed. Also, our experience has shown that employing “features,” rather than raw data directly, as training and testing inputs for the neural nets improves the level of accuracy. Although for a different application here, the clustering approach presented earlier and the neural network structure used in (60), have been utilized with slight modifications.

#### Clustering

A K-means clustering approach takes a set of observations  $(x_1, x_2, \dots, x_n)$ , and partitions the  $n$ -observations into  $k \leq n$  sets  $S = \{S_1, S_2, \dots, S_k\}$  so that the variance is minimized. Formally, the objective is,

$$\arg \min_S \sum_{i=1}^k \sum_{x \in S_i} \|x - \mu_i\|^2 = \arg \min_S \sum_{i=1}^k |S_i| Var S_i \quad , \quad (6.4)$$

where  $\mu_i$  is the mean of the points in  $S_i$ .

For clustering in our case, the voltage profile during the discharge pulses in the three-cell pack data set have been clustered with  $k$  set to 20, where the data was generated by discharging from 100% SoC to 0% SoC in twenty pulses, each causing a 5% decrements in SoC. After this, multiple drive cycles with 20 clusters each have been used as a part of the training set.

#### Neural Net Structure

As a final step, a deep neural net structure consisting of three layers has been employed to generate the voltage behavior in terms of clusters. In Chapters 4 and 5, the neural nets used

were simplified because an objective was to minimize the computational complexity toward possible on-board computations. In this case of synthetic generation, where all calculations can be considered off-line, larger networks are acceptable. The network developed has three hidden layers with 10, 100 and 10 neurons individually, and has been trained for 1000 epochs with a learning rate of 0.001. The optimizer used is the ADAM optimizer (61).

From the three-cell pack data set, the drive cycle profiles have been used for training the network. Once again, three inputs are used: current value at the beginning of each pulse, the SoC value at the beginning of the pulse, and corresponding capacity values obtained from the characterization test implemented directly prior to the drive profiles. Cluster points from clustering the voltage behavior during the discharge pulses were used as network targets. Ninety percent of the complete drive data was used for training, whereas ten percent was used for validation and testing.

For network input, an SoC profile corresponding to the synthetically generated current profile results from a Coulomb counting process,

$$SoC(t) = SoC(t - 1) + \frac{I(t)}{Q} \Delta t \quad , \quad (6.5)$$

where  $I$  is the current value,  $Q$  represents capacity and  $\Delta t$  is the time step. Along with a desired capacity value profile, the current and SoC profiles make up inputs to the network. The output from this network gives the voltage behavior corresponding to the synthetic current profile.

## 6.4 Results

Using the methodologies of the previous section, one can generate synthetic data sets with a wide degree of flexibility for desired operational scenarios. However, an inherent challenge with using synthetic data generation is in validating the process. There are several ideas to get at this challenge; here we utilize the mRPT test data generated from experimenting

on the three-cell pack for this purpose. The underlying reason for this lies in the fact that even though the drive cycle data set possesses current rates similar to that of the five pulses in the mRPT test, they occur at different SoC values, thus providing a basis to compare experimental and synthetic data at different capacity values.

Hence, in what follows we first describe a synthetic data profile where the same current profile has been applied at different capacity points. Then we present a novel validation idea where we compare against the actual mRPT data.

### **Synthetic Data**

The result of the proposed methodology is highlighted in Figure 6.3. For generating both the voltage responses, the same current profile is input to the neural net at different capacity points, with states limited to 50 A. The first voltage response is generated at the capacity value of 1.976 Ah and the second response is generated at 1.857 Ah. The profile consists of 18 current pulses and clearly highlights a variation in voltage centroids as the capacity fades. Although there are other means to illustrate the synthetic data, we remind the reader that voltage centroids are of interest because they would be used in the subsequent prediction phase of this work, such as when lengthy and complete data streams are used.

We note in Figure 6.3 that even though some of the voltage centroids are higher than a preceding value, this does not indicate presence of charge pulses. The nature of clustering of centroids, as well as the recovery phase in batteries, can lead to this phenomenon where a particular voltage value resulting from a current pulse of smaller magnitude may be marginally above the voltage centroid for a current pulse of a higher magnitude.

### **mRPT Based Validation**

Validation of these ideas can be approached from a case study viewpoint, and many realistic scenarios can be considered. We illustrate the idea behind this validation approach with one

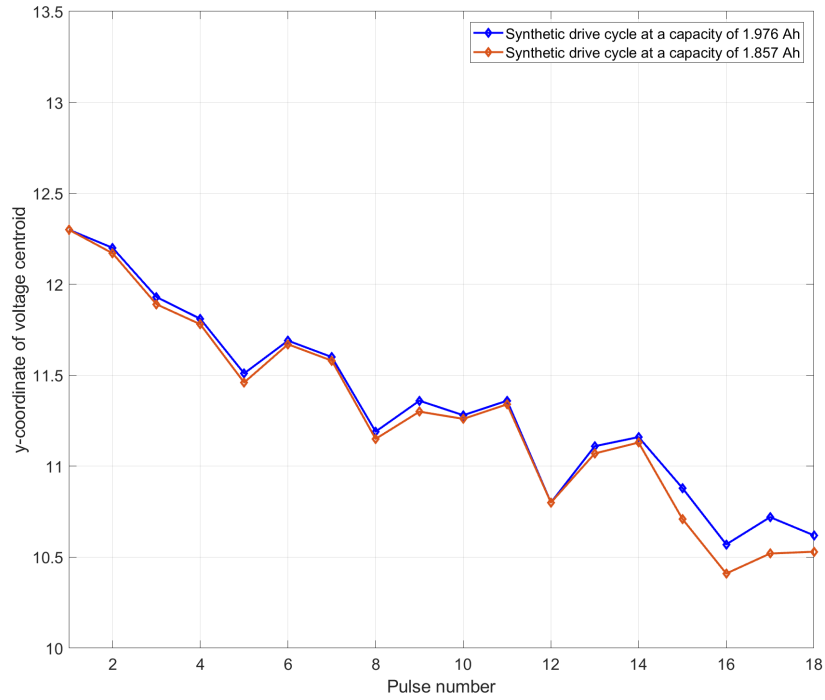


Figure 6.3: Comparison of true and synthetic voltage centroids during mRPT tests 1,5,7,10.

such case. Inputs to the network are the current values of each pulse and the corresponding SoC starting point from the mRPT profile at specific capacity values. In Figure 6.4 a comparison is shown between experimental (true) and synthetically generated voltage cluster points corresponding to mRPTs 1,5,7 and 10.

In Table 6.1, the mean square error is shown between the true mRPT voltage cluster values and the synthetically generated cluster values. As has been the case with estimation results in our investigation into predicting capacity fade, as the capacity of the battery fades, estimation errors tend to increase (as seen in the case of test 10). Although this typically happens when the battery is entering a failure mode, and not during typical operation ranges, these error margins are deemed tolerable.

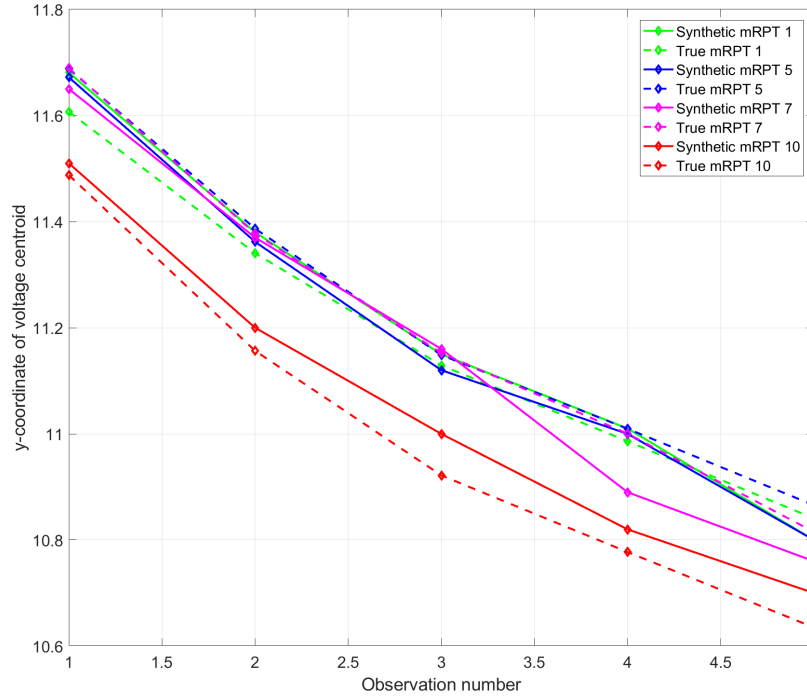


Figure 6.4: Comparison of true and synthetic Voltage centroids during mRPT 1,5,7,10.

Table 6.1: mRPT mean square error comparison

Test	1	5	7	10
MSE(%)	1.924	1.210	2.489	3.987

### Capacity Estimation Using Synthetic Data

The next step in using the synthetically generated data is an attempt to the methodology outlined in Chapter 5, where a drive cycle data is given as input to a network which predict features in line with what an mRPT test would depict. Following this, the predicted features are fed to a network which is trained and on the mRPT features and SoC behavior of the B-o-L data. This chain of approach will give us a method to go from a drive cycle to a predicted capacity number.

As is shown in Figure 6.5, the behavior of voltage centroids of one drive cycle is generated at three capacity points using a randomized current profile generated using the Markov

process. The current profile is such that each pulse can discharge the battery by 3 to 5% SoC with some pulses having no discharge at all. The nature of the three plots depicts that when there is marginal capacity change (1.976 Ahr to 1.938 Ahr), the plots do not show much variation. But with a large drop (1.938 Ahr to 1.754 Ahr), there are some drastic changes observed, especially in the lower ranges of SoC, where the plot tends to diverge from expected patterns (such as at pulse number 15).

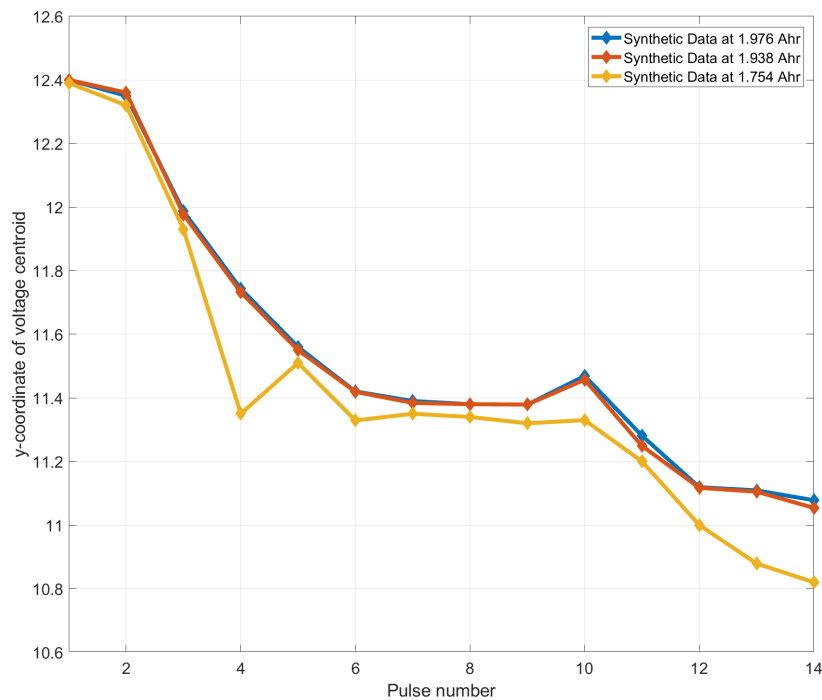


Figure 6.5: Synthetic drive cycle at different capacity values.

The three profiles which are generated are then fed to the feature generator which generated the voltage centroids for an mRPT data structure. The output of this network is fed to a second network and capacity predictions are obtained. The numbers obtained are shown in Table 6.2.

The predictions related to the 10<sup>th</sup> test shows a large error of 6.21% but this prediction is in a range where where the battery pack has lost around 22% of its rated capacity. In

Table 6.2: Capacity estimation results in the SoC range 50% to 10%.

Test No.	Estimated Capacity	True Capacity	% Error
1	1.981	1.976	0.25
5	1.967	1.938	1.49
10	1.645	1.754	6.21

order to reduce this error margin, the next step was to try and remove the large variations in the data observed from the 15<sup>th</sup> pulse onwards and observe the estimation numbers. The results of this step are shown in Table 6.3.

Table 6.3: Capacity estimation results in the SoC range 50% to 10%.

Test No.	Estimated Capacity	True Capacity	% Error
1	1.951	1.976	1.26
5	1.947	1.938	0.46
10	1.832	1.754	4.46

Reducing the data range did show some reduction in error margins for the 10<sup>th</sup> test without much effect on the 1<sup>st</sup> and 5<sup>th</sup>.

## 6.5 Summary

In this chapter a novel approach has been presented aimed at the challenges presented by data requirements in monitoring, predicting and controlling the state of health of modern battery pack systems. By using a limited experimentally derived data set, an approach is presented which provides essentially unlimited user-specified streams of synthetic data, based on capacity variations and varying scenarios. While challenges in this research still remain, this chapter has provided proof of concept and a basis for further study. In particular, a variety of scenarios may be tested in validating the approach, and ultimately the synthetic data approach can be used for capacity estimation and prediction trials for comparative studies in further experimentation.

While the approach presented in this chapter is early in its development, these techniques have great potential in providing realistic and verifiable baseline sets of training data for applications requiring large amounts of data, especially those that exhibit conditions that are known to be possible, but are too difficult to achieve in experimentation. The next steps to this work include applying broader heuristic verification and boundary analysis to the output of the Markov Chains to provide deeper confidence in the generated training data. With this analysis, the resulting trained predictions can be better anticipated and understood in real applications.

## CHAPTER 7

### CONCLUSION

From the initiation of this research there was a multitude of assumptions and uncertainties pertaining to both generation/availability of data to the use of largely black box approaches to modeling and estimation.

Testing and generating of data was the first hurdle where capturing gradual capacity fade was the primary focus. Through our initial testing, it was observed that, if the aim was to deplete the battery completely of its ability to get recharged, it was fairly easy to accomplish accurate estimation through deep discharge pulses and over-charging. On the other hand, making sure the capacity decays gradually even when the battery has reached a stage, where it loses around 8-10% of capacity with each cycling, was a tricky and delicate endeavor.

With the application of machine learning approaches, with every test type ( $Q_i$ , mRPT and drive cycle), the models had a tendency to generalize well on training but diverged on testing and simply increasing the network size was not a solution. More complicated solutions of regularization, scaling of inputs and use of advanced optimization algorithms needed careful implementation as the training time of these networks and the memory requirements had an exponential scale. With the generation of data synthetically, validating the quality of the generated data was of primary concern and it proved to be a difficult issue. Some of the challenges faced in each step of this research are discussed in detail in the following sections.

#### 7.1 Data Generation and Testing

As mentioned above, the aim of generating data was to capture the gradual decay in capacity fade in batteries as the ultimate objective. In order to do this a number of test profiles were studied, as well as examples of industry standardized testing. After the creation and

implementation of a few drive cycles, the upper and lower thresholds were tweaked because these limits had a bearing on how low or high the pack could be discharged or charged, respectively. This along with the study of a few drive cycles which were implemented on automotive grade cells created for testing the behavior of such batteries in different climate zones led us to create both drive cycles that have been used in this dissertation. As our focus shifted from profiles containing discharge/charge pulses to only discharge pulses, we observed an even slower and more gradual loss in capacity.

At the end of this refining approach, we were able to effectively generate data sets with gradual capacity loss at different temperatures without any situation where the packs lost capacity abruptly.

## 7.2 Characterization and mRPT Based Estimation

With neural nets, or in general any ML approaches, the two big factors which affect their ability to generalize are the quality of the data and the selection of the correct model. While using  $Q_i$  (characterization) tests, the main objective was to use beginning-of-life data in order to estimate capacity. The thought behind this was to facilitate a algorithm which did not require significant testing for a new battery and yet was able to capture the fade trends at later stages of the battery life. This training approach with a simple recurrent network gave good estimation numbers as the data used here was well defined and clearly showed trends with capacity fade.

When the estimation was attempted using mRPT data, a second objective of reducing the raw data volume was also incorporated. There were two issues encountered:

1. K-means clustering has a circular decision boundary, which means the number of cluster points in each cluster has to be of equal number. This was an issue with decreasing capacity as there were multiple CV modes occurring with the lower threshold being

reached and, as a result, data pre-processing with extrapolation we used to get around this issue.

2. FFNNs were unable to generalize well and increase in network size led to overfitting. At this stage, changing over to RNNs with their element of internal memory, and where their ability to remember important information related to the inputs they receive (e.g., the present state depends on the previous state in terms of SoC).
3. RNNs suffer from vanishing gradient and as a result, with higher capacity fade when the battery pack was approaching its end-of-life conditions, the estimation error kept rising. But, the network performed well in the capacity ranges which would be considered a standard and safe operating range for such batteries.

The approach developed and refined using mRPTs were extended to them them being applied on a microcontroller (Raspberry Pi) to test their feasibility for on-board and BMS implementation. With this implementation, the memory considerations were rigorously studied and they showed favourable numbers. But, the major issue that was observed was the requirement of large volumes of effective test data for the prediction of capacity fade. Making the best use of available data and the still maintaining low on-board memory consumption was achieved with intuitive use of clustering and within ranges of our interest, capacity fade predictions were obtained with very minimal training and testing time.

### **7.3 Drive Cycle Based Estimation**

In the estimation using drive cycle data, due to the lack of a structured profile, where there are discharge/charge pulses at regular intervals with constant rest phases between them, using I-V-T data directly as an input and target for NNs was counter productive as the network size grew (500 to 1000 nodes in 5 to 6 layers), thus leading to significant increases in training time (in the range of 8 to 9 hours). To combat this, a feature generator structure

was used to predict features which are similar to the features extracted from mRPTs. These features were fed to a second RNN, which was used to predict the SoC behavior and subsequent capacity prediction. The feature generator approach used multiple neural nets versus a single large net and used a fuzzy based selection technique to select which network was trained in the particular range of data. That network, which was a combination of networks, was used to predict the behavior of the features.

Also, using B-o-L data was insufficient while using drive cycles and the entire range of drive cycles were used to train the feature generator structure. This was a step away from what was implemented in the  $Q_i$  and mRPT based estimation, but in order to overcome the limited information available in the drive cycles, this was a necessary step.

Finally, with the increase in complexity in data and data pre-processing, estimation error showed an upward and gradually increasing trend. Once again, however such results produced errors that were below permissible limits in the capacity range of interest.

## **7.4 Synthetic Generation**

As a method to address the issue of quality data availability, probabilistic and synthetic data generation is a concept with a lot of promise. For this purpose, by the use of Markov chains, a concept has been demonstrated, which though in its infancy, can be used to combine multiple data sets in order to gain larger data sets which are beneficial to any ML implementation.

## **7.5 Final Comments**

Prediction and estimation of capacity fade in batteries and battery packs is a challenging problem due to the complexity of the relationships between many characteristics and features present in the battery pack system. In this study a conscious effort has been made to use some features which enable us to make effective predictions. But there is a vast scope

of exploration that is waiting to be looked into with larger number of features as well as combination of features.

The data requirements as has been elaborated upon, over long time intervals complicates the problem further, particularly because of the expensive and reliable testing environments required.

In the end, the research reported in this dissertation shows very promising results for a group of methodologies whereby simple ideas from machine learning are used to not only reduce the amount of data required in prediction of capacity fade, but also to shift reliance to more accessible data.

The research following this work is focused on several important off-shoots where packs can be looked at for fault detection and isolation, observation and estimation of other fade parameters such as impedance, exploration of simpler microcontrollers than a Raspberry Pi, incorporating cloud connectivity, and so on. The ultimate goal in capacity fade estimation, and prediction of general state of health for battery packs, is to be able to use typical drive cycle data for learning and prediction in automotive grade packs on-board a BMS in an EV.

## REFERENCES

- [1] W. J. McCracken, B. Parmley, C. Kelly, M. Crites, S. Wilson, Lithium-ion System Advances, *The Fifteenth Annual Battery Conference on Applications and Advances, 2000.*, pp. 287-291.
- [2] B. Pattipati, K. Pattipati, J. P. Christopherson, S. M. Namburu, D. V. Prokhorov, L. Qiao, Automotive Battery Management Systems, *IEEE AUTOTESTCON*, September 2008.
- [3] Thomas B. Reddy, Linden's handbook of batteries. Vol. 4. New York: McGraw-hill, 2011.
- [4] C. J. Mikolajczak, T. Hayes, M. V. Megerle and M. Wu, A Scientific Methodology for Investigation of a Lithium Ion Battery Failure, *2007 IEEE International Conference on Portable Information Devices*, pp. 1-6, Orlando, FL, 2007.
- [5] Bruce H. Kenknight, Eric G. Lovett, Robert J. Sweeney, Scott T. Mazar, and Yatheendhar Manicka, Method and apparatus for establishing context among events and optimizing implanted medical device performance, U.S. Patent 7,043,305, issued May 9, 2006.
- [6] C. Hendricks, N. Williard, S. Mathew, and M. Pecht, A failure modes, mechanisms, and effects analysis (FMMEA) of lithium-ion batteries. *Journal of Power Sources*, 297, pp.113-120, 2015.
- [7] A. Rahmoun, H. Biechl and A. Rosin, SOC estimation for Li-Ion batteries based on equivalent circuit diagrams and the application of a Kalman filter, *Electric Power Quality and Supply Reliability*, Tartu, pp. 1-4, 2012.
- [8] Pankaj Arora, Ralph E. White, and Marc Doyle, Capacity fade mechanisms and side reactions in lithiumion batteries, *Journal of the Electrochemical Society* 145, no. 10 (1998): 3647-3667.
- [9] T. Zheng, Y. Liu, E. W. Fuller, S. Tseng, U. Von Sacken, and J. R. Dahn, Lithium insertion in high capacity carbonaceous materials, *Journal of The Electrochemical Society* 142, no. 8 (1995): 2581-2590.
- [10] M. Doyle and J. Newman, A. S. Gozdz, C. N. Schmutz and J. M. Tarascon, *Journal of Electrocheical Society* 143 (1996): 1890.
- [11] M. Bolster and R. J. Staniewicz, Investigation of lithium intercalation metal oxides for thermal batteries, *Proceedings of the 34th International Power Sources Symposium*, Cherry Hill, pp. 136-140, NJ, USA, 1990.

- [12] A. Sakuda, K. Hirokazu, A. Hayashi, K. Tadanaga, and M. Tatsumisago, All-solid-state lithium secondary batteries with oxide-coated LiCoO<sub>2</sub> electrode and Li<sub>2</sub>SP<sub>2</sub>S<sub>5</sub> electrolyte, *Journal of Power Sources* 189, no. 1 (2009): 527-530.
- [13] F. Deligiannis, F. Harvey, R. J. Staniewicz and J. Willson, Lithium-Thionyl Chloride Batteries for the Mars Pathfinder Microover. No. N-96-24116; NASA-CP-3325; M-802; NAS-1.55: 3325; NIPS-96-39735; CONF-9511233-. National Aeronautics and Space Administration, Huntsville, AL (United States). George C. Marshall Space Flight Center, 1996.
- [14] N. Fitrianiingsih, H. Tarigan and R. Hidayat, Preliminary study on the preparation of hybrid polymer gel electrolyte for lithium battery applications and its ac impedance characteristics, *Joint International Conference on Rural Information and Communication Technology and Electric-Vehicle Technology (rICT and ICeV-T)*, Bandung, pp. 1-3, 2013
- [15] V. Muenzel, M. Brazil, I. Mareels, J. de Hoog and D. A. Thomas, Modeling reversible self-discharge in series-connected Li-ion battery cells, *IEEE Tencon - Spring*, Sydney, NSW, pp. 470-474, 2013.
- [16] R. N. Methekar, P. W. C. Northrop, K. Chen, R. D. Braatz and V. R. Subramanian, Kinetic Monte Carlo simulation of surface heterogeneity in graphite anodes for lithium-ion batteries: Passive layer formation, *Proceedings of the 2011 American Control Conference*, San Francisco, CA, pp. 1512-1517, 2011.
- [17] G. Nagasubramanian, Impedance studies on cathodes in Li-ion cells, *Collection of Technical Papers. 35th Intersociety Energy Conversion Engineering Conference and Exhibit (IECEC) (Cat. No.00CH37022)*, Las Vegas, NV, USA, pp. 968-975 vol.2, 2002.
- [18] C. Weng, J. Sun, H. Peng, An Open-Circuit-Voltage Model of Lithium-Ion Batteries for Effective Incremental Capacity Analysis, *ASME Dynamic Systems and Control Conference*, 2013.
- [19] L. Xintian, Z. Guojian, H. Yao, D. Bo, X. Xingwu, Research on the Capacity Fading Characteristics of a Li-ion Battery Based on an Equivalent Thermal Model, *International Conference on Intelligent Computing and Internet of Things (ICIT)*, May 2015.
- [20] J. Wang, P. Liu, J. Hicks-Garner, E. Sherman, S. Soukiazian, M. Verbrugge, H. Tataraia, J. Musser, P. Finamore, Cycle-Life Model for Graphite-LiFePO<sub>4</sub> Cells, *Journal of Power Sources*, Vol.196, Issue 8, Pages 3942-3948, April 2011.
- [21] Y. Lv, T. Mei, H. Gong, D. Wei, Z. Xing, Y. Zhu, Y. Qian, Synthesis of LiMnO<sub>2</sub> Porous Microsphere and its Electrochemical Behaviour as Cathode Material in Lithium-ion Batteries, *IET Micro & Nano Letters*, Vol. 7, Issue 5, Pages 439-442, June 2012.

- [22] T. Kim, Y. Wang, Z. Sahinoglu, T. Wada, S. Hara, W. Qiao, A Rayleigh Quotient-based Recursive Total-Least-Squares Online Maximum Capacity Estimation for Lithium-ion Batteries, *IEEE Transactions on Energy Conversion*, Vol. 30, Issue 3, Pages 842-851, September 2015.
- [23] Z. Fangdan, J. Jiuchun, Z. Weige, S. Bingxiang, Z. Caiping, W. Yukun, Capacity Estimation of Large-Scale Retired Li-ion Batteries for Second Use Based on Support Vector Machine, *IEEE 23rd International Symposium on Industrial Electronics (ISIE)*, July 2014.
- [24] X. Liu, D. Liu, Y. Zhang, Q. Wang, H. Wang, F. Zhang, Least Squares Support Vector Machine Based Lithium Battery Capacity Prediction, *International Conference on Mechatronics and Control (ICMC)*, July 2014.
- [25] L. Sturlaugson, J. W. Sheppard, Principal Component Analysis Preprocessing with Bayesian Networks for Battery Capacity Estimation, *IEEE Instrumentation and Measurement Technology Conference (I2MTC)*, July 2013.
- [26] A. A. Hussein, Capacity Fade Estimation in Electric Vehicle Li-ion Batteries Using Artificial Neural Networks, *IEEE Transactions on Industry Applications*, Vol. 51, Issue 3, Pages 2321-2330, October 2014.
- [27] Md. Sarvi, S. Adeli, A Neural Network Method for Estimation of Battery Available Capacity, *45th International Universities Power Engineering Conference (UPEC)*, August-September 2010.
- [28] L. Chen, B. Ji, W. P. .Cao, H. H. Pan, B. B. Tian, W. L. Lin, Grey system Theory-Based Capacity Estimation Method for Li-ion Batteries, *7th IET International Conference on Power Electronics, Machines and Drives (PEMD)*, April 2014.
- [29] C. Weng, Y. Cui, J. Sun, H. Peng, On-Board State of Health Monitoring of Lithium-ion Batteries Using Incremental Capacity Analysis with Support Vector Regression, *Journal of Power Sources*, Vol. 235, Pages 36-44, August 2013.
- [30] M. Pyne, S. Yurkovich, Data Driven Modeling and Simulation for Energy Storage Systems, *IEEE Mult-Conference on Systems and Control*, September 2016.
- [31] L. Tang, G. Rizzoni and S. Onori, Energy Management Strategy for HEVs Including Battery Life Optimization, *IEEE Transactions on Transportation Electrification*, October 2015, vol. 1, no. 3, pages 211-222.
- [32] S. Dey, S. Mohon, P. Pisu and B. Ayalew, Sensor Fault Detection, Isolation, and Estimation in Lithium-Ion Batteries, *IEEE Transactions on Control Systems Technology*, November 2016, vol. 24, no. 6, pages 2141-2149.

- [33] Q. Gong, S. Midlam-Mohler, V. Marano, and G. Rizzoni, An Iterative Markov Chain Approach for Generating Vehicle Driving Cycles, *SAE International Journal of Engines* no. 4, 2011-01-0880 (2011): 1035-1045.
- [34] J. Chen, J. S. Kim, and C Rabiti, Probabilistic Analysis of Hybrid Energy Systems using Synthetic Renewable and Load Data, *American Control Conference*, pp. 4723-4728. IEEE, 2017.
- [35] S. Yang, Y. Zhou, Y. Guo, R. A. Farneth, I. Marsic and B. S. Randall, Semi-Synthetic Trauma Resuscitation Process Data Generator, *International Conference on Healthcare Informatics (ICHI)*, pp. 573-573. IEEE, 2017.
- [36] P. E. Jacob, S. Md. Mahdi Alavi, A. Mahdi, S. J. Payne and D. A. Howey, Bayesian Inference in Non-Markovian State-Space Models With Applications to Battery Fractional-Order Systems, *IEEE Transactions on Control Systems Technology* 2017.
- [37] F. R. S. Sevilla, C. Park, V. Knazkins and P. Korba, Model Predictive Control of Energy Systems with Hybrid Storage, *Power and Energy Society General Meeting (PESGM)*, pp. 1-5. IEEE, 2016.
- [38] T. Ganu, D. P. Seetharam, V. Arya, J. Hazra, D. Sinha, R. Kunnath, L. C. De Silva, S. A. Husain and S. Kalyanaraman, nplug: An Autonomous Peak Load Controller, *IEEE Journal on Selected Areas in Communications* 31, no. 7 pp. 1205-1218, 2013.
- [39] L. Guo, M. Ramaswamy, M. Pyne, B. J. Yurkovich, and S. Yurkovich, Modeling and Experimental Validation of Series Connected Battery Pack Modules, *Conference on Control Technology and Applications (CCTA)*, pp. 859-865, IEEE, 2017.
- [40] F. Jin and He Yong-ling, State-Of-Charge Estimation of Li-Ion Battery Using Extended Kalman Filter, *Indonesian Journal of Electrical Engineering and Computer Science* no. 12 pp.7707-7714, IEEE, 2013.
- [41] H. Hu, S. Yurkovich, Y. Guezennec, and B. J. Yurkovich, Electro-thermal Battery Model Identification for Automotive Applications, *Journal of Power Sources* 196, no. 1 pp. 449-457, Elsevier, 2011.
- [42] S. Malkhandi, Fuzzy Logic-Based Learning System and Estimation of State-of-Charge of Lead-acid Battery, *Engineering Applications of Artificial Intelligence* no. 5, pp. 479-485 Elsevier, 2006.
- [43] Aurlien Gron, Hands-on Machine Learning with Scikit-Learn and TensorFlow: Concepts, Tools, and Techniques to build Intelligent Systems, O'Reilly Media, Inc., 2017.
- [44] C. Boutsidis, A. Zouzias, M. W. Mahoney, P. Drineas, Randomized Dimensionality Reduction for K-means Clustering, *Transactions on Information Theory*, Vol. 61, Issue 2, Pages 1045-1062, February 2015.

- [45] Simon Haykin, *Neural Networks: A Comprehensive Foundation*, Prentice Hall PTR, 1994.
- [46] Richard M. Golden, *Mathematical Methods for Neural Network Analysis and Design*, MIT Press, 1996.
- [47] D. Luo, H. Xu, Y. Zhen, B. Dilkina, H. Zha, X. Yang and W. Zhang, Learning Mixtures of Markov Chains from Aggregate Data with Structural Constraints, *IEEE Transactions on Knowledge and Data Engineering* 28, no. 6 pp. 1518-1531, 2016.
- [48] M. Jafari, A. Gauchia, S. Zhao, K. Zhang and L. Gauchia, Electric Vehicle Battery Cycle Aging Evaluation in Real-World Daily Driving and Vehicle-to-Grid Services, *IEEE Transactions on Transportation Electrification*, vol. 4, no. 1, pp. 122-134, March 2018.
- [49] A. Guha and A. Patra, State of Health Estimation of Lithium-Ion Batteries Using Capacity Fade and Internal Resistance Growth Models, *IEEE Transactions on Transportation Electrification*, vol. 4, no. 1, pp. 135-146, March 2018.
- [50] A. Natarajan, M. Pyne, B. J. Yurkovich, S. Yurkovich, On-Board Application of Supervised Learning for Capacity Estimation, *IEEE Conference on Control Technology and Applications*, August 2019 (submitted).
- [51] M. Pyne, B. J. Yurkovich, S. Yurkovich, Capacity Fade Estimation Using Supervised Learning, *IEEE Conference on Control Technology and Applications*, August 2017.
- [52] M. A. Hannan, M. S. H. Lipu, A. Hussain, M. H. Saad and A. Ayob, Neural Network Approach for Estimating State of Charge of Lithium-ion Battery Using Backtracking Search Algorithm, *IEEE Access*, Vol. PP, Issue 99, 2018.
- [53] L. Chen et al., A Novel State-of-Charge Estimation Method of Lithium-ion Batteries Combining the Grey Model and Genetic Algorithms, *IEEE Transactions on Power Electronics*, Vol. PP, Issue 99, 2017.
- [54] Y. K. Wu, G. T. Ye, L. T. Chang, T. Y. Hsieh and B. S. Jan, Capacity Determination of a Dynamic Energy Storage System in an Island Power System with High Renewable Energy Penetration, *International Conference on Applied System Innovation (ICASI)*, Pages 1698-1701, Sapporo, 2017.
- [55] M. Sarvi, M. A. S. Masoum, A Neural Network Model for Ni-Cd Batteries, *43rd International Universities Power Engineering Conference*, Pages 1-5, Padova, September, 2008.
- [56] J. Randles, J. E. Brough, Kinetics of Rapid Electrode Reactions, *Discussions of the Faraday Society 1*, Pages 11-19, 1947.

- [57] Casas-Cabanas, Montse, and M. Rosa Palacn, Electrode Materials for Lithium-Ion Rechargeable Batteries, *Advanced Materials for Clean Energy*, Page 229, 2017.
- [58] C. Pillot, Micro hybrid, HEV, P-HEV and EV market 20122025 impact on the battery business, *World Electric Vehicle Symposium and Exhibition (EVS27)*, Barcelona, pp. 1-6, 2013.
- [59] T. R. Hawkins, B. Singh, G. MajeauBettez and A. H. Strmman, Comparative environmental life cycle assessment of conventional and electric vehicles, *Journal of Industrial Ecology* 17, no. 1, pp. 53-64, 2013.
- [60] M. Pyne, B. J. Yurkovich and S. Yurkovich, Toward the Use of Operational Cycle Data for Capacity Estimation, *IEEE Conference on Control Technology and Applications (CCTA)*, Copenhagen, pp. 1389-1394, August 2018.
- [61] A. M. Taqi, A. Awad, F. Al-Azzo and M. Milanova, The Impact of Multi-Optimizers and Data Augmentation on TensorFlow Convolutional Neural Network Performance, *IEEE Conference on Multimedia Information Processing and Retrieval (MIPR)*, Miami, FL, pp. 140-145, 2018.

## **BIOGRAPHICAL SKETCH**

Moinak Pyne is currently pursuing his PhD at the Energy Storage Systems Laboratory at The University of Texas at Dallas. He received his MS from The University of Texas at Dallas in 2015. His thesis was titled Design and Evaluation of a Microgrid for PEV Charging with Flexible Distribution of Energy Sources and Storage. He received the B.Tech. degree in Electrical Engineering from West Bengal University of Technology, Kolkata, India, in 2013. His current research interests include modeling estimation and control of energy storage systems and use of data science as an analytic tool. He has had multiple publications over the years and has been recognised with scholarships and a Teaching Assistantship award. He has previously worked as a Battery Engineering Intern at Car Technologies in Summer 2016 and as a Visiting Scholar at the Center for Automotive Research at The Ohio State University in Summer 2017. He will be joining Peterbilt Motor Company in Denton, TX as a Data Scientist in the Summer of 2019.

## CURRICULUM VITAE

# Moinak Pyne

### **Educational History:**

BS, Electrical Engineering, West Bengal University of Technology, 2013

MS, Electrical Engineering, The University of Texas at Dallas, 2015

PhD, Electrical Engineering, The University of Texas at Dallas, 2019

*Supervised Battery Capacity Fade Estimation*

PhD Dissertation

Electrical Engineering Department, The University of Texas at Dallas

Advisor: Dr. Stephen Yurkovich

*Design and Evaluation of Microgrid for PEV Charging with Flexible Distribution of Energy Sources and Storage*

MS Thesis

Electrical Engineering Department, The University of Texas at Dallas

Advisor: Dr. Stephen Yurkovich

### **Employment History:**

Visiting Scholar, Center for Automotive Research, The Ohio State University, 2017

Battery Engineering Intern, Car Technologies, LLC, 2016

### **Professional Recognitions:**

Semi-Finalist, Go Green in the City Competition, by Schneider Electric, 2017

Best Teaching Assistant Award, UT Dallas, 2015

Jonsson School Graduate Fellowship Recipient for MS Thesis, 2014-2015

Student Member, IEEE-Control Systems Society, 2013-Present